Copy 1
RM E55K01a

NACA

RESEARCH MEMORANDUM

This is chapter 6 - Volume III of NACA RM E52B03a

AERODYNAMIC DESIGN OF AXIAL-FLOW COMPRESSORS

VI - EXPERIMENTAL FLOW IN TWO-DIMENSIONAL CASCADES

By Seymour Lieblein

Lewis Flight Propulsion Laboratory
Cleveland, Ohio

NATIONAL ADVISORY COMMITTEE FOR AERONAUTICS

WASHINGTON

167

TABLE OF CONTENTS

NATIONAL ADVISORY COMMITTEE FOR AERONAUTICS

RESEARCH MEMORANDUM

AERODYNAMIC DESIGN OF AXIAL-FLOW COMPRESSORS

VI - EXPERIMENTAL FLOW IN TWO-DIMENSIONAL CASCADES

By Seymour Lieblein

SUMMARY

Available experimental two-dimensional cascade data for conventional compressor blade sections are correlated. The two-dimensional cascade and some of the principal aerodynamic factors involved in its operation are first briefly described. Then the data are analyzed by examining the variation of cascade performance at a reference incidence angle in the region of minimum loss. Variations of reference incidence angle, total-pressure loss, and deviation angle with cascade geometry, inlet Mach number, and Reynolds number are investigated.

From the analysis and the correlations of the available data, rules and relations are evolved for the prediction of the magnitude of the reference total-pressure loss and the reference deviation and incidence angles for conventional blade profiles. These relations are developed in simplified forms readily applicable to compressor design procedures.

INTRODUCTION

Because of the complexity and three-dimensional character of the flow in multistage axial-flow compressors, various simplified approaches have been adopted in the quest for accurate blade-design data. The prevailing approach has been to treat the flow across individual compressor blade sections as a two-dimensional flow. The use of two-dimensionally derived flow characteristics in compressor design has generally been satisfactory for conservative units (ref. 1).

In view of the limitations involved in the theoretical calculation of the flow about two-dimensional blade sections (refs. 2 and 3), experimental investigations of two-dimensional cascades of blade sections were adopted as the principal source of blade-design data. Early experimental cascade results (e.g., refs. 4 to 6), however, were marked by a sensitivity to individual tunnel design and operation. This was largely a result of the failure to obtain true two-dimensional flow. Under these circumstances,

the correlation of isolated data was very difficult. Some efforts were made, however, to correlate limited experimental data for use in compressor design (e.g., ref. 7). The British, in particular, through the efforts primarily of Carter and Howell, appear to have made effective use of their early cascade investigations (refs. 8 to 11).

In recent years, the introduction of effective tunnel-wall boundary-layer removal for the establishment of true two-dimensional flow gave a substantial impetus to cascade analysis. In particular, the porous-wall technique of boundary-layer removal developed by the NACA (ref. 12) was a notable contribution. The use of effective tunnel boundary-layer control has resulted in more consistent systematic test data (refs. 13 to 16) and in more significant two-dimensional comparisons between theoretical and experimental performance (refs. 17 to 19). With the availability of a considerable amount of consistent data, it has become feasible to investigate the existence of general relations among the various cascade flow parameters. Such relations curtail the amount of future experimental data needed and also result in more effective use of the data currently available.

Inasmuch as the primary function of cascade information is to aid in the design of compressors, the present paper expresses the existing cascade data in terms of parameters applicable to compressor design. Such expression not only facilitates the design of moderate compressors but also makes possible a rapid comparison of cascade data with data obtained from advanced high-speed compressor configurations. Since the bulk of the available cascade data has been obtained at low speed (Mach numbers of the order of 0.1), the question of applicability to such high-speed units is very significant. It is necessary to determine which flow parameters can or cannot be applied, to what extent the low-speed data are directly usable, and whether corrections can be developed in those areas where the low-speed data cannot be used directly.

In the present report, the available cascade data obtained from a large number of tunnels are reworked in terms of what are believed to be significant parameters and, wherever possible, correlated in generalized forms. The performance parameters considered in the correlation are the outlet-air deviation angle and the cascade losses expressed in terms of blade-wake momentum thickness. The correlations are based on the variations of the performance parameters with cascade geometry (blade profile shape, solidity, chord angle) and inlet flow conditions. In view of the difficulties involved in establishing correlations over the complete range of operation of the cascade at various Mach number levels, the analysis is restricted to an examination of cascade performance at a reference incidence-angle location in the region of minimum loss.

The report is divided into four main sections: (1) a brief description of the two-dimensional cascade and of the parameters, concepts, and

data involved in the analysis, (2) an analysis of the variation of the reference incidence angle with cascade geometry and flow conditions, (3) an analysis of the variation of total-pressure loss at the reference incidence angle, and (4) an analysis of the variation of deviation angle at the reference incidence angle.

SYMBOLS

The following symbols are used in this report:

A	flow area
b	exponent in deviation-angle relations
C_D	drag coefficient
C_L	lift coefficient
c	chord length
D	diffusion factor (based on over-all velocities)
D_l	local diffusion factor (based on local velocities)
d	exponent in wake velocity-distribution relations
f	function
H	wake form factor, δ^*/θ
i	incidence angle, angle between inlet air-flow direction and tangent to blade mean camber line at leading edge, deg
i_o	incidence angle of uncambered blade section, deg
K_C	compressibility correction in loss equation
K_s	blade-shape correction factor in incidence- and deviation-angle relations
K_t	blade maximum-thickness correction factor in incidence- and deviation-angle relations
M	Mach number

[redacted]

m, m_c factors in deviation-angle rule

n slope factor in incidence-angle rule

P total pressure

p static pressure

q dynamic pressure, $\rho V^2/2$

Re_c blade-chord Reynolds number

s blade spacing

t blade maximum thickness

V air velocity

y direction normal to axis

z direction along axis

α angle of attack, angle between inlet air-flow direction and blade chord, deg

β angle between air-flow direction and axis, deg

γ^o angle between blade chord and axis, deg

δ wake full thickness

δ^* wake displacement thickness

δ^o deviation angle, angle between outlet air-flow direction and tangent to blade mean line at trailing edge, deg

δ_o^o deviation angle of uncambered blade section, deg

θ wake momentum-defect thickness

ρ density

σ solidity, c/s

φ blade camber angle, difference between angles of tangents to mean camber lines at leading and trailing edges, deg

$\bar{\omega}$ total-pressure-loss coefficient

Subscripts:

av average

i incidence angle

i.e. incompressible equation

inc incompressible

l lower surface

max maximum

ref reference

u upper surface

z component along axis

δ deviation angle

θ tangential

0 free stream

1 cascade inlet

2 cascade outlet (measuring station)

10 10 percent thick

PRELIMINARY CONSIDERATIONS

Description of Cascade

A schematic diagram of a low-speed two-dimensional-cascade tunnel is shown in figure 1 to illustrate the general tunnel layout. The principal components of the conventional tunnel are a blower, a diffuser section, a large settling chamber with honeycomb and screens to remove any swirl and to ensure a uniform velocity distribution, a contracting section to accelerate the flow, the cascade test section, and some form of outlet-air guidance. The test section contains a row or cascade of blades set in a mounting device that can be altered to obtain a range of air inlet angles (angle β_1 in figs. 1 and 2). Variations in blade angle of attack

[redacted]

are obtained either by rotating the blades on their individual mounting axes (i.e., by varying the angle between the blade chord and the cascade axis γ^{o}) at fixed air inlet angle or by keeping the blade-chord angle fixed and varying the air inlet angle by rotating the entire cascade. Outlet flow measurements are obtained from a traverse along the cascade usually between $\frac{1}{2}$ to $1\frac{1}{2}$ chord lengths behind the blade trailing edge at the blade midspan. In the analysis, blade outlet refers to the cascade measuring station.

In most cases, some form of wall boundary-layer control in the cascade is provided by means of suction through slots or porous-wall surfaces. Examples of different tunnel designs or detailed information concerning design, construction, and operation of the two-dimensional-cascade tunnel can be obtained from references 12, 13, and 20 to 22.

Nomenclature and symbols designating cascade blade characteristics are given in figure 2. As in isolated-airfoil practice, cascade blade shapes are normally evolved by adding a basic thickness distribution to a mean camber line. The mean camber line (as indicated in fig. 2) represents the basic curvature of the profile. Some frequently used curvatures are the NACA (A_{10}) and related mean lines (refs. 13 and 15), the circular-arc mean line (ref. 8), and the parabolic-arc mean line (ref. 14). Two popular basic thickness distributions are the NACA 65-series thickness distribution (ref. 13) and the British C.4 thickness distribution (ref. 8). A high-speed profile has also been obtained from the construction of a circular-arc upper and lower surface (ref. 23); this profile is referred to as the double-circular-arc blade.

Performance Parameters

The performance of cascade blade sections has generally been presented as plots of the variation of air-turning angle, lift coefficient, and flow losses against blade angle of attack (or incidence angle) for a given cascade solidity and blade orientation. Blade orientation is expressed in terms of either fixed air inlet angle or fixed blade-chord angle. Flow losses have been expressed in terms of coefficients of the drag force and the defects in outlet total pressure or momentum. A recent investigation (ref. 24) demonstrates the significance of presenting cascade losses in terms of the thickness and form characteristics of the blade wakes.

In this analysis, the cascade loss parameters considered are the wake momentum-thickness ratio θ/c (ref. 24) and the total-pressure-loss coefficient $\bar{\omega}_1$, defined as the ratio of the average loss in total pressure across the blade to the inlet dynamic head. Cascade losses are considered

in terms of $\bar{\omega}_1$, since this parameter can be conveniently used for the determination of compressor blade-row efficiency and entropy gradients. The parameter θ/c represents the basic wake development of the blade profile and, as such, constitutes a significant parameter for correlation purposes. Values of θ/c were computed from the cascade loss data according to methods similar to those presented in reference 24. The diffusion factor D of reference 25 was used as a measure of the blade loading in the region of minimum loss.

In the present analysis, it was necessary to use a uniform nomenclature and consistent correlation technique for the various blade shapes considered. It was believed that this could best be accomplished by considering the approach characteristics of the blade in terms of air incidence angle i, the camber characteristics in terms of the camber angle φ, and the air-turning characteristics in terms of the deviation angle δ° (fig. 2). As indicated in figure 2, these angles are based on the tangents to the blade mean camber line at the leading and trailing edges. The use of the deviation angle, rather than the turning angle, as a measure of the air outlet direction has the advantage, for correlation purposes, of a generally small variation with incidence angle. Air-turning angle is related to the camber, incidence, and deviation angles by

$$\Delta\beta = \varphi + i - \delta^\circ \qquad (1)$$

Incidence angle is considered positive when it tends to increase the air-turning angle, and deviation angle is considered positive when it tends to decrease the air-turning angle (fig. 2).

The use of incidence and deviation angles requires a unique and reasonable definition of the blade mean-line angle at the leading and trailing edges, which may not be possible for some blade shapes. The principal difficulty in this respect is in the 65-(A_{10})-series blades (ref. 13), whose mean-line slope is theoretically infinite at the leading and trailing edges. However, it is still possible to render these sections usable in the analysis by arbitrarily establishing an equivalent circular-arc mean camber line. As shown in figure 3, the equivalent circular-arc mean line is obtained by drawing a circular arc through the leading- and trailing-edge points and the point of maximum camber at the midchord position. Equivalent incidence, deviation, and camber angles can then be established from the equivalent circular-arc mean line as indicated in the figure. The relation between equivalent camber angle and isolated-airfoil lift coefficient of the NACA 65-(A_{10})-series mean line is shown in figure 4.

A typical plot of the cascade performance parameters used in the analysis is shown in figure 5 for a conventional blade section at fixed solidity and air inlet angle.

Data Selection

In selecting data sources for use in the cascade performance correlations, it is necessary to consider the degree of two-dimensionality obtained in the tunnel and the magnitude of the test Reynolds number and turbulence level.

Two-dimensionality. - As indicated previously, test results for a given cascade geometry obtained from different tunnels may vary because of a failure to achieve true two-dimensional flow across the cascade. Distortions of the true two-dimensional flow are caused by the tunnel-wall boundary-layer growth and by nonuniform inlet and outlet flow distributions (refs. 12 and 20). In modern cascade practice, good flow two-dimensionality is obtained by the use of wall-boundary-layer control or large tunnel size in conjunction with a large number of blades, or both. Examples of cascade tunnels with good two-dimensionality are given by references 13 and 21.

The lack of good two-dimensionality in cascade testing affects primarily the air-turning angles and blade-surface pressure distributions. Therefore, deviation-angle data were rejected when the two-dimensionality of the tunnel appeared questionable (usually the older and smaller tunnels). Practically all the cascade loss data were usable, however, since variations in the measured loss obtained from a given cascade geometry in different tunnels will generally be consistent with the measured diffusion levels (unless the blade span is less than about 1 or 2 inches and there is no extensive boundary-layer removal).

Reynolds number and turbulence. - For the same conditions of two-dimensionality and test-section Mach number, test results obtained from cascades of the same geometry may vary because of large differences in the magnitude of the blade-chord Reynolds number and the free-stream turbulence. Examples of the effect of Reynolds number and turbulence on the losses obtained from a given blade section at fixed incidence angle are presented in figure 6. Similar pronounced effects are observed on the deviation angle. As discussed in reference 3, the loss variation with Reynolds number is associated primarily with a local or complete separation of the laminar boundary layer on the blade surfaces. The data used in the correlation are restricted to values of blade-chord Reynolds number from about 2.0×10^5 to 2.5×10^5 in order to minimize the effects of different Reynolds numbers. Free-stream turbulence level was not generally determined in the various cascade tunnels.

In some cases (refs. 13 and 26, e.g.), in tunnels with low turbulence levels, marked local laminar-separation effects were observed in the range of Reynolds number selected for the correlation. Illustrative plots of the variation of total-pressure-loss coefficient with angle of attack for a cascade with local laminar separation are shown in figure 7. In such

instances, it was necessary to estimate the probable variation of loss (and deviation angle) in the absence of the local separation (as indicated in the figure) and use values obtained from the faired curves for the correlations.

The specific sources of data used in the analysis are indicated by the references listed for the various performance correlations. Details of the tunnel construction and operation and other pertinent information are given in the individual references.

Approach

In a correlation of two-dimensional-cascade data that is intended ultimately for use in compressor blade-element design, the variations of performance parameters should be established over a wide range of incidence angles. Experience shows (fig. 8) that the variation of loss with incidence angle for a given blade section changes markedly as the inlet Mach number is increased. Consequently, correlated low-speed blade performance at high and low incidence angles is not applicable at high Mach numbers. The low-speed-cascade performance is therefore considered at some reference point on the general loss-against-incidence-angle curve that exhibits the least variation in location and in magnitude of performance parameters as Mach number is increased.

The reference location herein is selected as the point of minimum loss on the curve of total-pressure loss against incidence angle. For conventional low-speed-cascade sections, the region of low-loss operation is generally flat, and it is difficult to establish precisely the value of incidence angle that corresponds to the minimum loss. For practical purposes, therefore, since the curves of loss coefficient against incidence angle are generally symmetrical, the reference minimum-loss location was established at the middle of the low-loss range of operation. Specifically, as shown in figure 9, the reference location is selected as the incidence angle at the midpoint of the range, where range is defined as the change in incidence angle corresponding to a rise in loss coefficient equal to the minimum value. Thus, for conventional cascade sections, the midrange reference location is considered coincident with the point of minimum loss. In addition to meeting the abovementioned requirement of small variation with inlet Mach number, the reference minimum-loss incidence angle (as compared with the optimum or nominal incidence settings of ref. 27 or the design incidence setting of ref. 13) requires the use of only the loss variation and also permits the use of the diffusion factor (applicable in region of minimum loss) as a measure of the blade loading.

At this point, it should be kept in mind that the reference minimum-loss incidence angle is not necessarily to be considered as a recommended design point for compressor application. The selection of the best

incidence angle for a particular blade element in a multistage-compressor design is a function of many considerations, such as the location of the blade row, the design Mach number, and the type and application of the design. In general, there is no one universal definition of design or best incidence angle. The cascade reference location is established primarily for purposes of analysis.

Of the many blade shapes currently in use in compressor design practice (i.e., NACA 65-series, C-series circular arc, parabolic arc, double circular arc), data sufficient to permit a reasonably complete and significant correlation have been published only for the 65-(A_{10})-series blades of reference 13. Therefore, a basic correlation of the 65-(A_{10})-series data had to be established first and the results used as a guide or foundation for determining the corresponding performance trends for the other blade shapes for which only limited data exist.

Since the ultimate objective of cascade tests is to provide information for designing compressors, it is desirable, of course, that the structure of the data correlations represent the compressor situation as closely as possible. Actually, a blade element in a compressor represents a blade section of fixed geometry (i.e., fixed profile form, solidity, and chord angle) with varying inlet-air angle. In two-dimensional-cascade practice, however, variations in incidence angle have been obtained by varying either the inlet-air angle or the blade-chord angle. The available systematic data for the NACA 65-(A_{10})-series blades (ref. 13) have been obtained under conditions of fixed inlet-air angle and varying blade-chord angle. Since these data form the foundation of the analysis, it was necessary to establish the cascade performance correlations on the basis of fixed inlet-air angle. Examination of limited unpublished low-speed data indicate that, as illustrated in figure 10, the loss curve for constant air inlet angle generally falls somewhat to the right of the constant-chord-angle curve for fixed values of β_1 and γ° in the low-loss region of the curve. Values of minimum-loss incidence angle for fixed β_1 operation are indicated to be of the order of 1° or 2° greater than for fixed γ° operation. An approximate allowance for this difference is made in the use of reference-incidence-angle data from these two methods.

With the definition of reference incidence angle, performance parameters, and analytical approach established, the procedure is first to determine how the value of the reference minimum-loss incidence angle varies with cascade geometry and flow conditions for the available blade profiles. Then the variation of the performance parameters is determined at the reference location (as indicated in fig. 5) as geometry and flow are changed. Thus, the various factors involved can be appraised, and correlation curves and charts can be established for the available data. The analysis and correlation of cascade reference-point characteristics are presented in the following sections.

INCIDENCE-ANGLE ANALYSIS

Preliminary Analysis

In an effort to obtain a general empirical rule for the location of the reference minimum-loss incidence angle, it is first necessary to examine the principal influencing factors.

It is generally recognized that the low-loss region of incidence angle is identified with the absence of large velocity peaks (and subsequent decelerations) on either blade surface. For infinitely thin sections, steep velocity gradients are avoided when the front stagnation point is located at the leading edge. This condition has frequently been referred to as the condition of "impact-free entry." Weinig (ref. 28) used the criterion of stagnation-point location to establish the variation of "impact-free-entry" incidence angle for infinitely thin circular-arc sections from potential-flow theory. Results deduced from reference 28 are presented in figure 11(a). The minimum-loss incidence angle is negative for infinitely thin blades and decreases linearly with camber for fixed solidity and blade-chord angle.

While there is no definite corresponding incidence-angle theory for thick-nose blades with rounded leading edges, some equivalent results have been obtained based on the criterion that the location of the stagnation point in the leading-edge region of a thick blade is the controlling factor in the determination of the surface velocity distributions. Carter, in reference 11, showed semitheoretically on this basis that optimum incidence angle (angle at maximum lift-drag ratio) for a conventional 10-percent-thick circular-arc blade decreases with increasing camber angle. The results of reference 11 were followed by generalized plots of optimum incidence angle in reference 27, which showed, as in figure 11(a), that optimum incidence angle for a 10-percent-thick C-series blade varies with camber angle, solidity, and blade orientation. (In these references, blade orientation was expressed in terms of air outlet angle rather than blade-chord angle.) The plot for an outlet-air angle of 20° is shown in figure 11(b). Apparently, the greater the blade circulation, the lower in magnitude the minimum-loss incidence angle must be. It is reasonable to expect, therefore, that the trends of variation of minimum-loss incidence angle for conventional blade sections will be similar to those established by thin-airfoil theory.

A preliminary examination of experimental cascade data showed that the minimum-loss incidence angles of uncambered sections ($\varphi = 0$) of conventional thicknesses were not zero, as indicated by theory for infinitely thin blades (fig. 11(a)), but always positive in value. The appearance of positive values of incidence angle for thick blades is attributed to the existence of velocity distributions at zero indicence angle that are not symmetrical on the two surfaces. Typical plots illustrating the high

velocities generally observed in the inlet region of the lower (pressure) surface of thick uncambered blades at zero incidence angle are shown in figure 12. Apparently, an increase in incidence angle from the zero value is necessary in order to reduce the lower-surface velocity to a more equitable distribution that results in a minimum of the over-all loss. This zero-camber thickness effect will appear only for blade-chord angles between 0° and 90°, since, as indicated by the highly simplified one-dimensional model of the blade passage flow in figure 13, the velocity distributions at these limit angles are symmetrical.

The effect of blade-thickness blockage on "impact-free-entry" incidence angle for straight (uncambered) blades of constant chordwise thickness in incompressible two-dimensional flow is investigated in reference 29. The results of reference 29, plotted in terms of the parameters used in this analysis, are shown in figure 14. It is reasonable to expect that similar trends of variations of zero-camber reference minimum-loss incidence angle will be obtained for compressor blade profiles.

On the basis of the preceding analysis, therefore, it is expected that, for low-speed-cascade flow, reference minimum-loss incidence angle will generally be positive at zero camber and decrease with increasing camber, depending on solidity and blade-chord angle. The available theory also indicates that the variation of reference incidence angle with camber at fixed solidity and chord angle might be essentially linear. If so, the variations could be expressed in terms of slope and intercept values, where the intercept value represents the magnitude of the incidence angle for the uncambered section (function of blade thickness, solidity, and blade-chord angle). Reference minimum-loss incidence angle may also vary with inlet Mach number and possibly with Reynolds number.

Data Correlations

Form of correlation. - Although preliminary theory indicates that blade-chord angle is the significant blade orientation parameter, it was necessary to establish the data correlations in terms of inlet-air angle, as mentioned previously. The observed cascade data were found to be represented satisfactorily by a linear variation of reference incidence angle with camber angle for fixed solidity and inlet-air angle. The variation of reference minimum-loss incidence angle can then be described in equation form as

$$i = i_0 + n\varphi \tag{2}$$

where i_0 is the incidence angle for zero camber, and n is the slope of the incidence-angle variation with camber $(i - i_0)/\varphi$.

Since the existence of a finite blade thickness is apparently the cause of the positive values of i_o, it is reasonable to assume that both the magnitude of the maximum thickness and the thickness distribution contribute to the effect. Therefore, since the 10-percent-thick 65-series blades of reference 13 are to be used as the basis for a generalized correlation of all conventional blade shapes, it is proposed that the zero-camber reference incidence angle be expressed in the form

$$i_o = (K_s)_i(K_t)_i(i_o)_{10} \tag{3}$$

where $(i_o)_{10}$ represents the variation of zero-camber incidence angle for the 10-percent-thick 65-series thickness distribution, $(K_t)_i$ represents any correction necessary for maximum blade thicknesses other than 10 percent, and $(K_s)_i$ represents any correction necessary for a blade shape with a thickness distribution different from that of the 65-series blades. (For a 10-percent-thick 65-series blade, $(K_t)_i = 1$ and $(K_s)_i = 1$.)

The problem, therefore, is reduced to finding the values of n and i_o (through eq. (3)) as functions of the pertinent variables involved for the various blade profiles considered.

NACA 65-(A_{10})-series blades. - From the extensive low-speed-cascade data for the 65-(A_{10})-series blades (ref. 13), when expressed in terms of equivalent incidence and camber angles (figs. 3 and 4), plots of i_o and n can be deduced that adequately represented the minimum-loss-incidence-angle variations of the data. The deduced values of i_o and n as functions of solidity and inlet-air angle are given for these blades in figures 15 and 16. The subscript 10 in figure 15 indicates that the i_o values are for 10-percent maximum-thickness ratio. Values of intercept i_o and slope n were obtained by fitting a straight line to each data plot of reference incidence angle against camber angle for a fixed solidity and air inlet angle. The straight lines were selected so that both a satisfactory representation of the variation of the data points and a consistent variation of the resulting n and i_o values were obtained.

The deduced rule values and the observed data points compared in figure 17 indicate the effectiveness of the deduced representation. In several configurations, particularly for low cambers, the range of equivalent incidence angle covered in the tests was insufficient to permit an accurate determination of a minimum-loss value. Some of the scatter of the data may be due to the effects of local laminar separation in altering the range characteristics of the sections.

[redacted]

Although the cascade data in reference 13 include values of inlet-air angle from 30° to 70° and values of solidity from 0.5 to 1.5, the deduced variations in figures 15 and 16 are extrapolated to cover wider ranges of β_1 and σ. The extrapolation of i_o to zero at $\beta_1 = 0$ is obvious. According to theory (fig. 11), the value of the slope term does not vanish at $\beta_1 = 0$. In figure 16, therefore, an arbitrary fairing of the curves down to nonzero values of n was adopted as indicated. Actually, it is not particularly critical to determine the exact value of the slope term at $\beta_1 = 0$ necessary to locate the reference incidence angle precisely, since, for such cases (inlet guide vanes and turbine nozzles), a wide low-loss range of operation is usually obtained. The solidity extrapolations were attempted because of the uniform variations of the data with solidity. However, caution should be exercised in any further extrapolation of the deduced variations.

C-Series circular-arc blades. - The various thickness distributions used in combination with the circular-arc mean line have been designated C.1, C.2, C.3, and so forth (refs. 27, 30, and 31). In general, the various C-series thickness distributions are fairly similar, and have their maximum thickness located at between 30- and 40-percent of the chord length. The 65-series and two of the more popular C-series thickness distributions (C.1 and C.4) are compared on an exaggerated scale in figure 18. (The 65-series profile shown is usually thickened near the trailing edge in actual blade construction.)

In view of the somewhat greater thickness blockage in the forward portions of the C-series blades (fig. 18), it may be that the minimum-loss incidence angles for zero camber for the C-series blades are somewhat greater than those for the 65-series profiles; that is, $(K_s)_i > 1$. In the absence of any definitive cascade data, the value of $(K_s)_i$ for the C-series profiles was arbitrarily taken to be 1.1. Observed minimum-loss incidence angles for an uncambered 10-percent-thick C.4 profile (obtained from ref. 32) are compared in figure 19 with values predicted from the deduced $(i_o)_{10}$ values for the 65-series blade (fig. 15 and eq. (3)) with an assumed value of $(K_s)_i = 1.1$. (For 10-percent thickness, $(K_t)_i = 1$.)

In view of the similarity between the 65-(A_{10})-series mean line and a true circular arc (fig. 3), the applicability of the slope values in figure 16 to the circular-arc mean line was investigated. For the recent cascade data obtained from tunnels having good boundary-layer control (refs. 17 and 33), a check calculation for the 10-percent-thick C.4 circular-arc blades using figures 15 and 16 with $(K_s)_i = 1.1$ revealed good results. For the three configurations in reference 33 tested at constant β_1 ($\varphi = 30°$), the agreement between observed and predicted

minimum-loss incidence angles was within 1°. For the one configuration in reference 15 tested at constant γ° ($\varphi = 31^{\circ}$), the predicted value of minimum-loss incidence angle was 1.7° greater than the observed value. However, in view of the general 1° to 2° difference between fixed β_1 and fixed γ° operation (fig. 10), such a discrepancy is to be expected. On the basis of these limited data, it appears that the low-speed minimum-loss incidence angles for the C-series circular-arc blade can be obtained from the i_o and n values of the 65-series blade with $(K_s)_i = 1.1$.

Double-circular-arc blades. - The double-circular-arc blade is composed of circular-arc upper and lower surfaces. The arc for each surface is drawn between the point of maximum thickness at midchord and the tangent to the circles of the leading- and trailing-edge radii. The chordwise thickness distribution for the double-circular-arc profile with 1-percent leading- and trailing-edge radius is shown in figure 18. Lack of cascade data again prevents an accurate determination of a reference incidence-angle rule for the double circular arc. Since the double-circular-arc blade is thinner than the 65-series blade in the inlet region, the zero-camber incidence angles for the double-circular-arc blade should be somewhat different from those of the 65-series section, with perhaps $(K_s)_i \leq 1$. It can also be assumed, as before, that the slope-term values of figure 16 are valid for the double-circular-arc blade. From an examination of the available cascade data for the double-circular-arc blade ($\varphi = 25^{\circ}$, $\sigma = 1.333$, ref. 23; and $\varphi = 40^{\circ}$, $\sigma = 1.064$, ref. 30), it appears that the use of figures 15 and 16 with a value of $(K_s)_i = 0.7$ in equations (2) and (3) results in a satisfactory comparison between predicted and observed values of reference incidence angle.

Other blades. - Similar procedures can be applied to establish reference incidence-angle correlations for other blade shapes. Cascade data are also available for the C-series parabolic-arc blades (refs. 14, 23, 32, 34, and 35) and the NACA 65-(A1) series blade (ref. 15); but, in view of the limited use of these forms in current practice, no attempt was made at this time to deduce corresponding incidence-angle rules for these blades.

Effect of blade maximum thickness. - As indicated previously, some correction (expressed here in terms of $(K_t)_i$, eq. (3)) of the base values of $(i_o)_{10}$ obtained from the 10-percent-thick 65-series blades in figure 15 should exist for other values of blade maximum-thickness ratio. According to the theory of the zero-camber effect, $(K_t)_i$ should be zero for zero thickness and increase as maximum blade thickness is increased, with a value of 1.0 for a thickness ratio of 0.10. Although the very limited low-speed data obtained from blades of variable thickness ratio (refs. 36 and 37) were not completely definitive, it was possible to establish a preliminary thickness correction factor for reference zero-camber incidence angle as indicated in figure 20 for use in conjunction with equation (3).

Effect of inlet Mach number. - The previous correlations of reference minimum-loss incidence angle have all been based on low-speed-cascade data. It appears from limited high-speed data, however, that minimum-loss incidence angle will vary with increasing inlet Mach number for certain blade shapes.

The variations of minimum-loss incidence angle with inlet Mach number are plotted for several blade shapes in figures 21 and 22. The extension of the test data points to lower values of inlet Mach number could not generally be made because of reduced Reynolds numbers or insufficient points to establish the reference location at the lower Mach numbers. In some instances, however, it was possible to obtain low-speed values of incidence angle from other sources.

The blades of figure 21 show essentially no variation of minimum-loss incidence angle with inlet Mach number, at least up to a Mach number of about 0.8. The blades of figure 22, however, evidence a marked increase in incidence angle with Mach number. The difference in the variation of minimum-loss incidence angle with Mach number in figures 21 and 22 is associated with the different way the general pattern of the loss variation changes with increasing Mach number for the two types of blades. For the thick-nose blades, as illustrated in figures 8(a) and (b), the loss coefficient increases with Mach number at both the high and low incidence angles; thus tending to maintain the same point of minimum loss. For the sharp-nose blade, as illustrated by figures 8(c) and (d), the increase in loss occurs primarily on the low-incidence-angle side; and a positive shifting of the minimum-loss incidence angle results. Data for other thick-nose sections in reference 35 show the rise in loss to occur at both ends of the curve, but plots of reference incidence angle against Mach number could not validly be made for these blades because of evidence of strong local laminar-separation effects.

Since the most obvious difference between the blades in figures 21 and 22 is the construction of the leading-edge region, the data suggest that blades with thick-nose inlet regions tend to show, for the range of inlet Mach number covered, essentially no Mach number effect on minimum-loss incidence angle, while blades with sharp leading edges will have a significant Mach number effect. The available data, however, are too limited to conclusively confirm this observation at this time. Furthermore, for the blades that do show a Mach number effect, the magnitude of the variation of reference incidence angle with Mach number is not currently predictable.

Summary

The analysis of blade-section reference minimum-loss incidence angle shows that the variation of the reference incidence angle with cascade

geometry at low speed can be established satisfactorily in terms of an intercept value i_o and a slope value n as given by equation (2). Deduced values of i_o and n were obtained as a function of β_1 and σ from the data for the 10-percent-thick 65-(A_{10})-series blades of reference 13 as equivalent circular-arc sections (figs. 15 and 16). It was then shown that, as a first approach, the deduced values of $(i_o)_{10}$ and n in figures 15 and 16 could also be used to predict the reference incidence angles of the C-series and double-circular-arc blades by means of a correction $(K_s)_i$ to the $(i_o)_{10}$ values of figure 15 (eq. (3)).

The procedure involved in estimating the low-speed reference minimum-loss incidence angle of a blade section is as follows: From known values of β_1 and σ, $(i_o)_{10}$ and n are selected from figures 15 and 16. The value of $(K_t)_i$ for the blade maximum-thickness ratio is obtained from figure 20, and the appropriate value of $(K_s)_i$ is selected for the type of thickness distribution. For NACA 65-series blades, $(K_s)_i = 1.0$; and it is proposed that $(K_s)_i$ be taken as 1.1 for the C-series circular-arc blade and as 0.7 for the double-circular-arc blade. The value of i_o is then computed from equation (3); and, finally, i is determined from the blade camber angle according to equation (2).

It should be noted that the values of $(K_s)_i$ given for the circular-arc blades are rather tenuous values obtained from very limited data. The use of the proposed values is not critical for good accuracy; the values were included primarily for completeness as a reflection of the anticipated differences in the blade-thickness blockage effects. Further experimental data will be necessary to establish the significance of such a correction. Also, a marked increase in reference minimum-loss incidence angle is to be expected for sharp-nose blade sections. The magnitude of the Mach number correction for these blades is currently unpredictable.

LOSS ANALYSIS

With the location of the low-speed reference minimum-loss incidence angle established for several conventional blade sections, the magnitude of the losses occurring at this reference position (fig. 5) will now be investigated. Accordingly, the nature of the loss phenomena and the various factors influencing the magnitude of the loss over a range of blade configurations and flow conditions are first analyzed. The available experimental loss data are then examined to establish fundamental loss correlations in terms indicated by the analysis.

Preliminary Analysis

Two-dimensional-cascade losses arise primarily from the growth of boundary layer on the suction and pressure surfaces of the blades. These surface boundary layers come together at the blade trailing edge, where they combine to form the blade wake, as shown in figure 23. As a result of the formation of the surface boundary layers, a local defect in total pressure is created, and a certain mass-averaged loss in total pressure is determined in the wake of the section. The loss in total pressure is measured in terms of the total-pressure-loss coefficient $\bar{\omega}$, defined generally as the ratio of the mass-averaged loss in total pressure $\overline{\Delta P}$ across the blade row from inlet to outlet stations to some reference free-stream dynamic pressure $(P_0 - p_0)_{ref}$, or

$$\bar{\omega}_{ref} = \frac{\overline{\Delta P}}{(P_0 - p_0)_{ref}} \tag{4}$$

For incompressible flow, $P_0 - p_0$ is equal to the conventional free-stream dynamic pressure $\rho_0 V_0^2/2$. The total-pressure-loss coefficient is usually determined from consideration of the total-pressure variation across a blade spacing s (fig. 23).

A theoretical analysis of incompressible two-dimensional-cascade losses in reference 24 shows that the total-pressure-loss coefficient at the cascade-outlet measuring station (where the static pressure is essentially uniform across the blade spacing) is given by

$$\bar{\omega}_1 = 2\left(\frac{\theta}{c}\right)_2 \frac{\sigma}{\cos \beta_2}\left(\frac{\cos \beta_1}{\cos \beta_2}\right)^2 \left\{ \frac{\frac{2H_2}{3H_2 - 1}}{\left[1 - \left(\frac{\theta}{c}\right)_2 \frac{\sigma H_2}{\cos \beta_2}\right]^3} \right\} \tag{5}$$

where $\bar{\omega}_1$ is the loss coefficient based on inlet dynamic head, θ/c is the ratio of wake momentum thickness to blade-chord length, σ is cascade solidity, β_2 is the air outlet angle, and H_2 is the wake form factor (displacement thickness divided by momentum thickness). The wake characteristics in equation (5) are expressed in terms of conventional thickness in a plane normal to the wake (i.e., normal to the outlet flow) at the measuring station. Definitions of wake characteristics and variations in velocity and pressure assumed by the analysis are given in reference 24. The analysis further indicates that the collection of terms within the brackets is essentially secondary (since H_2 is generally $\leq$ about 1.2 at the measuring station), with a magnitude of nearly 1 for conventional unstalled configurations. The principal determinants of the loss

in total pressure at the cascade measuring station are, therefore, the cascade geometry factors of solidity, air outlet and air inlet angles, and the aerodynamic factor of wake momentum-thickness ratio.

Since the wake is formed from a coalescing of the pressure- and suction-surface boundary layers, the wake momentum thickness naturally depends on the development of the blade-surface boundary layers and also on the magnitude of the blade trailing-edge thickness. The results of references 24, 36, and 38 indicate, however, that the contribution of conventional blade trailing-edge thickness to the total loss is not generally large for compressor sections; the preliminary factor in the wake development is the blade-surface boundary-layer growth. In general, it is known (ref. 3, e.g.) that the boundary-layer growth on the surfaces of the blade is a function primarily of the following factors: (1) the surface velocity gradients (in both subsonic and supersonic flow), (2) the blade-chord Reynolds number, and (3) the free-stream turbulence level.

Experience has shown that blade-surface velocity distributions that result in large amounts of diffusion in velocity tend to produce relatively thick blade boundary layers. The magnitude of the velocity diffusion in low-speed flow generally depends on the geometry of the blade section and its incidence angle. As Mach number is increased, however, compressibility exerts a further influence on the velocity diffusion of a given cascade geometry and orientation. If local supersonic velocities develop at high inlet Mach numbers, the velocity diffusion is altered by the formation of shock waves and the interaction of these shock waves with the blade-surface boundary layers. The losses associated with local supersonic flow in a cascade are generally greater than for subsonic flow in the same cascade. The increases in loss are frequently referred to as shock-separation losses.

Cascade-inlet Mach number also influences the magnitude of the subsonic diffusion for a fixed cascade. This Mach number effect is the conventional effect of compressibility on the blade velocity distributions in subsonic flow. Compressibility causes the maximum local velocity on the blade surface to increase at a faster rate than the inlet and outlet velocities. Accordingly, the magnitude of the surface diffusion from maximum velocity to outlet velocity becomes greater as inlet Mach number is increased. A further secondary influence of Mach number on losses is obtained because of an increase in losses associated with the eventual mixing of the wake with the surrounding free-stream flow (ref. 39).

On the basis of the foregoing considerations, therefore, it is expected that the principal factors upon which to base empirical cascade-wake-thickness correlations should be velocity diffusion, inlet Mach number, blade-chord Reynolds number, and, if possible, turbulence level.

Data Correlations

Velocity diffusion based on local velocities. - Recently, several investigations have been reported in references 24, 25, and 40 on the establishment of simplified diffusion parameters and the correlation of cascade losses in terms of these parameters. The general hypothesis of these diffusion correlations states that the wake thickness, and consequently the magnitude of the loss in total pressure, is proportional to the diffusion in velocity on the suction surface of the blade in the region of the minimum loss. This hypothesis is based on the consideration that the boundary layer on the suction surface of conventional compressor blade sections contributes the major share of the wake in these regions, and therefore the suction-surface velocity distribution becomes the governing factor in the determination of the loss. It was further established in these correlations that, for conventional velocity distributions, the diffusion in velocity can be expressed significantly as a parameter involving the difference between some function of the measured maximum suction-surface velocity V_{max} and the outlet velocity V_2.

Reference 40 presents an analysis of blade-loading limits for the 65-(A_{10})10 blade section in terms of drag coefficient and a diffusion parameter given for incompressible flow by $(V_{max}^2 - V_2^2)/V_{max}^2$. Results of an unpublished analysis of cascade losses in terms of the momentum thickness of the blade wake (as suggested in ref. 24) indicate that a local diffusion parameter in the form given previously or in the form $(V_{max} - V_2)/V_{max}$ can satisfactorily correlate experimental cascade loss data. The term "local diffusion parameter" is used to indicate that a knowledge of the maximum local surface velocity is required. The correlation obtained between calculated wake momentum-thickness ratio θ/c and local diffusion factor given by

$$D_l = \frac{V_{max} - V_2}{V_{max}} \tag{6}$$

obtained for the NACA 65-(A_{10})-series cascade sections of reference 13 at reference incidence angle is shown in figure 24. Values of wake momentum-thickness ratio for these data were computed from the reported wake coefficient values according to methods similar to those discussed in reference 24. Unfortunately, blade-surface velocity-distribution data are not available for the determination of the diffusion factor for other conventional blade shapes.

The correlation of figure 24 indicates the general validity of the basic diffusion hypothesis. At high values of diffusion (greater than about 0.5), a separation of the suction-surface boundary layer is

suggested by the rapid rise in the momentum thickness. The indicated nonzero value of momentum thickness at zero diffusion represents the basic friction loss (surface shear stress) of the flow and also, to a smaller extent, the effect of the finite trailing-edge thickness. The correlation of figure 24 further indicates that wake momentum-thickness ratio at reference incidence angle can be estimated from the computed local diffusion factor for a wide range of solidities, cambers, and inlet-air angles. The loss relations of equation (5) and reference 24 can then be used to compute the resulting loss in the total pressure.

Velocity diffusion based on over-all velocities. - In order to include the cases of blade shapes for which velocity-distribution data are not available, a diffusion parameter has been established in reference 25 that does not require a specific knowledge of the peak local suction-surface velocity. Although originally derived for use in compressor design and analysis, the diffusion factor of reference 25 can also be applied in the analysis of cascade losses. The diffusion factor of reference 25 attempts, through several simplifying approximations, to express the local diffusion on the blade suction surface in terms of over-all (inlet or outlet) velocities or angles, quantities that are readily determined. The basis for the development of the over-all diffusion factor is presented in detail in reference 25 and is indicated briefly in figure 25. The diffusion factor is given by

$$D = \left(1 - \frac{V_2}{V_1}\right) + \frac{\Delta V_\theta}{2\sigma V_1} \tag{7}$$

which, for incompressible two-dimensional-cascade flow, becomes

$$D = \left(1 - \frac{\cos \beta_1}{\cos \beta_2}\right) + \frac{\cos \beta_1}{2\sigma} (\tan \beta_1 - \tan \beta_2) \tag{8}$$

As in the case of the local diffusion factor, the diffusion factor of equation (8) is restricted to the region of minimum loss.

Cascade total-pressure losses at reference minimum-loss incidence angle are presented in reference 25 as a function of diffusion factor for the blades of reference 13. In a further unpublished analysis, a composite plot of the variation of computed wake momentum-thickness ratio with D factor at reference minimum-loss incidence angle was obtained from the available systematic cascade data (refs. 13, 14, and 32) as shown in figure 26. Blade maximum thickness was 10 percent in all cases. A separation of the suction-surface boundary layer at high blade loading is indicated by the increased rise in the wake momentum thickness for values of diffusion factor greater than about 0.6.

For situations in which the determination of a wake momentum-thickness ratio cannot be made, a significant loss analysis may be obtained if a simplified total-pressure-loss parameter is used that closely approximates the wake thickness. Since the terms within the brackets of equation (5) are generally secondary factors, a loss parameter of the form $\bar{\omega}_1 \frac{\cos \beta_2}{2\sigma}\left(\frac{\cos \beta_2}{\cos \beta_1}\right)^2$ should constitute a more fundamental expression of the basic loss across a blade element than the loss coefficient alone. The effectiveness of the substitute loss parameter $\bar{\omega}_1 \frac{\cos \beta_2}{2\sigma}\left(\frac{\cos \beta_2}{\cos \beta_1}\right)^2$ in correlating two-dimensional-cascade losses is illustrated in figure 27(a) for all the data for the NACA 65-(A_{10})-series blades of reference 13. (Total-pressure-loss coefficients were computed for the data from relations given in ref. 25.) A generalized correlation can also be obtained in terms of $\bar{\omega}_1 \frac{\cos \beta_2}{2\sigma}$, as shown in figure 27(b), but its effectiveness as a separation indicator does not appear to be as good. Such generalized loss parameters are most effective if the wake form does not vary appreciably among the various data considered.

Effect of blade maximum thickness. - Since an increase in blade maximum-thickness ratio increases the magnitude of the surface velocities (and therefore the diffusion), higher values of wake momentum-thickness ratio would be expected for thicker blades. From an analysis of limited available data on varying blade maximum-thickness ratio (refs. 36 and 37), it appears that the effect of blade thickness on wake momentum-thickness ratio is not large for conventional cascade configurations. For example, for an increase in blade maximum-thickness ratio from 0.05 to 0.10, an increase in θ/c of about 0.003 at D of about 0.55 and an increase of about 0.002 at D of about 0.35 are indicated. The greater increase in wake θ/c at the higher diffusion level is understandable, since the rate of change of θ/c with D_1 increases with increasing diffusion (see fig. 24).

If blade-surface velocity ditributions can be determined, then the thickness effect will automatically be included in the evaluation of the resulting local diffusion factor. When an over-all diffusion factor such as equation (7) is used, variations in blade thickness are not reflected in the corresponding loss prediction. However, in view of the small observed effect and the scatter of the original θ/c against D correlation of figure 26, it is believed that a thickness correction is unwarranted for conventional thickness ranges. However, the analysis does indicate that, for high diffusion and high solidity levels, it may be advisable to maintain blade thickness as small as practicable in order to obtain the lowest loss at the reference condition.

Thus, the plots of figures 24, 26, and 27 show that, when diffusion factor and wake momentum-thickness ratio (or total-pressure-loss parameter) are used as the basic blade-loading and loss parameters, respectively, a generalized correlation of two-dimensional-cascade loss data is obtained. Although several assumptions and restrictions are involved in the use and calculation of these parameters, the basic diffusion approach constitutes a useful tool in cascade loss analysis. In particular, the diffusion analysis should be investigated over the complete range of incidence angle in an effort to determine generalized off-design loss information.

Effect of Reynolds number and turbulence. - The effect of blade-chord Reynolds number and turbulence level on the measured losses of cascade sections is discussed in the section on Data Selection and in references 3, 13, 17, and 41. In all cases, the data reveal an increasing trend of loss coefficient with decreasing Reynolds number and turbulence. Examples of the variation of the total-pressure-loss coefficient with incidence angle for conventional compressor blade sections at two different values of Reynolds number are illustrated in figure 28. Loss variations with Reynolds number over a range of incidence angles for a given blade shape are shown in figure 29. A composite plot of the variation of total-pressure-loss coefficient at minimum loss with blade-chord Reynolds number for a large number of blade shapes is shown in figure 30. Identification data for the various blades included in the figure are given in the references. For the blades whose loss data are reported in terms of drag coefficient, conversion to total-pressure-loss coefficient was accomplished according to the cascade relations presented in reference 25. The effect of change in tunnel turbulence level through the introduction of screens is indicated for some of the blades.

It is apparent from the curves in figure 30 that it is currently impossible to establish any one value of limiting Reynolds number that will hold for all blade shapes. (The term limiting Reynolds number refers to the value of Reynolds number at which a large rise in loss is obtained.) On the basis of the available cascade data presented in figure 30, however, it appears that serious trouble in the minimum-loss region may be encountered at Reynolds numbers below about 2.5×10^5. Carter in reference 11 places the limiting blade-chord Reynolds number based on outlet velocity at 1.5 to 2.0×10^5. Considering that outlet Reynolds number is less than inlet Reynolds number for decelerating cascades, this quoted value is in effective agreement with the value of limiting Reynolds number deduced herein.

The desirability of conducting cascade investigations in the essentially flat range of the curve of loss coefficient against Reynolds number in order to enhance the correlation of data from various tunnels, as well as from the various configurations of a given tunnel, is indicated. Cascade operation in the flat range of Reynolds number may also yield a more significant comparison between observed and theoretically computed loss.

Reynolds number and turbulence level should always be defined in cascade investigations. Furthermore, the development of some effective Reynolds number (ref. 3) which attempts to combine the effects of both blade-chord Reynolds number and turbulence should be considered for use as the independent variable.

Effect of inlet Mach number. - In the previous correlations, attention was centered on the various factors affecting the loss of cascade blades for essentially incompressible or low Mach number flow. Tests of cascade sections at higher Mach number levels have been relatively few, primarily because of the large power requirements and operational difficulties of high-velocity tunnels. As a consequence, it has not been possible to establish any empirical correlations that will permit the estimation of Mach number effects for conventional blade sections. The limited available data indicate, however, that a marked rise in loss is eventually obtained as Mach number is increased.

A typical example of the variation of total-pressure-loss coefficient with inlet Mach number for a conventional cascade section at fixed incidence angle in the region of minimum loss is presented in figure 31(a). The inlet Mach number at which the sharp rise in loss occurs is referred to as the limiting Mach number. The variation of the wake profile downstream of the blade as Mach number is increased is shown in figure 31(b) to illustrate the general deterioration of the suction-surface flow. The flow deterioration is the result of a separation of the suction-surface boundary layer induced by shock-wave and boundary-layer interactions.

In view of the complex nature of the shock-wave development and its interaction effects, the estimation of the variation of minimum total-pressure loss with inlet Mach number for a given blade is currently impossible. At the moment, this pursuit must be primarily an experimental one. Schlieren photographs showing the formation of shocks in a cascade are presented in references 42 to 44, and detailed discussions of shock formations and high-speed performance of two-dimensional-cascade sections are treated in references 42 and 44 to 47. Cascade experience (refs. 23 and 42) and theory (refs. 44, 47, and 48) indicate that a location of the point of maximum thickness at about the 50-percent-chord position and a thinning of the blade leading and trailing edges are favorable for good high Mach number performance. The avoidance of a throat area within the blade passage is also indicated in order to minimize the effects of flow choking. Discussions of the choking problem are presented in references 37 and 46, and blade throat areas are given for several blade shapes in references 15, 49, and 50. The effects of camber distribution on high Mach number performance are discussed extensively in the literature (refs. 15, 34, and 35). Results indicate that, for the range of blade shapes and Mach numbers normally covered, camber distribution does not have a large effect on maximum Mach number performance as obtained in the two-dimensional cascade.

Summary

From the foregoing correlations and considerations, the low-speed loss in total pressure of conventional two-dimensional-cascade sections can readily be estimated. If blade-surface velocity distributions are available, the suction-surface local diffusion factor D_l is determined according to equation (6) and a value of θ/c is then selected from figure 24. In the absence of blade-surface velocity data, the diffusion factor D is computed from over-all conditions by means of equation (7) and θ/c is selected from figure 26. With θ/c determined, the total-pressure-loss coefficient is computed according to equation (5) from the cascade geometry and a pertinent value of wake form factor H.

According to reference 24, for cascade measuring stations located more than about 1/2 chord length downstream of the blade trailing edge, the value of H will generally be less than about 1.2. For practical purposes, it was indicated that a constant value of H of about 1.1 can be used over a wide range of cascade configurations and incidence angles for measuring stations located between $\frac{1}{2}$ to $1\frac{1}{2}$ chord lengths behind the trailing edge. Loss coefficients based on inlet dynamic head can then be determined, if desired, from equation (8). The estimation of losses based on the diffusion factor D can, for example, produce a value of solidity that results in the least computed loss coefficient for a given velocity diagram.

The accuracy of the results obtained from the prediction procedure outlined is subject to the limitations and approximations involved in the diffusion analysis and wake momentum-thickness correlations. Strictly speaking, the procedure gives essentially a band of probable loss values at the cascade measuring station about $\frac{1}{2}$ to $1\frac{1}{2}$ chord lengths downstream of the blade trailing edge for the reference incidence-angle setting and Reynolds numbers of about 2.5×10^5 and greater at low speed (up to about 0.3 inlet Mach number). It should also be noted at this point that the loss values obtained in this manner represent the low-speed profile loss of the cascade section. Such loss values are not generally representative of the losses of the section in a compressor blade row or in a high-speed cascade.

A corresponding loss-estimation technique for high Mach number flow is currently unavailable because of the unknown magnitude of the compressibility effect on the wake momentum-thickness ratio of a given cascade geometry. Furthermore, both the wake form factor H and the relation between θ/c and $\bar{\omega}$ (given for incompressible flow by eq. (5)) vary with Mach number. For example, if the velocity variation in each leg of

the wake is assumed to vary according to the power relation

$$\frac{V}{V_0} = \left(\frac{y}{\delta}\right)^d \tag{9}$$

where δ is the thickness of the wake and d is some constant, then variations of H and θ and of the relation between θ/c and $\bar{\omega}$ with outlet free-stream Mach number can be established analytically to illustrate the nature of the compressibility effects.

Curves of the variation of the ratios of compressible to incompressible form factor H/H_{inc} and momentum thickness θ/θ_{inc} with outlet Mach number for various d values obtained from numerical integration of the wake parameters involved are shown in figures 32 and 33. Recently, the increasing trend of H with M_2 was substantiated experimentally at the NACA Lewis laboratory in an investigation of the wake characteristic of a turbine nozzle (unpublished data). Curves of the ratio of the integrated value of $\bar{\omega}$ obtained from a given value of θ/c in a compressible flow to the value of $\bar{\omega}$ computed from the same value of θ/c according to the incompressible relation of equation (5) are shown in figure 34. It should be noted that for compressible flow the denominator in the loss-coefficient definition (eq. (4)) is now given by $P - p$.

In summary, therefore, an accurate prediction of the variation of reference total-pressure loss with inlet Mach number for a given cascade blade is currently impossible. At the moment, this pursuit is primarily an experimental one. Families of curves of wake momentum thickness and form factor against diffusion factor are required (with appropriate definitions for subsonic or supersonic flow) as in figure 24 or 26 for a wide range of inlet Mach number. Analytically, a simple compressible relation is needed between θ/c and $\bar{\omega}$ as a function of Mach number.

DEVIATION-ANGLE ANALYSIS

Preliminary Analysis

The correct determination of the outlet flow direction of a cascade blade element presents a problem, because the air is not discharged at the angle of the blade mean line at the trailing edge, but at some angle δ° to it (fig. 2). Inasmuch as the flow deviation is an expression of the guidance capacity of the passage formed by adjacent blades, it is expected that the cascade geometry (camber, thickness, solidity, and chord angle) will be the principal influencing factor involved.

From cascade potential-flow theory (ref. 28, e.g.), it is found that the deviation angle increases with blade camber and chord angle and decreases with solidity. Weinig in reference 28 shows that the deviation angle varies linearly with camber for a given value of solidity and chord angle. Furthermore, with deviation angle equal to zero at zero camber angle in the theory, it is possible to express the deviation angle as a ratio of the camber angle. Values of the ratio of deviation angle to camber angle for an infinitely thin circular-arc blade of small camber deduced from the theory of reference 28 are presented in figure 35 for a range of solidities and chord angles. The values in figure 35 are for the incidence angle for "impact-free entry" previously mentioned, which corresponds essentially to the condition of minimum loss.

The results of figure 35 show that, for a blade of zero thickness, the minimum-loss deviation angle is zero at zero camber angle. Analysis indicates, however, that this is not the case for blades of conventional thicknesses. A recent theoretical demonstration of the existence of a positive value of zero-camber deviation angle according to potential-flow calculations is given by Schlichting in reference 18. The computed variation of zero-camber deviation angle for a conventional 10-percent-thick profile at zero incidence angle as obtained in the reference is shown in figure 36.

It will be recalled from the discussion of the zero-camber minimum-loss incidence angle that, for the conventional staggered cascade ($0^\circ < \gamma^\circ < 90^\circ$) with finite blade thickness set at zero incidence angle, a greater magnitude of velocity occurs on the blade lower (concave) surface than on the upper (convex) surface (fig. 12). Such velocity distributions result in a negative blade circulation and, consequently (as indicated by the solid vectors in fig. 37), in a positive deviation angle. Furthermore, since the deviation angle increases slightly with increasing incidence angle ($d\delta^\circ/di$ is positive in potential cascade flow), positive values of deviation angle will likewise be obtained at the condition of minimum-loss incidence angle (as illustrated by the dashed vectors in fig. 37). Since the zero-camber deviation angle arises from essentially a thickness blockage effect, the characteristics of the variation of minimum-loss zero-camber deviation angle with cascade geometry would be expected to roughly parallel the variation of the minimum-loss zero-camber incidence angle in figure 15. The low-speed reference deviation-angle correlations may, therefore, involve intercept values as in the case of the reference incidence-angle correlations.

In addition to the cascade-geometry factors mentioned, the low-speed deviation angles can also be affected by Reynolds number, turbulence, and Mach number. The thickened surface boundary layers resulting from low levels of Reynolds number and turbulence tend to increase the deviation angle. Variations in inlet Mach number can affect the deviation angle of a fixed two-dimensional-cascade geometry because of the associated changes

in blade circulation, boundary-layer development, and outlet to inlet axial-velocity ratio (compressibility effect on ρV_z).

Data Correlations

Form of correlation. - Examination of deviation-angle data at reference incidence angle reveals that the observed data can be satisfactorily represented by a linear variation of reference deviation angle with camber angle for fixed solidity and air inlet angle. The variation of reference deviation angle can then be expressed in equation form as

$$\delta^\circ = \delta_o^\circ + m\varphi \tag{10}$$

where δ_o° is the reference deviation angle for zero camber, m is the slope of the deviation-angle variation with camber $(\delta^\circ - \delta_o^\circ)/\varphi$, and φ is the camber angle. As in the case of the analogous terms in the reference incidence-angle relation (eq. (2)), δ_o° and m are functions of inlet-air angle and solidity.

The influence of solidity on the magnitude of the slope term m could also be directly included as a functional relation in equation (10), so that equation (10) could be expressed as

$$\frac{\delta^\circ - \delta_o^\circ}{\varphi} = \frac{m_{\sigma=1}}{\sigma^b} \tag{11}$$

where $m_{\sigma=1}$ represents the value of m (i.e., $(\delta^\circ - \delta_o^\circ)/\varphi$) at a solidity of 1, b is the solidity exponent (variable with air inlet angle), and the other terms are as before. It will be noted that equation (11) is similar in form to the frequently used deviation-angle rule for circular-arc blades originally established by Constant in reference 6 and later modified by Carter in reference 48. Carter's rule for the condition of nominal incidence angle is given by

$$\frac{\delta^\circ}{\varphi} = \frac{m_c}{\sqrt{\sigma}} \tag{12}$$

in which m_c is a function of blade-chord angle. Values of m_c determined from theoretical considerations for circular-arc and parabolic-arc mean lines (ref. 48) are shown in figure 38. In the ensuing correlations, both forms of the deviation-angle relation (eqs. (10) and (11)) are used, since each has a particular advantage. Equation (10), with m plotted as a function of β_1 and δ°, is easier to use for prediction, especially if the calculation of a required camber angle is involved. Equation (11) may be better for extrapolation and for comparison with Carter's rule.

As in the case for the zero-camber reference minimum-loss incidence angle, the zero-camber deviation angle can be represented as a function of blade thickness as

$$\delta_o^o = (K_s)_\delta (K_t)_\delta (\delta_o^o)_{10} \tag{13}$$

where $(\delta_o^o)_{10}$ represents the basic variation for the 10-percent-thick 65-series thickness distribution, $(K_s)_\delta$ represents any correction necessary for a blade shape with a thickness distribution different from that of the 65-series blade, and $(K_t)_\delta$ represents any correction necessary for maximum blade thicknesses other than 10 percent. (For a 10-percent-thick 65-series blade, $(K_t)_\delta$ and $(K_s)_\delta$ are equal to 1.) The problem, therefore, is reduced to finding the values of m, b, and δ_o^o (through eq. (13)) as functions of the pertinent variable involved for the various blade shapes considered.

NACA 65-(A_{10})-series blades. - From an examination of the plots of equivalent deviation angle against equivalent camber angle at reference minimum-loss incidence angle obtained from the cascade data, values of zero-camber deviation angle can be determined by extrapolation. The deduced plots of zero-camber deviation angle $(\delta_o^o)_{10}$ and slope term m as functions of solidity and air inlet angle are presented in figures 39 and 40 for these blades. The subscript 10 indicates that the i_o values are for 10-percent maximum-thickness ratio. Values of the intercept term δ_o^o and the slope term m were obtained by fitting a straight line to each data plot of reference equivalent deviation angle against equivalent camber angle for a fixed solidity and air inlet angle. The straight lines were selected so that both a satisfactory representation of the variation of the data points and a consistent variation for the resulting δ_o^o and m values were obtained. The extrapolation of the values of m to $\beta_1 = 0$ was guided by the data for the 65-$(12A_{10})$10 blade at solidities of 1 and 1.5 reported in the cascade guide-vane investigation of reference 51 (for an aspect ratio of 1, as in ref. 13).

For the deviation-angle rule as given by equation (11), deduced values of $m_{\sigma=1}$ and exponent b as functions of inlet-air angle are presented in figures 41 and 42. The deduced rule values (eq. (10) or (11)) and the observed data points are compared in figure 43 to indicate the effectiveness of the deduced representations. The flagged symbols in the high-camber range in the figure represent blade configurations for which boundary-layer separation is indicated (D greater than about 0.62). In view of the higher loss levels for this condition, an increase in the magnitude of the deviation angle is to be expected compared with the values extrapolated from the smaller cambers for which a lower loss level existed.

C-series circular-arc blades. - In view of the absence of systematic cascade data for the C-series circular-arc blade, an accurate determination of the rule constants cannot be made for this blade shape. However, a preliminary relation can be deduced on the basis of limited data. It appears that, for the uncambered C.4 section (refs. 14 and 32), if a value of $(K_s)_\delta$ equal to 1.1 (as for the determination of i_o) is used, a satisfactory comparison between predicted and observed δ_o^o values is obtained.

The characteristic number $m_{\sigma=1}$ in the deviation-angle design rule of equation (11) for a given blade mean line corresponds to the value of $(\delta^o - \delta_o^o)/\varphi$ at a solidity of unity. Cascade data for a C.4 circular-arc profile obtained from tunnels with good boundary-layer control are presented in references 17 and 33 for a solidity of 1.0 for $\beta_1 = 30^o$, 42.5^o, 45^o, and 60^o. Values of $(\delta^o - \delta_o^o)/\varphi$ were computed for these blades according to the δ_o^o variations of figure 39. A value of $m_{\sigma=1}$ for $\beta_1 = 0^o$ was obtained from the performance data of a free-stream circular-arc inlet guide vane presented in reference 52. These values of m are plotted in figure 44 against inlet-air angle, and the proposed variation of $m_{\sigma=1}$ for the circular-arc mean line is shown by the solid line.

In the absence of data covering a range of solidities, it was assumed that the solidity exponent b in the deviation-angle rule of equation (11) is independent of the profile shape and will therefore also be applicable for the circular-arc mean line. This assumption agrees with limited experimental data. The variation of ratio of deviation angle to camber angle obtained from constant-thickness circular-arc guide-vane sections of reference 53 ($\delta_o^o = 0^o$ for guide vanes) over a wide range of solidities is shown in figure 45. A computed variation based on values of b and $m_{\sigma=1}$ obtained from figures 42 and 44, respectively, is shown in the figure by the solid line. A satisfactory agreement with these circular-arc data is thus demonstrated for the value of b obtained from the 65-series data. On the basis of these results, deduced curves of m against β_1 for a range of solidities (for use in conjunction with eq. (10)) were computed for the C-series circular-arc blade as indicated in figure 46.

Double-circular-arc blades. - Although limited data are available for the double-circular-arc blade (refs. 23 and 30), it was felt that these data could not be reliably utilized in the construction of a deviation-angle rule because of the questionable two-dimensionality of the respective test tunnels. However, since the C-series and the double-circular-arc blades differ only in thickness distribution, it is reasonable to expect that, as in the case of the reference incidence-angle correlations, only the zero-camber deviation angles will be materially affected.

Therefore, the slope-term value m deduced for the C-series circular-arc blade (fig. 46) might also be used for the double-circular-arc blade, but the δ_0° values may be different. An arbitrarily selected value of 0.7 for $(K_s)_\delta$ in equation (13) (as for the reference-incidence-angle determination) is suggested for the double-circular-arc blade.

Comparison of rules. - In view of the widespread use of Carter's rule (eq. (12)) with fig. 38) for predicting the deviation angle of circular-arc-mean-line blades, some results obtained from the use of Carter's rule were compared with the deduced rule of equation (11) with figures 39, 42, and 44. The principal difference between the two rules occurs in the blade orientation parameter used for the m variation and in the δ_0° and b variations. The value of the solidity exponent of 1/2 in equation (12) was originally obtained from limited data. Carter, in a later work, (ref. 11) proposes a variable solidity exponent and indicates values close to 1 for accelerating cascades and close to 1/2 for decelerating cascades. The variation of b obtained from the NACA 65-(A_{10})-series blades as equivalent circular arcs in figure 42 essentially confirms this trend. Actually, the deviation-angle rule in the form of equation (11) constitutes a modification of Carter's rule.

In addition to the basic differences between the rules in the magnitudes of the m, b, and δ_0° values, it is noted that Carter's rule was originally developed for the condition of nominal incidence angle, whereas the modified rule pertains to the reference minimum-loss incidence angle. However, since Carter's rule has frequently been used over a wide range of reference angle in its application, both rules were evaluated, for simplicity, for the reference minimum-loss incidence angle.

An illustrative comparison of predicted reference deviation angle as obtained from Carter's rule and the modified rule for a 10-percent-thick, thick-nosed circular-arc blade is shown by the calculated results in figure 47 for ranges of camber angle, solidity, and inlet-air angle. Deviation angles in figure 47 were restricted to cascade configurations producing values of diffusion factor less than 0.6. Blade-chord angle for Carter's rule was computed from the equation

$$\gamma^\circ = \beta_1 - i - \frac{\varphi}{2} \tag{14}$$

Reference incidence angle was determined from equations (2) and (3) and figures 15 and 16.

The plots of figure 47 show that, in practically all cases, the deviation angles given by the modified rule are somewhat greater in magnitude than those predicted by Carter's rule for the 10-percent-thick

[redacted]

blade. This is particularly true for the high inlet-air angles. Thus, greater camber angles are required for a given turning angle according to the modified rule. Differences are even less for the double-circular-arc blade, as indicated in figure 48, since the δ_0^o values are smaller for these blades. However, it should be kept in mind that the magnitude of the factors in the modified rule are proposed values based on limited data. Further research is required to establish the modified rule on a firmer foundation.

Effect of maximum blade thickness. - Available data on the variation of reference deviation angle with blade maximum-thickness ratio obtained from cascade investigations of the 65-$(12A_{10})$ blade of reference 36 are shown in figure 49. The solid symbols representing the values of deviation angle at zero thickness were determined by subtracting the values of $(\delta_0^o)_{10}$ obtained from figure 39 from the measured value of deviation angle at 10-percent maximum thickness obtained from the data in figure 49. A very reasonable variation with thickness ratio, as indicated by the faired curves, is thus obtained for all three configurations. The increasing slope of the deviation-angle variation with increasing thickness ratio is believed due to some extent to the accompanying increase in wake losses.

Preliminary values of a correction factor for maximum-thickness ratio $(K_t)_\delta$ deduced from the data of figure 49 are shown in figure 50. In the absence of further data, it is proposed that this correction curve is also applicable to other conventional blade shapes.

Effect of Reynolds number. - In view of the large rise in loss as blade-chord Reynolds number is reduced (fig. 30), a corresponding rise in deviation angle (or decrease in turning angle) is to be expected. Experimental confirmation of the marked effect of Reynolds number on blade deviation angle at fixed incidence angle is illustrated in figure 51 for several compressor blade shapes. The variation of deviation angle with Reynolds number over a range of incidence angle is demonstrated in figure 52. In all cases the variation of the deviation or turning angle closely parallels the variation of the loss. Therefore, factors involved in the deviation-angle variation are the same as those for the loss behavior. Correspondingly, no Reynolds number correction factors that will be applicable for all blade configurations have been established. The deduced deviation-angle rule developed herein is applicable at a Reynolds number of about 2.5×10^5 and greater.

Effect of inlet Mach number. - Experimental variations of minimum-loss deviation angle with inlet Mach number are presented in figure 53 for two circular-arc blades. Further cascade data in terms of air-turning angle at fixed angle of attack are shown in figure 54 for two other

compressor blade shapes. (Inasmuch as the data in fig. 54 were obtained at constant angle of attack, the variation of turning angle is an inverse reflection of the variation of deviation angle.) The data of figures 53 and 54 indicate that deviation angle varies with inlet Mach number up to the limiting value. As indicated in the Preliminary Analysis section (p. 27), the resultant Mach number effect for a given blade configuration will depend on the relative magnitude of the various factors involved. Apparently, the net effect is small up to the limiting value of inlet Mach number. Large increases in deviation angle can be expected, however, when the loss rises rapidly at the limiting Mach number because of the adverse effects of the shock formation. (The rise in deviation angle in the data is always associated with the sharp rise in loss.)

Variation with incidence angle. - Thus far, of necessity, the analysis has been conducted for flow conditions at only one reference position on the general curve of loss against incidence angle. Ultimately, of course, it is desired to predict flow variations over the entire range of incidence angle. The variation of deviation angle with incidence angle for a fixed geometry in the two-dimensional cascade is primarily a function of the change in the guidance capacity of the cascade arising from the change in orientation of the approaching flow (a potential-flow effect) and of the variation in the wake loss. Since no information is currently available on the effect of losses, attention is centered on deviation-angle variations in the region of low loss, where the trend of variation approaches that of the potential flow.

Examination of potential-flow theory (Weinig, ref. 28, e.g.) shows that a positive slope of deviation angle against incidence angle exists (i.e., deviation angle increases with incidence angle). Calculations based on the theory of Weinig reveal that the magnitude of the slope varies with solidity and blade-chord angle. The deviation-angle slope approaches zero for infinite solidity (deviation angle is essentially constant at high solidity) and increases as solidity is reduced. At constant solidity, the slope of deviation angle against incidence angle increases as the chord angle is increased. These trends indicate physically that the greater the initial guidance effect (high solidity and low blade angle), the less sensitive the deviation angle is to changes in incidence angle.

For analysis purposes, since the region of low loss is generally small, the variation of deviation angle with incidence angle for a given cascade geometry in the region of minimum loss can be represented as

$$\delta^{\circ} = \delta^{\circ}_{ref} + (i - i_{ref})\left(\frac{d\delta^{\circ}}{di}\right)_{ref} \qquad (15)$$

where $(d\delta^{\circ}/di)_{ref}$ represents the slope of the deviation-angle variation

at the reference incidence angle. An empirical determination of the magnitude of the slope of the variation of deviation angle with incidence angle was obtained from an analysis of the low-speed experimental data for the 65-(A_{10})10 blades of reference 13. From the plot of deviation angle against incidence angle for each configuration (as in fig. 5, e.g.), the slope of the curve at the minimum-loss incidence angle was evaluated graphically. The deduced variation of reference slope magnitude $d\delta^o/di$ obtained from fairings of these values is presented in figure 55 as a function of solidity and inlet-air angle. Qualitative agreement with theory is strongly indicated by the data. Inasmuch as the phenomenon is essentially a guidance or channel effect, it is anticipated that the slope values of figure 55 will also be applicable for other conventional blade shapes. Thus, it is possible to predict the deviation angle at incidence angles other than the reference location within the low-loss range of operation from the use of equation (15) and figure 55.

Summary

The analysis of blade-section deviation angle shows that the variation of reference deviation angle with cascade geometry at low speed can be satisfactorily established in terms of an intercept value δ_o^o and a slope value m as given by equation (10). The experimental data could also be expressed in terms of a rule similar in form to Carter's rule, as indicated by equation (11). Deduced values of δ_o^o and m were obtained as a function of β_1 and σ from the data for the 10-percent-thick 65-(A_{10})-series blades of reference 13 as equivalent circular arc (figs. 39 and 40). Rules for predicting the reference deviation angle of the C-series and double-circular-arc blades were also deduced based on the correlations for the 65-(A_{10})-series blades and on limited data for the circular-arc blade (figs. 39 and 46).

The procedure involved in estimating the low-speed reference deviation angle of a blade section is as follows: From known values of β_1 and σ, $(\delta_o^o)_{10}$ is selected from figure 39, and m is selected from figure 40 for the 65-(A_{10})-series blades or from figure 46 for circular-arc-mean-line blades. The value of $(K_t)_\delta$ for the blade maximum-thickness ratio is obtained from figure 50, and the approximate value of $(K_s)_\delta$ is selected for the type of thickness distribution. For the 65-series blades, $(K_s)_\delta = 1.0$, and it is proposed that $(K_s)_\delta$ be taken as 1.1 for the C-series blades and as 0.7 for the double-circular-arc blade. The value of δ_o^o is then computed from equation (13), and finally δ^o is determined from the blade camber angle according to equation (10). As in the case of reference i_o values, the use of the proposed values of $(K_s)_\delta$ is not

[redacted]

critical for good accuracy in the final determination of δ^o. Reference deviation angle can also be computed according to the rule in the form of equation (11) in conjunction with figures 41, 42, and 44.

The camber angle required to produce a given turning angle at the reference condition at low speed can readily be calculated by means of the preceding incidence-angle and deviation-angle correlations when the inlet-air angle and blade solidity are known. From equations (1), (2), and (10), the camber angle as a function of the turning, deviation, and incidence angle is

$$\varphi = \frac{\Delta\beta - (i_o - \delta_o^o)}{1 - m + n} \tag{16}$$

or, in terms of the thickness corrections (eqs. (3) and (13)),

$$\varphi = \frac{\Delta\beta - \left[(K_s)_i(K_t)_i(i_o)_{10} - (K_s)_\delta(K_t)_\delta(\delta_o^o)_{10}\right]}{1 - m + n} \tag{17}$$

For simplicity, since $(K_s)_i = (K_s)_\delta = K_s$, equation (17) can be expressed in the form

$$\varphi = \frac{\Delta\beta - K_s\bar{K}_t\left[(i_o)_{10} - (\delta_o^o)_{10}\right]}{1 - m + n} \tag{18}$$

where $\bar{K}_t$ represents some correction factor for blade thickness, such that

$$\bar{K}_t\left[(i_o)_{10} - (\delta_o^o)_{10}\right] \cong (K_t)_i(i_o)_{10} - (K_t)_\delta(\delta_o^o)_{10} \tag{19}$$

Curves of the values of $(i_o)_{10} - (\delta_o^o)_{10}$ as a function of β_1 and σ are given in figure 56; curves of the values of $1 - m + n$ as a function of β_1 and σ are given in figure 57(a) for the 65-(A_{10})-series mean line and in figure 57(b) for the circular-arc mean line; and values of $\bar{K}_t$ are plotted as a function of β_1 and t/c in figure 58. The use of the chart values of $\bar{K}_t$ in equation (18) gives results within about 0.1^o of the exact values given by equation (17). Required camber angle can thus be determined readily by equation (18) in conjunction with figures 56 to 58.

CONCLUDING REMARKS

The foregoing analysis has presented a correlation of available two-dimensional experimental cascade data in terms of parameters significant

in compressor design. The work essentially presents a summary of the state of experimental cascade research with regard to cascade performance at the reference incidence angle. Rules and procedures were evolved for the prediction of the magnitude of the reference total-pressure loss and the reference incidence and deviation angles in satisfactory agreement with existing cascade data. The rules may also be of help in reducing the necessary experimental effort in the accumulation of further cascade data.

However, the present analysis is incomplete. Many areas, such as the deviation-angle rule for the double-circular-arc blade, require further data to substantiate the correlations. Furthermore, additional information concerning the influence of high Mach number and off-design incidence angles of cascade performance is needed.

Finally, it is recognized that the performance of a given blade geometry in the compressor configuration will differ from the performance established in the two-dimensional cascade. These differences result from the effects of the various three-dimensional phenomena that occur in compressor blade rows. It is believed, however, that a firm foundation in two-dimensional-cascade flow constitutes an important step toward the complete understanding of the compressor flow. The extent to which cascade-flow performance can be successfully utilized in compressor design can only be established from further comparative evaluations. Such comparisons between observed compressor performance and predicted two-dimensional-cascade performance on the basis of the rules derived herein are presented in part VII of this series (ref. 54).

Lewis Flight Propulsion Laboratory
National Advisory Committee for Aeronautics
Cleveland, Ohio, November 7, 1955

REFERENCES

1. Bullock, Robert O., Johnsen, Irving A., and Lieblein, Seymour: Aerodynamic Design of Axial-Flow Compressors. III - Compressor Design System. NACA RM

2. Roudebush, William H.: Aerodynamic Design of Axial-Flow Compressors. IV - Potential Flow in Two-Dimensional Cascades. NACA RM E54H26.

3. Roudebush, William H., and Lieblein, Seymour: Aerodynamic Design of Axial-Flow Compressors. V - Viscous Flow in Two-Dimensional Cascades. NACA RM E55J06.

4. Kantrowitz, Arthur, and Daum, Fred L.: Preliminary Experimental Investigation of Airfoils in Cascade. NACA WR L-231, 1942. (Supersedes NACA CB.)

5. Bogdonoff, Seymour M., and Bogdonoff, Harriet E.: Blade Design Data for Axial-Flow Fans and Compressors. NACA WR L-635, 1945. (Supersedes NACA ACR L5F07a.)

6. Constant, H.: Performance of Cascades of Aerofoils. Note No. E.3696, British R.A.E., 1939.

7. Davis, Hunt: A Method of Correlating Axial-Flow-Compressor Cascade Data. A.S.M.E. Trans., vol. 70, no. 8, Nov. 1948, pp. 951-955.

8. Howell, A. R.: The Present Basis of Axial Flow Compressor Design. Pt. I - Cascade Theory and Performance. R. & M. No. 2095, British A.R.C., June 1942.

9. Howell, A. R., and Carter, A. D. S.: Fluid Flow Through Cascades of Aerofoils. Rep. No. R.6, British N.G.T.E., Sept. 1946.

10. Carter, A. D. S., and Hounsell, A. F.: General Performance Data for Aerofoils Having C.1, C.2, or C.4 Base Profiles on Circular Arc Camber Lines. Memo. No. M.62, British N.G.T.E., Sept. 1949.

11. Carter, A. D. S.: The Low Speed Performance of Related Aerofoils in Cascade. Rep. No. R.55, British A.R.C., Sept. 1949. (See also C.P. No. 29, British M.O.S., Sept. 1949.)

12. Erwin, John R., and Emery, James C.: Effect of Tunnel Configuration and Testing Technique on Cascade Performance. NACA Rep. 1016, 1951. (Supersedes NACA TN 2028.)

13. Herrig, L. Joseph, Emery, James C., and Erwin, John R.: Systematic Two-Dimensional Cascade Tests of NACA 65-Series Compressor Blades at Low Speeds. NACA RM L51G31, 1951.

14. Fletcher, P. J.: Low Speed Tests on Compressor Cascades of Parabolic Cambered Airfoils. Pt. II. Pitch/Chord Ratio = 0.75. Memo. No. M.159, British N.G.T.E., Nov. 1952.

15. Erwin, John R., Savage, Melvyn, and Emery, James C.: Two-Dimensional Low-Speed Cascade Investigation of NACA Compressor Blade Sections Having a Systematic Variation in Mean-Line Loading. NACA RM L53I30b, 1953.

16. Felix, A. Richard: Summary of 65-Series Compressor-Blade Low-Speed Cascade Data by the Use of the Carpet-Plotting Technique. NACA RM L54H18a, 1954.

[redacted]

17. Blight, F. G., and Howard, W.: Tests of Four Aerofoil Cascades. Pt. I - Deflection, Drag and Velocity Distribution. Aero. Res. Lab. Rep. E.74, Dept. Supply, Commonwealth of Australia, July, 1952.

18. Schlichting, Herman: Problems and Results of Investigations on Cascade Flow. Jour. Aero. Sci., vol. 21, no. 3, Mar. 1954, pp. 163-178.

19. Katzoff, S., and Hannah, Margery E.: Further Comparisons of Theoretical and Experimental Lift and Pressure Distributions on Airfoils in Cascade at Low-Subsonic Speed. NACA TN 2391, 1951.

20. Carter, A. D. S., Andrews, S. J., and Shaw, H.: Some Fluid Dynamic Research Techniques. Proc. Inst. Mech. Eng. (London), vol. 163, 1950, pp. 249-263.

21. Blight, F. G., Howard, W., and McCallum, H.: The Design and Performance of a Low Speed Cascade Tunnel. Eng. Note 133, Aero. Lab., Fishermen's Bend, Melbourne (Australia), June 1949.

22. Briggs, William B.: Effect of Mach Number on the Flow and Application of Compressibility Corrections in a Two-Dimensional Subsonic-Transonic Compressor Cascade Having Varied Porous-Wall Suction at the Blade Tips. NACA TN 2649, 1952.

23. Andrews, S. J.: Tests Related to the Effect of Profile Shape and Camber Line on Compressor Cascade Performance. Rep. No. R.60, British N.G.T.E., Oct. 1949.

24. Lieblein, Seymour, and Roudebush, William H.: Theoretical Loss Relations for Low-Speed Two-Dimensional-Cascade Flow. NACA TN

25. Lieblein, Seymour, Schwenk, Francis C., and Broderick, Robert L.: Diffusion Factor for Estimating Losses and Limiting Blade Loadings in Axial-Flow-Compressor Blade Elements. NACA RM E53D01, 1953.

26. Korbacher, G. K.: A Test on a Compressor Cascade of Aerofoils Having Their Position of Maximum Thickness 40% of the Chord from the Leading Edge and a Pitch/Chord Ratio of 0.75. Memo. No. M.89, British N.G.T.E., June 1950.

27. Jeffs, R. A., Hounsell, A. F., and Adams, R. G.: Further Performance Data for Aerofoils Having C.1, C.2, or C.4 Base Profiles on Circular Arc Camber Lines. Memo. No. M.139, British N.G.T.E., Dec. 1951.

28. Weinig, Fritz: The Flow Around the Blades of Turbomachines. Johann Ambrosius Barth (Leipzig), 1935.

29. Stanitz, John D.: Effect of Blade-Thickness Taper on Axial-Velocity Distribution at the Leading Edge of an Entrance Rotor-Blade Row with Axial Inlet, and the Influence of This Distribution on Alinement of the Rotor Blade for Zero Angle of Attack. NACA TN 2986, 1953.

30. Howell, A. R.: A Note on Compressor Base Aerofoils C.1, C.2, C.3, C.4, C.5, and Aerofoils Made up of Circular Arcs. Memo. No. M.1011, Power Jets (Res. and Dev.), Ltd., Sept. 1944.

31. Hughes, Hazel P.: Base Profiles C.7. Memo. M.1210, British N.G.T.E., May 1946.

32. Fletcher, P. J.: Low Speed Tests on Compressor Cascades of Parabolic Cambered Aerofoils. Pt. I - Pitch/Chord Ratio = 1.0. Memo. No. M.81, British N.G.T.E., Mar. 1950.

33. Felix, A. Richard, and Emery, James C.: A Comparison of Typical National Gas Turbine Establishment and NACA Axial-Flow Compressor Blade Sections in Cascade at Low Speed. NACA RM L53B26a, 1953.

34. Andrews, S. J., Andrews, Patricia M., and Baines, Margaret: A Comparison Between Two Compressor Cascades Using C.4 Profile on Parabolic and Circular Arc Camber Lines. Memo. No. M.6, British N.G.T.E., Sept. 1946.

35. Carter, A. D. S.: Some Tests on Compressor Cascades of Related Aerofoils Having Different Positions of Maximum Camber. Rep. No. R.47, British N.G.T.E., Dec. 1948.

36. Herrig, L. Joseph, Emery, James C., and Erwin, John R.: Effect of Section Thickness and Trailing-Edge Radius on the Performance of NACA 65-Series Compressor Blades in Cascades at Low Speeds. NACA RM L51J16, 1951.

37. Bailey, W., and Jefferson, J. L.: Compressibility Effects on Cascades of Low Cambered Compressor Blades. Rep. No. E.3972, British R.A.E., May 1943.

38. Reeman, J., and Simonis, E. A.: The Effect of Trailing Edge Thickness on Blade Loss. Tech. Note No. 116, British R.A.E., Mar. 1943.

39. Stewart, Warner L.: Investigation of Compressible Flow Mixing Losses Obtained Downstream of a Blade Row. NACA RM E54I20, 1954.

40. Savage, Melvyn: Analysis of Aerodynamic Blade-Loading-Limit Parameters for NACA 65-$(C_{l_0}A_{10})$10 Compressor-Blade Sections at Low Speeds. NACA RM L5402a, 1955.

[redacted]

41. Lawson, T. V.: An Investigation into the Effect of Reynolds Number on a Cascade of Blades with Parabolic Arc Camber Lines. Memo. No. M.195, British N.G.T.E., Nov. 1953.

42. Todd, K. W.: An Experimental Study of Three-Dimensional High-Speed Air Conditions in a Cascade of Axial-Flow Compressor Blades. R. & M. No. 2792, British A.R.C., Oct. 1949.

43. Bogdonoff, Seymour M.: N.A.C.A. Cascade Data for the Blade Design of High-Performance Axial-Flow Compressors. Jour. Aero. Sci., vol. 15, no. 2, Feb. 1948, pp. 89-95.

44. Klapproth, John F.: General Considerations of Mach Number Effects on Compressor-Blade Design. NACA RM E53L23a, 1954.

45. Savage, Melvyn, Felix, A. Richard, and Emery, James C.: High-Speed Cascade Tests for Typical High-Flow Transonic Rotor Hub Conditions. NACA RM L55F07, 1955.

46. Carter, A. D. S., and Hughes, Hazel P.: A Note on the High Speed Performance of Compressor Cascades. Memo. No. M.42, British N.G.T.E., Dec. 1948.

47. Staniforth, R.: A Note on Compressor Operation at Transonic Relative Inlet Mach Numbers. Memo. M.224, British N.G.T.E., July 1954.

48. Carter, A. D. S., and Hughes, Hazel P.: A Theoretical Investigation into the Effect of Profile Shape on the Performance of Aerofoils in Cascade. R. & M. No. 2384, British A.R.C., 1946.

49. Carter, A. D. S.: Throat Areas of Compressor Blade Cascades Derived for the Base Aerofoil C.4. Memo. No. M.1025, Power Jets, Ltd., Oct. 1944.

50. Hughes, Hazel P.: Throat Areas for the Parabolic Arc Cambered Aerofoil C.4 in Cascade. Memo. No. M.157, British N.G.T.E., Aug. 1952.

51. Dunavant, James C.: Cascade Investigation of a Related Series of 6-Percent-Thick Guide-Vane Profiles and Design Charts. NACA RM L54I02, 1954.

52. Alsworth, Charles C., and Iura, Toru: Theoretical and Experimental Investigations of Axial Flow Compressors. Pt. 3 - Progress Report on Loss Measurements in Vortex Blading. Mech. Eng. Lab., C.I.T., July 1951. (Navy Contract N6-ORI-102, Task Order IV.)

53. Mankuta, Harry, and Guentert, Donald C.: Some Effects of Solidity on Turning Through Constant-Thickness Circular-Arc Guide Vanes in Axial Annular Flow. NACA RM E51E07, 1951.

54. Robbins, William H., Jackson, Robert J., and Lieblein, Seymour: Aerodynamic Design of Axial-Flow Compressors. VII - Blade-Element Flow in Annular Cascades. NACA RM E55G02.

55. Korbacher, G. K.: A Test on a Compressor Cascade of Aerofoils Having Their Position of Maximum Thickness 40% of the Chord and a Position of Maximum Camber of 45% of the Chord from the Leading Edge. Memo. No. M.80, British N.G.T.E., Mar. 1950.

56. Wilson, Robert E.: Turbulent Boundary-Layer Characteristics at Supersonic Speeds - Theory and Experiment. Jour. Aero. Sci., vol. 17, no. 9, Sept. 1950, pp. 585-594.

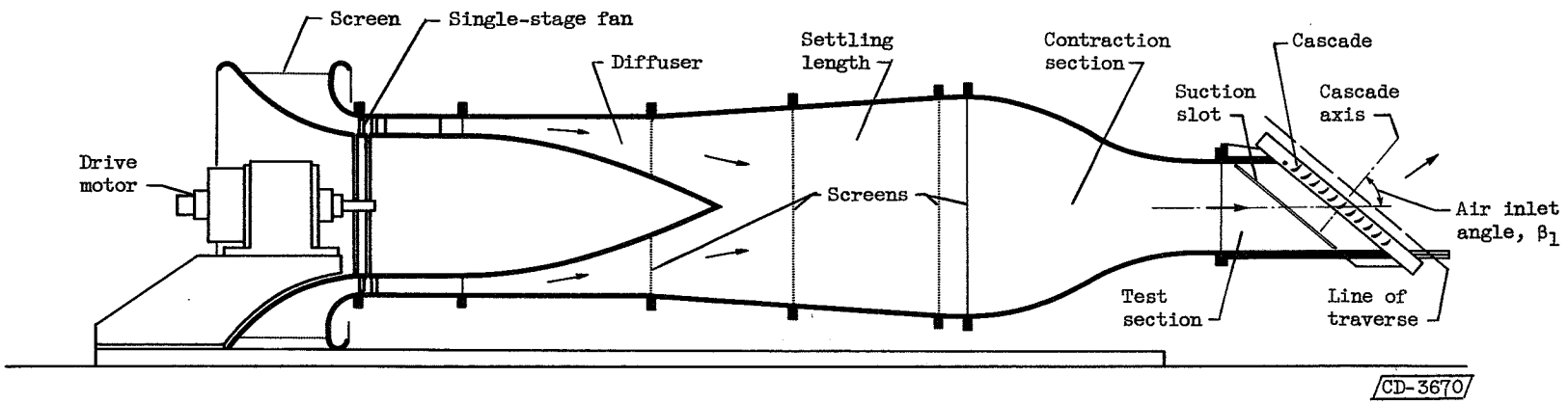

Figure 1. - Layout of conventional low-speed cascade tunnel (ref. 20).

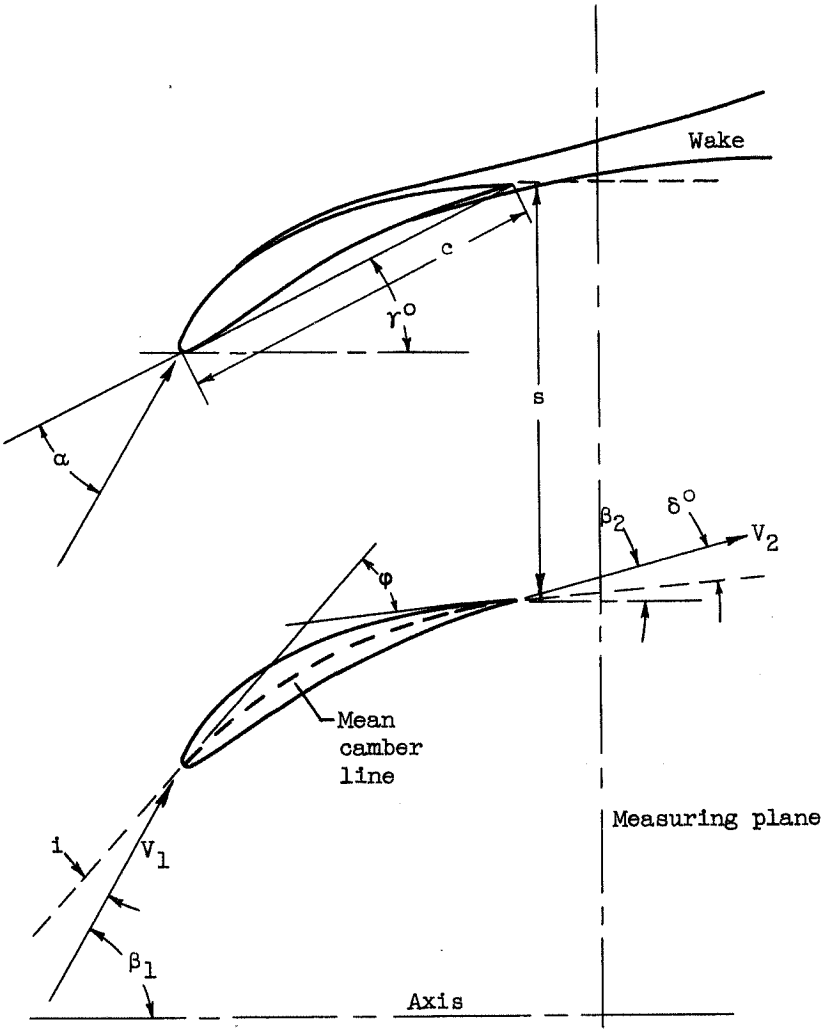

c	blade chord
i	incidence angle, angle between tangent to mean camber line at leading edge and inlet-air velocity
s	blade spacing
V_1	inlet-air velocity
V_2	outlet-air velocity
α	angle of attack, angle between chord and inlet-air velocity
β_1	inlet-air angle, angle between inlet-air velocity and axis
β_2	outlet-air angle, angle between outlet-air velocity and axis
$\Delta\beta$	air-turning angle, $\beta_1 - \beta_2$
γ^o	blade-chord angle, angle between chord and axis
δ^o	deviation angle, angle between tangent to mean camber line at trailing edge and outlet-air velocity
σ	solidity, ratio of chord to spacing, c/s
φ	blade camber angle, difference between angles of tangents to mean camber lines at leading and trailing edges

Figure 2. - Nomenclature for cascade blade.

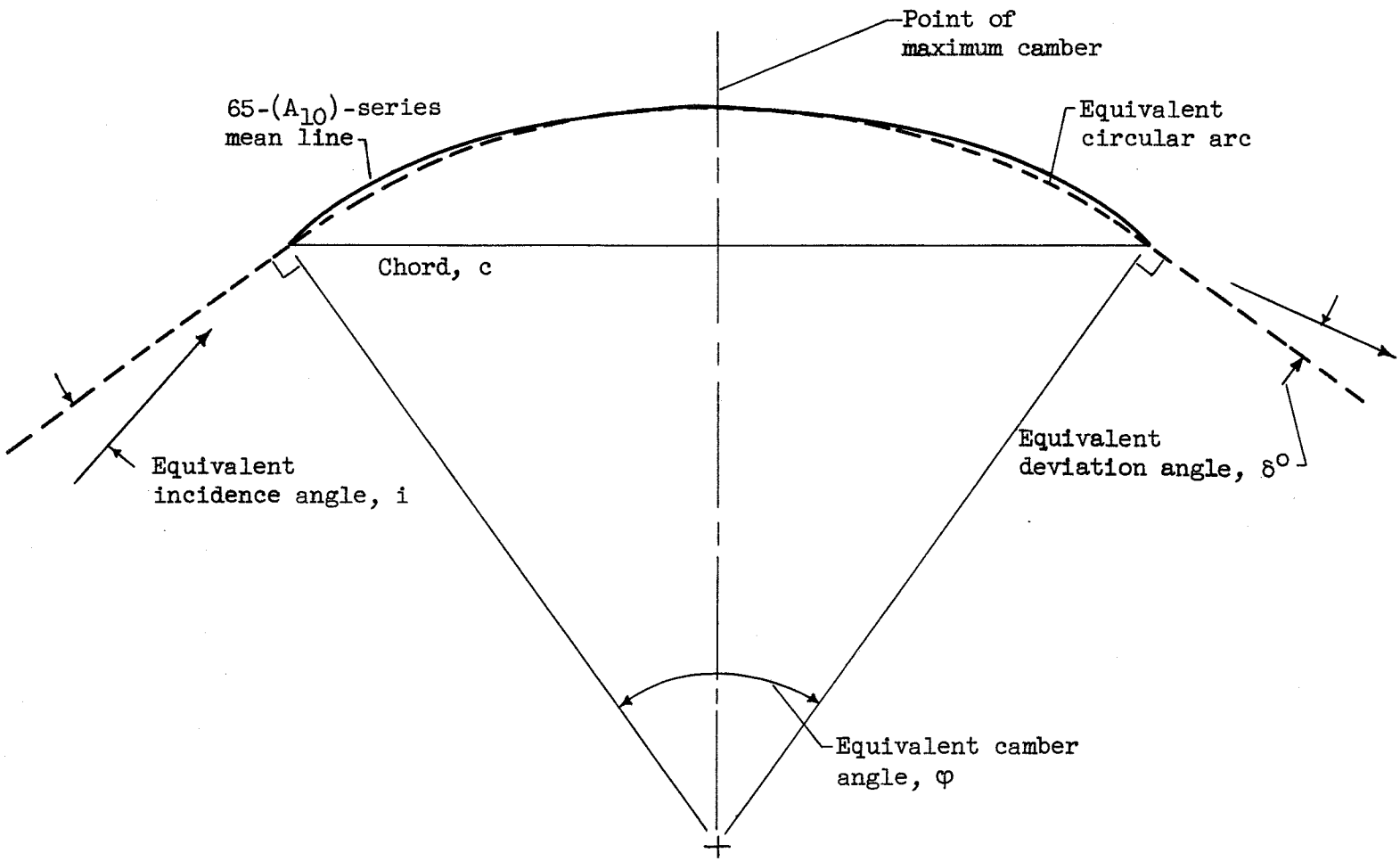

Figure 3. - Equivalent circular-arc mean line for NACA 65-(A_{10})-series blades.

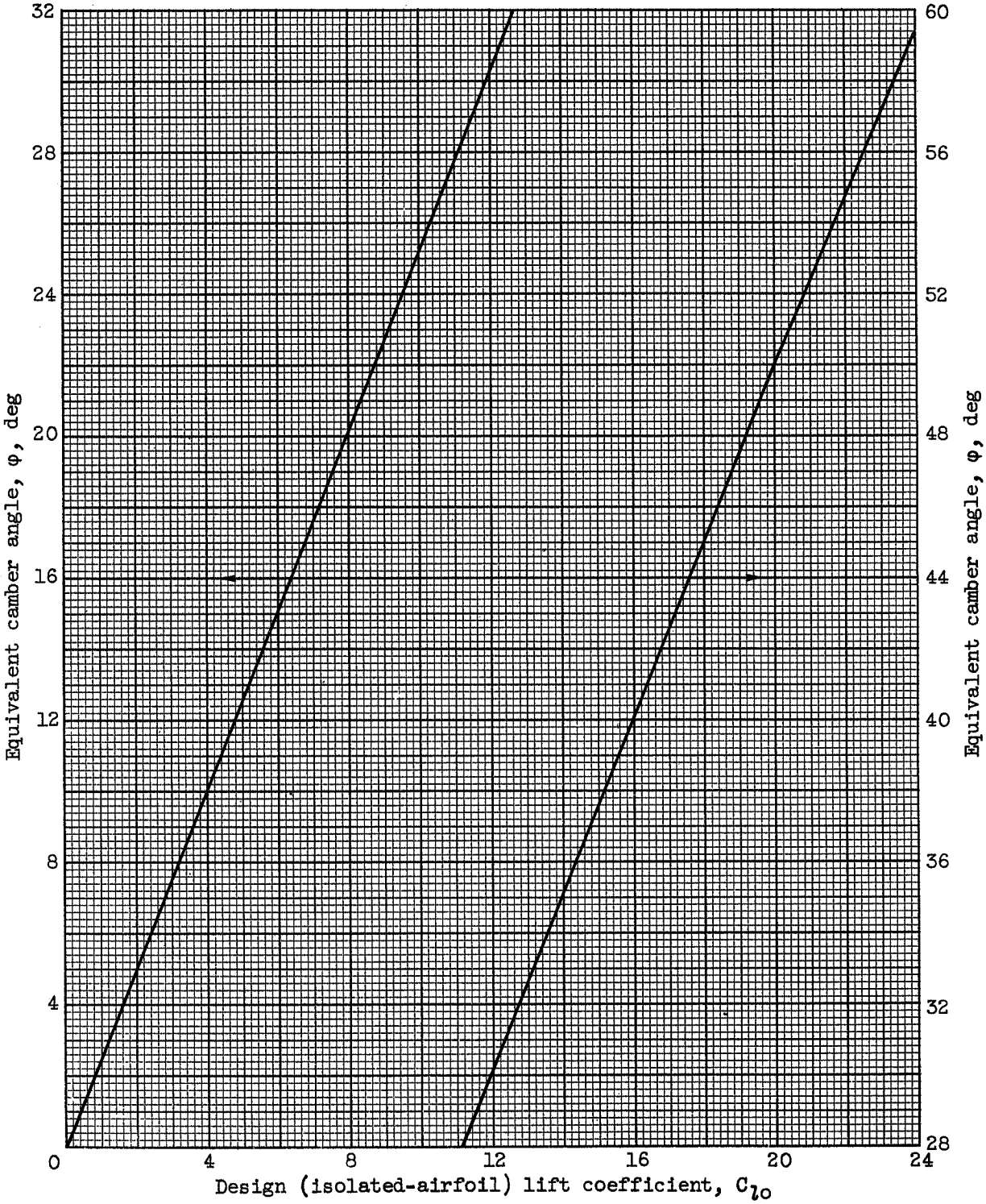

Figure 4. - Equivalent camber angles for NACA 65-($C_{l_o}A_{10}$) mean camber line as equivalent circular arc (fig. 3).

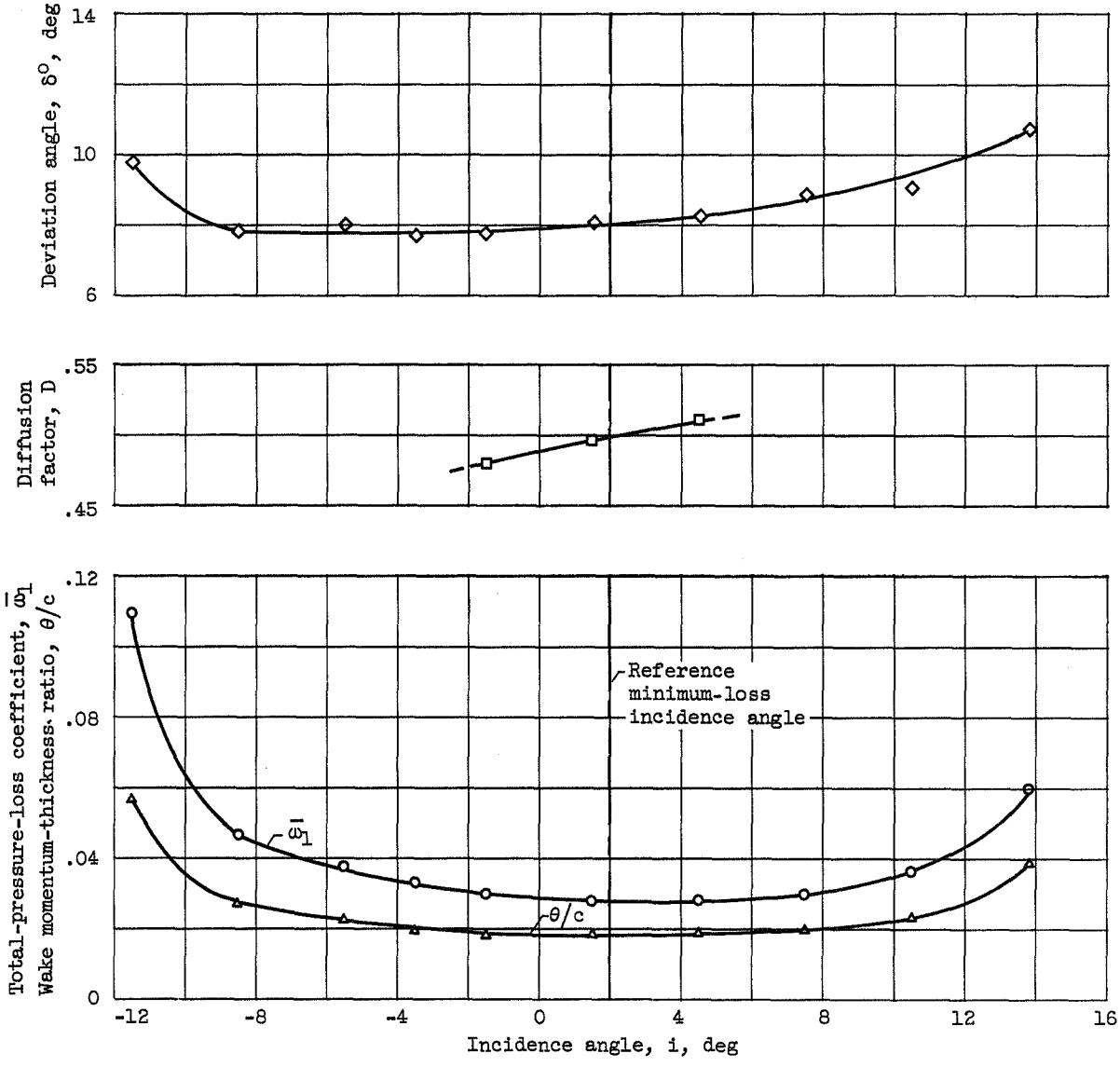

Figure 5. - Illustration of basic performance parameters for cascade analysis. Data obtained from conventional blade geometry in low-speed two-dimensional tunnel.

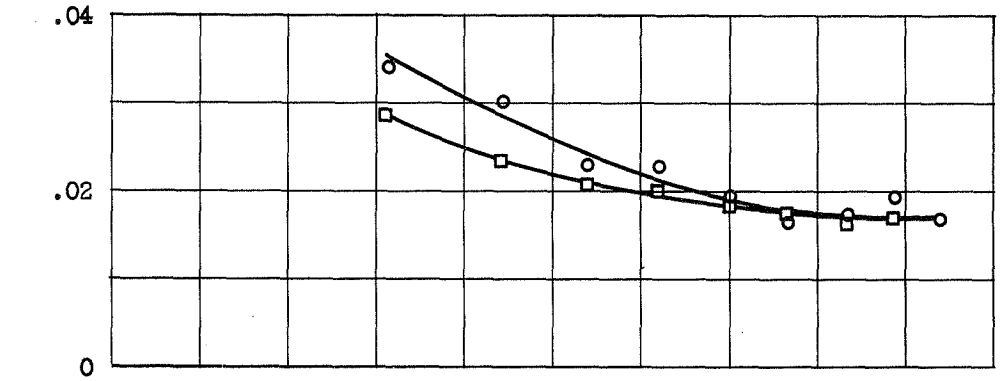

(a) NACA 65-(12)10 blade. Inlet-air angle, 45°; solidity, 1.5 (ref. 13).

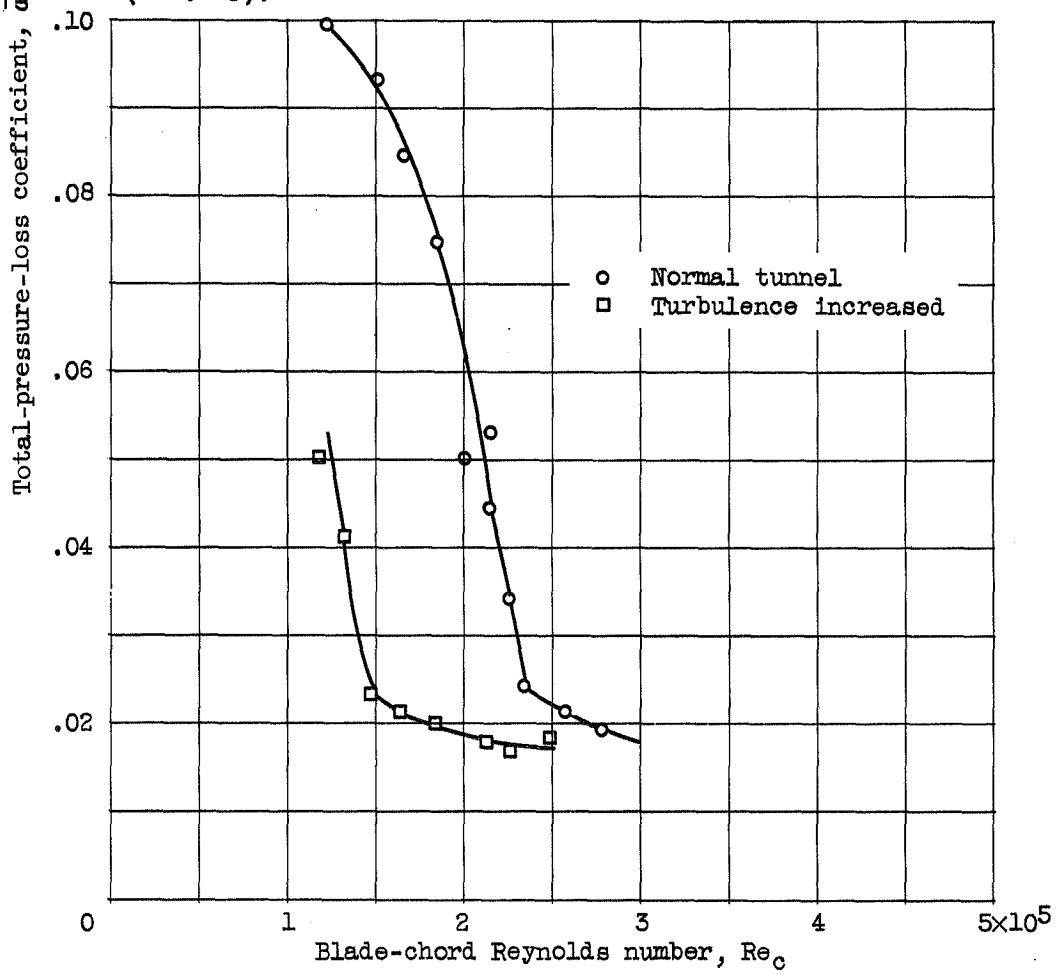

(b) Lighthill blade, 50 percent laminar flow. Inlet-air angle, 45.5°; solidity, 1.0 (ref. 17).

Figure 6. - Effect of blade-chord Reynolds number and free-stream turbulence on minimum-loss coefficient of cascade blade section in two-dimensional tunnel.

[redacted]

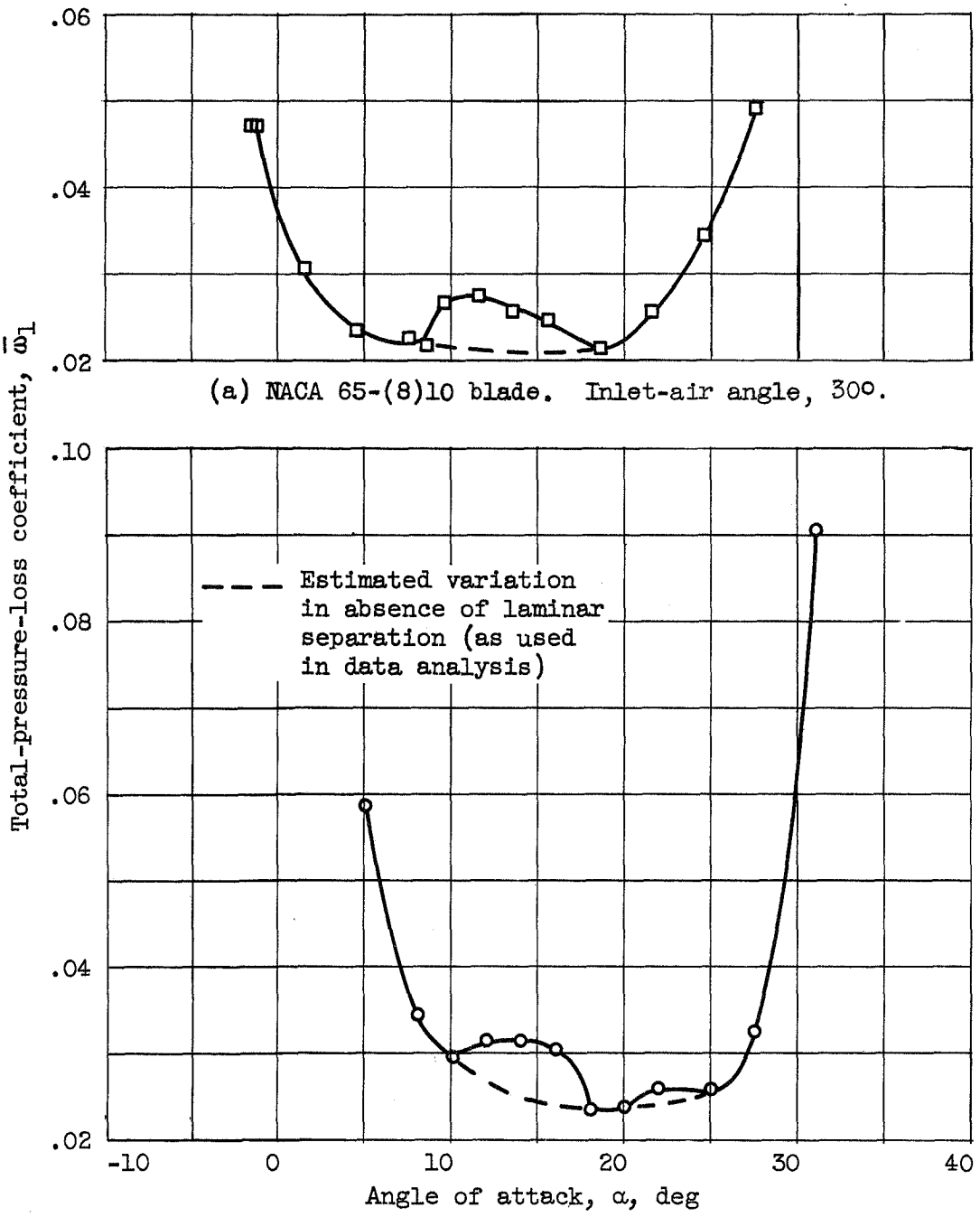

(a) NACA 65-(8)10 blade. Inlet-air angle, 30°.

(b) NACA 65-(12)10 blade. Inlet-air angle, 45°.

Figure 7. - Loss characteristics of cascade blade with local laminar separation. Solidity, 1.5; blade-chord Reynolds number, 2.45×10^5 (ref. 13).

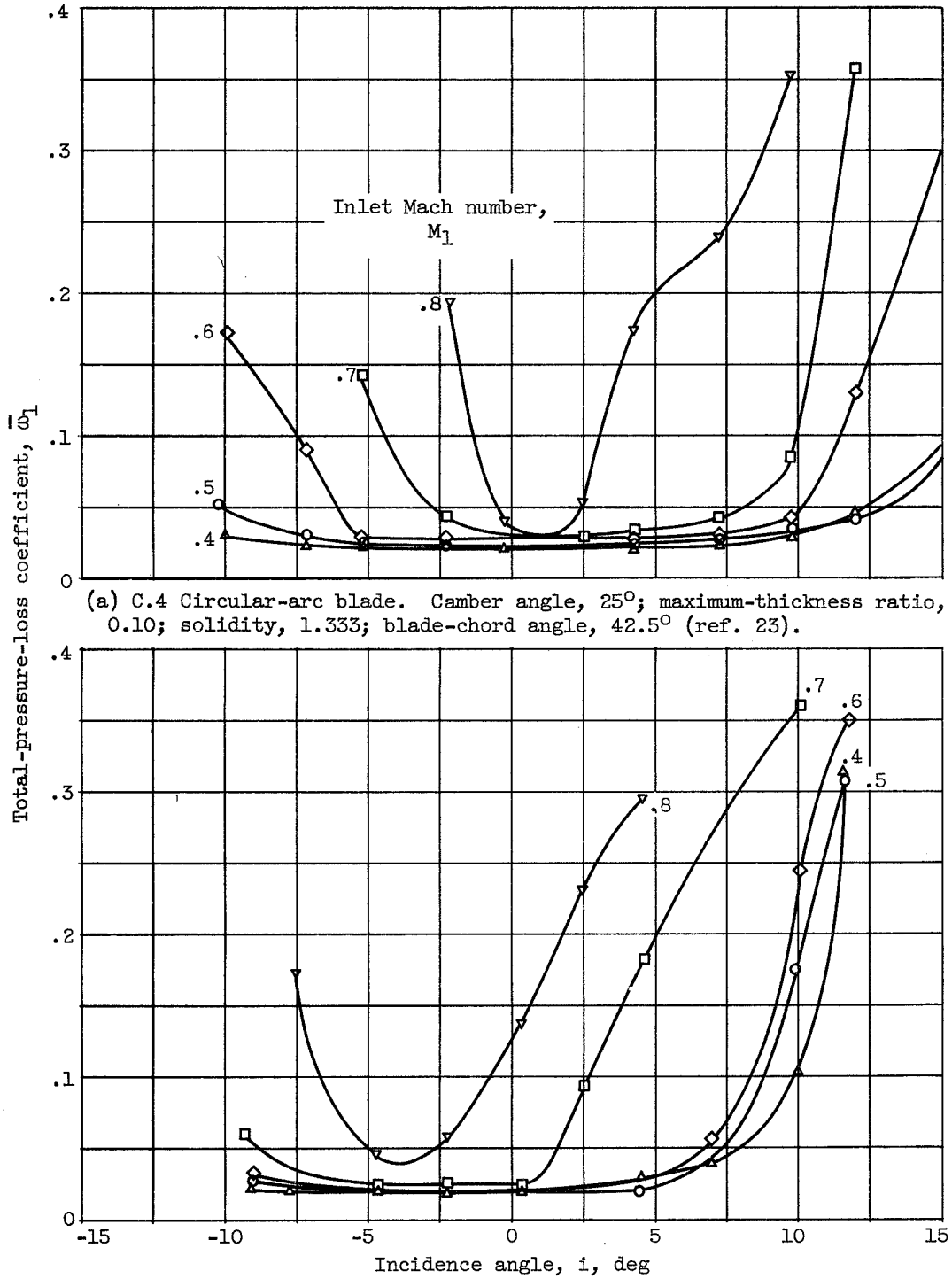

(a) C.4 Circular-arc blade. Camber angle, 25°; maximum-thickness ratio, 0.10; solidity, 1.333; blade-chord angle, 42.5° (ref. 23).

(b) C.4 Parabolic-arc blade. Camber angle, 25°; maximum-thickness ratio, 0.10; solidity, 1.333; blade-chord angle, 37.6° (ref. 23).

Figure 8. - Effect of inlet Mach number on loss characteristics of cascade blade sections.

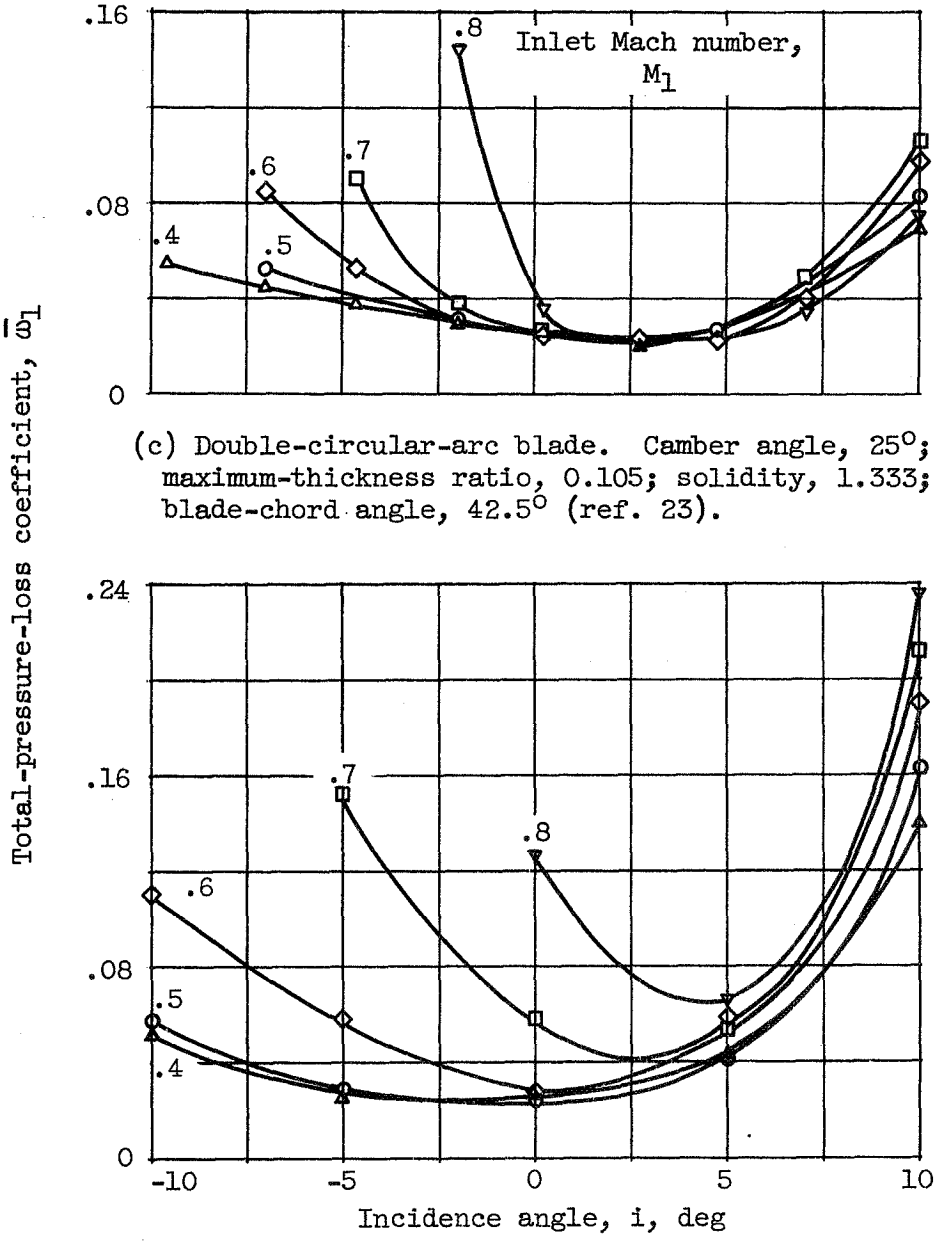

(c) Double-circular-arc blade. Camber angle, 25°; maximum-thickness ratio, 0.105; solidity, 1.333; blade-chord angle, 42.5° (ref. 23).

(d) Sharp-nose blade. Camber angle, 27.5°; maximum-thickness ratio, 0.08; solidity, 1.15; blade-chord angle, 30° (ref. 42).

Figure 8. - Concluded. Effect of inlet Mach number on loss characteristics of cascade blade sections.

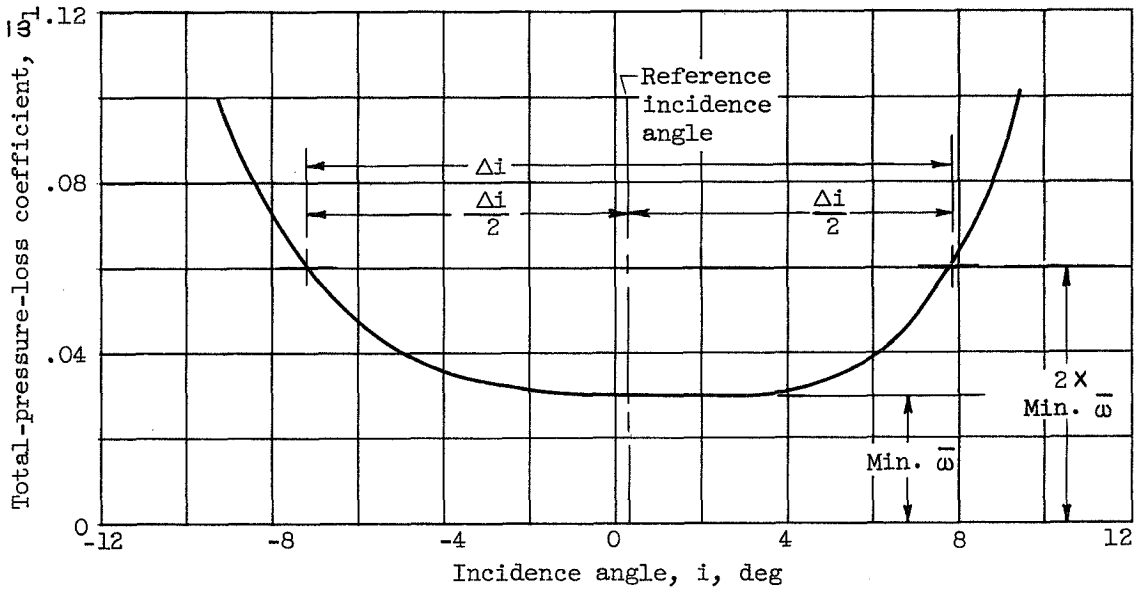

Figure 9. - Definition of reference minimum-loss incidence angle.

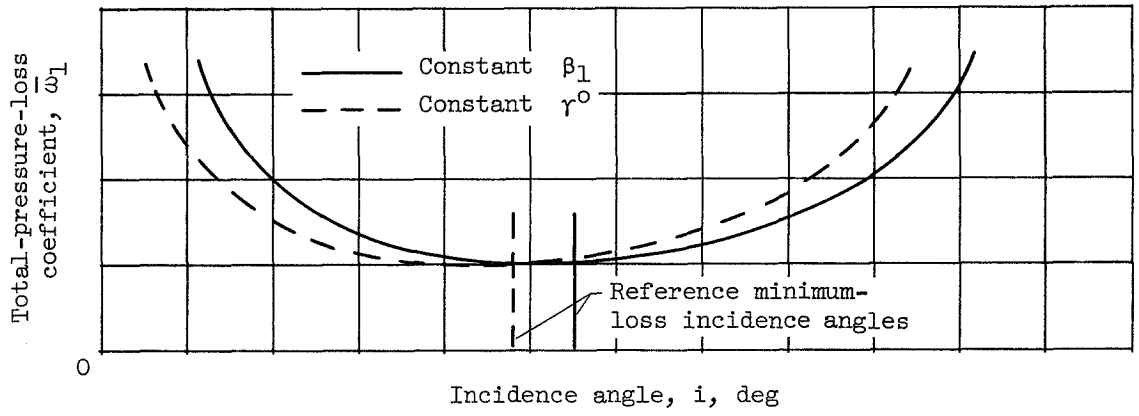

Figure 10. - Qualitative comparison of cascade range characteristics at constant blade-chord angle and constant inlet-air angle (for same value of β_1 in region of minimum loss).

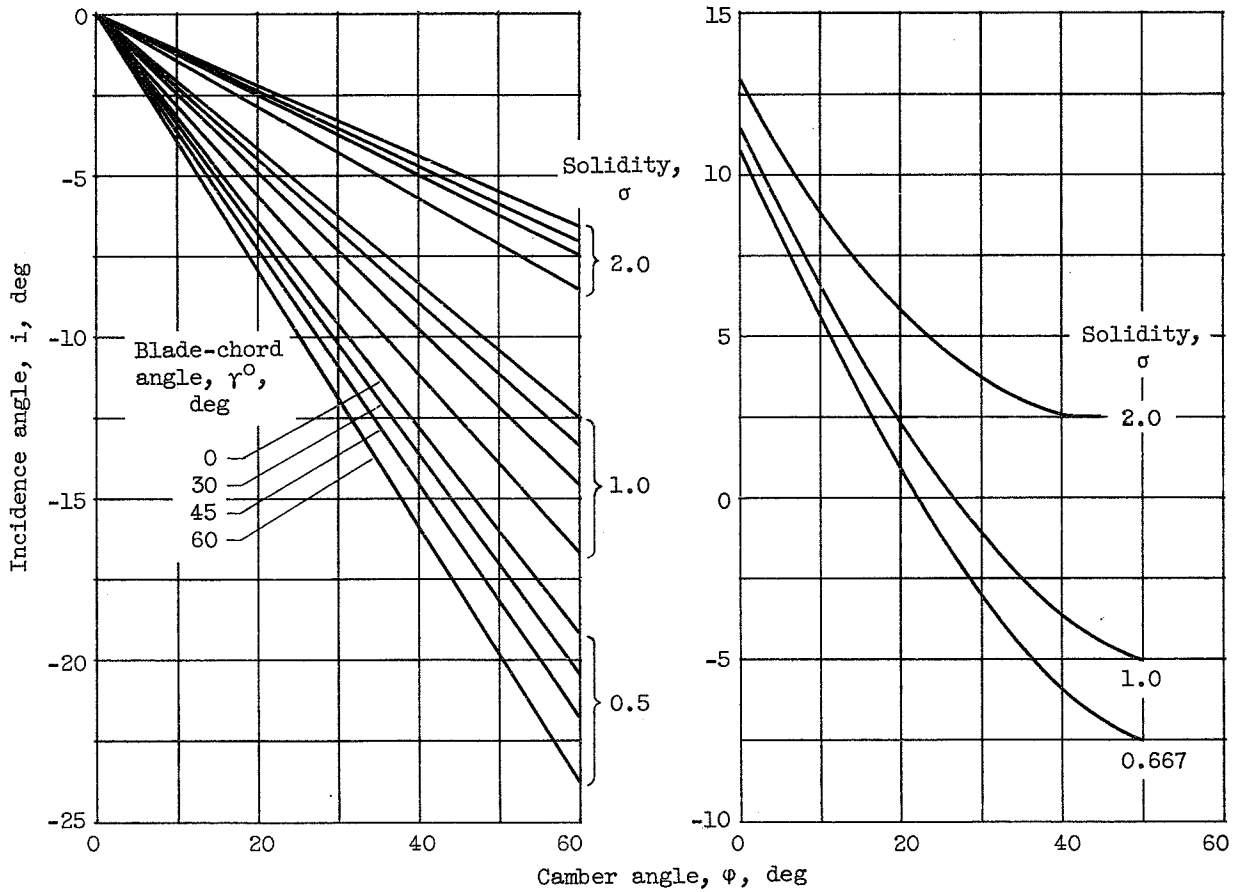

(a) "Inpact-free-entry" incidence angle for infinitely thin blades according to potential theory of Weinig (ref. 28).

(b) "Optimum" incidence angle for 10-percent-thick C-series profiles according to semitheoretical developments of Carter et al. (refs. 27 and 11). Outlet-air angle, 20°.

Figure 11. - Variation of reference incidence angle for circular-arc-mean-line blades obtained from theoretical or semitheoretical investigations.

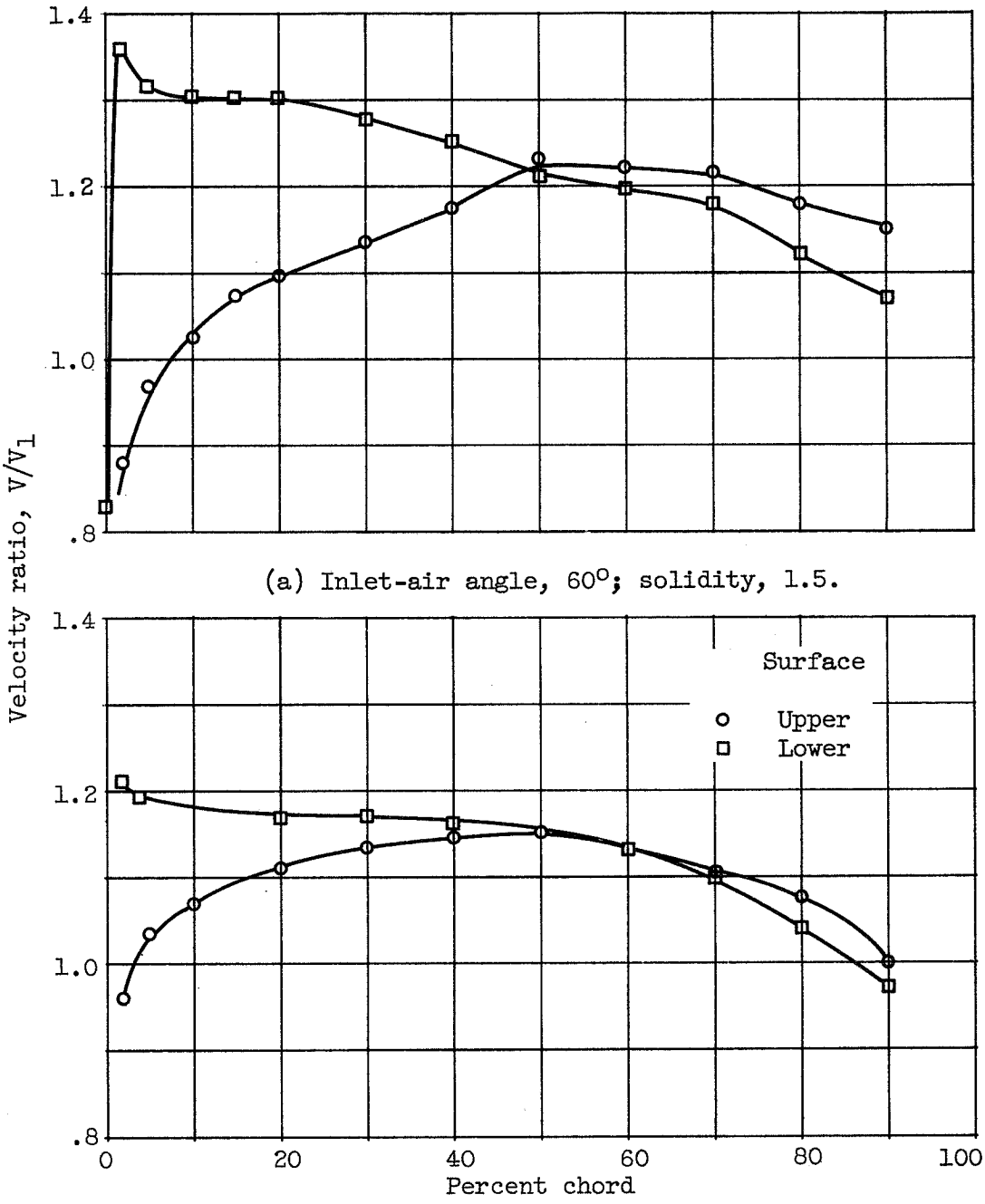

(a) Inlet-air angle, 60°; solidity, 1.5.

(b) Inlet-air angle, 30°; solidity, 1.0.

Figure 12. - Illustration of velocity distribution for uncambered blade of conventional thickness at zero incidence angle. Data for 65-(0)10 blade of reference 13.

[redacted]

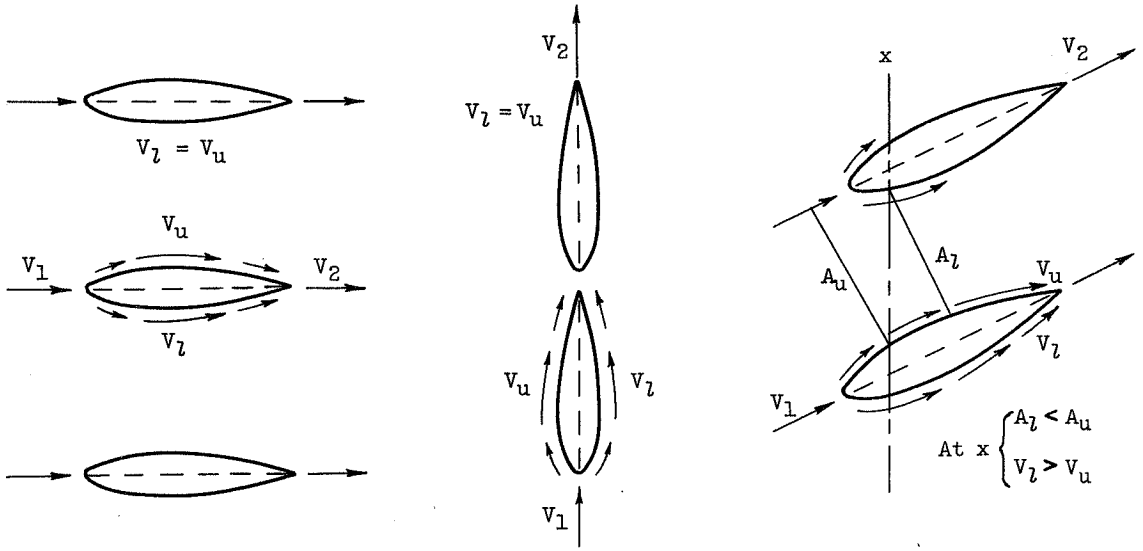

(a) $\gamma^o = 0^o$. (b) $\gamma^o = 90^o$. (c) $0^o < \gamma^o < 90^o$.

Figure 13. - Effect of blade thickness on surface velocity at zero incidence angle for uncambered airfoil section according to simplified one-dimensional model.

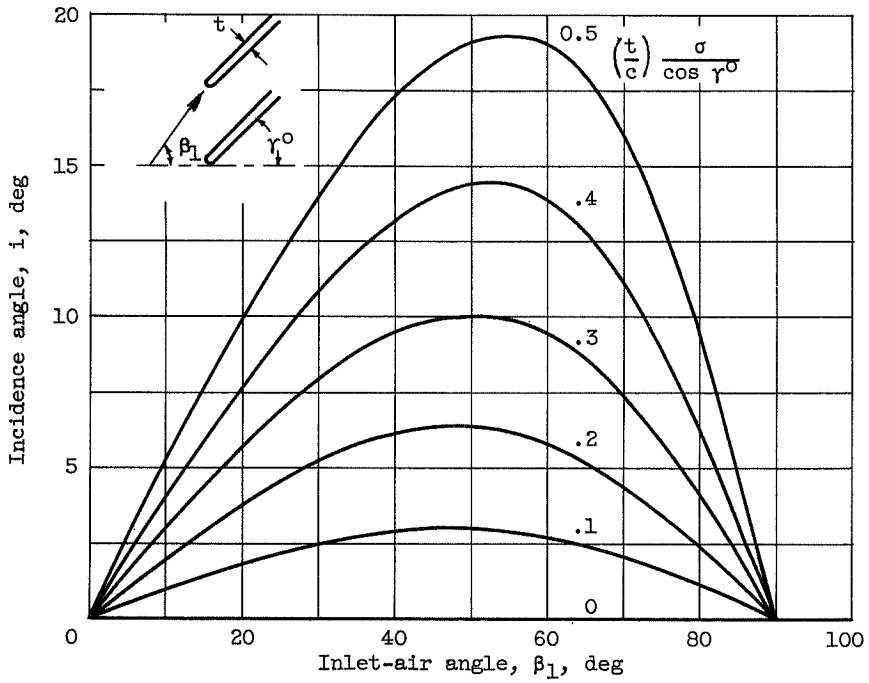

Figure 14. - Theoretical variation of "impact-free-entry" incidence angle for constant-thickness uncambered sections according to developments of reference 29.

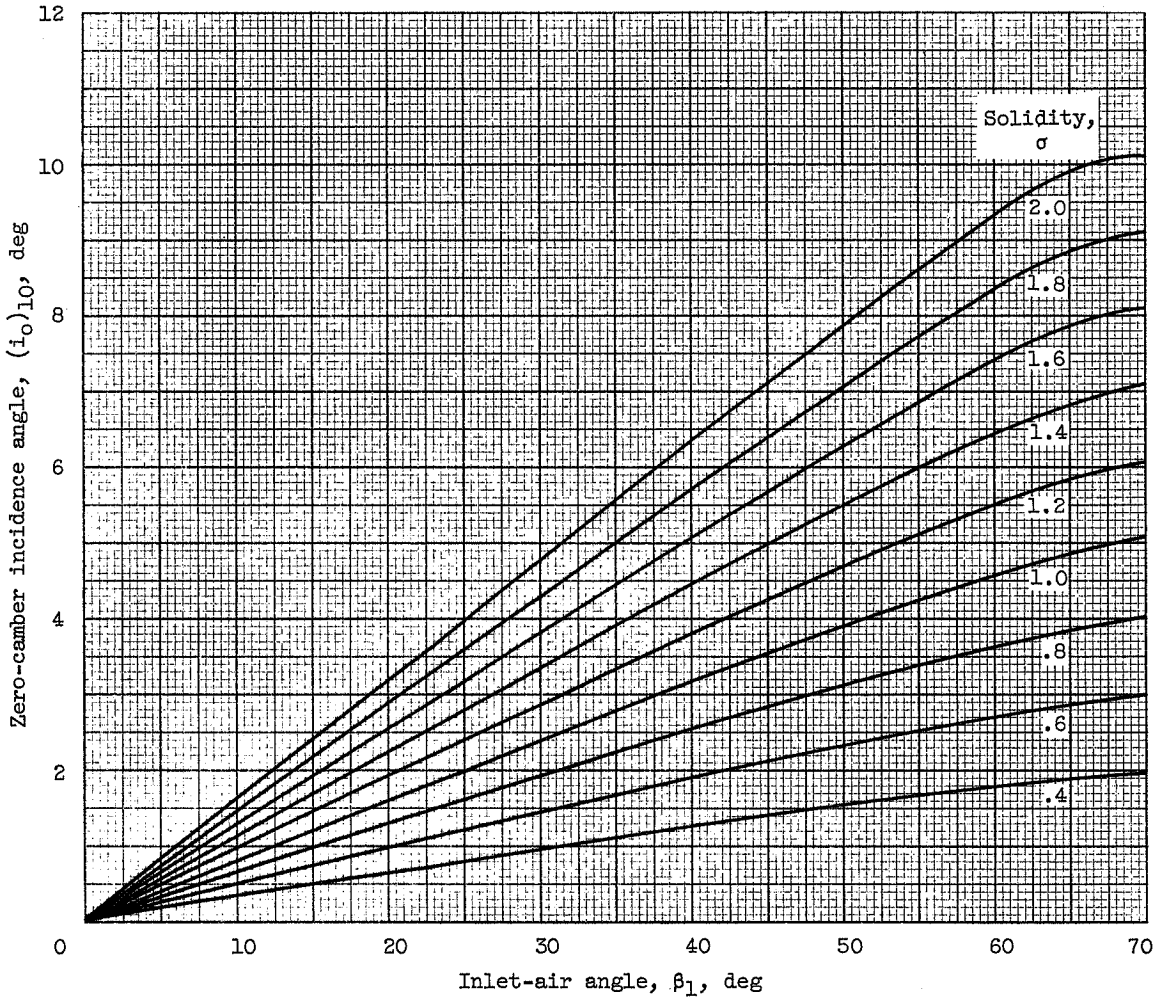

Figure 15. - Reference minimum-loss incidence angle for zero camber deduced from low-speed-cascade data of 10-percent-thick NACA 65-(A_{10})-series blades (ref. 13).

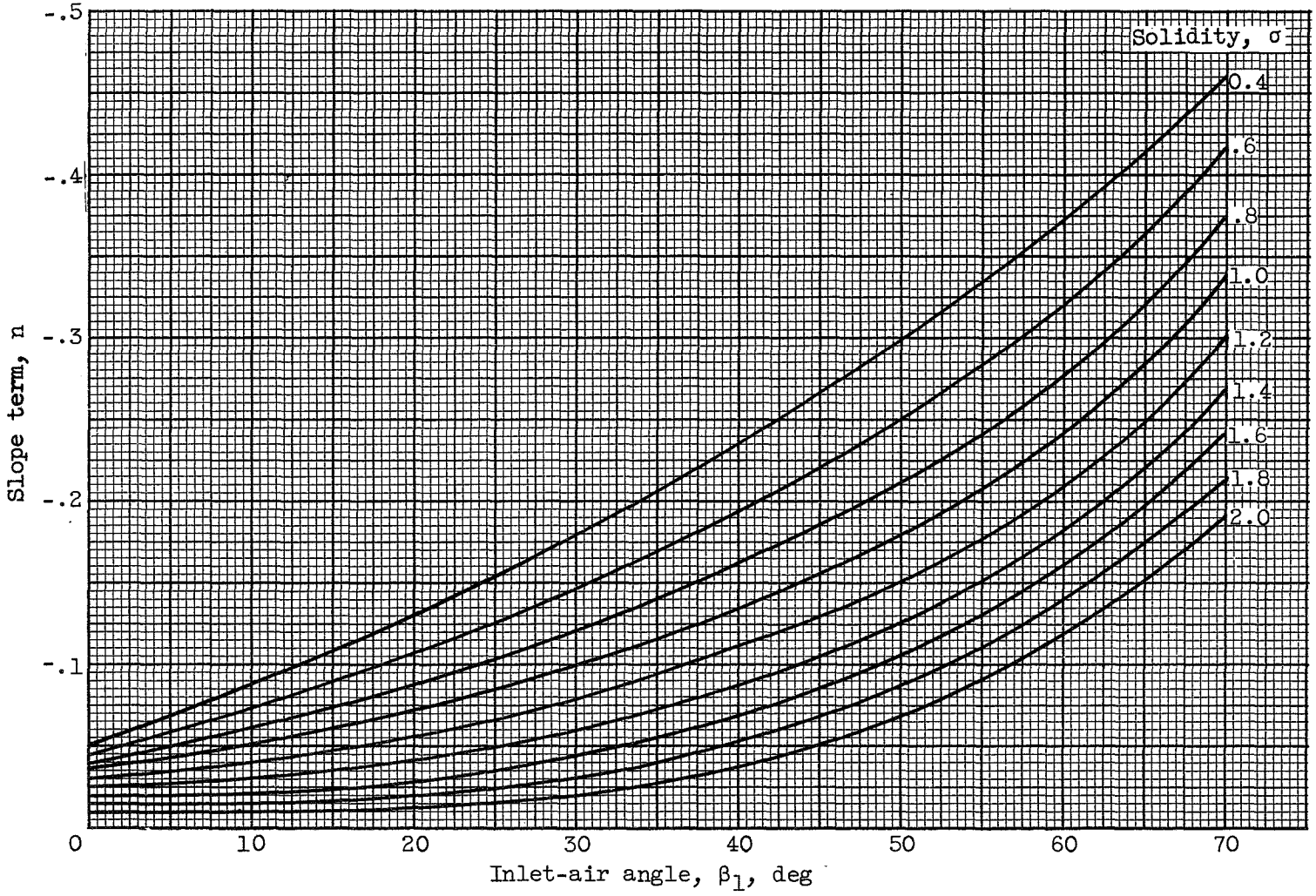

Figure 16. - Reference minimum-loss-incidence-angle slope term deduced from low-speed-cascade data for NACA 65-(A_{10})-series blades as equivalent circular arcs.

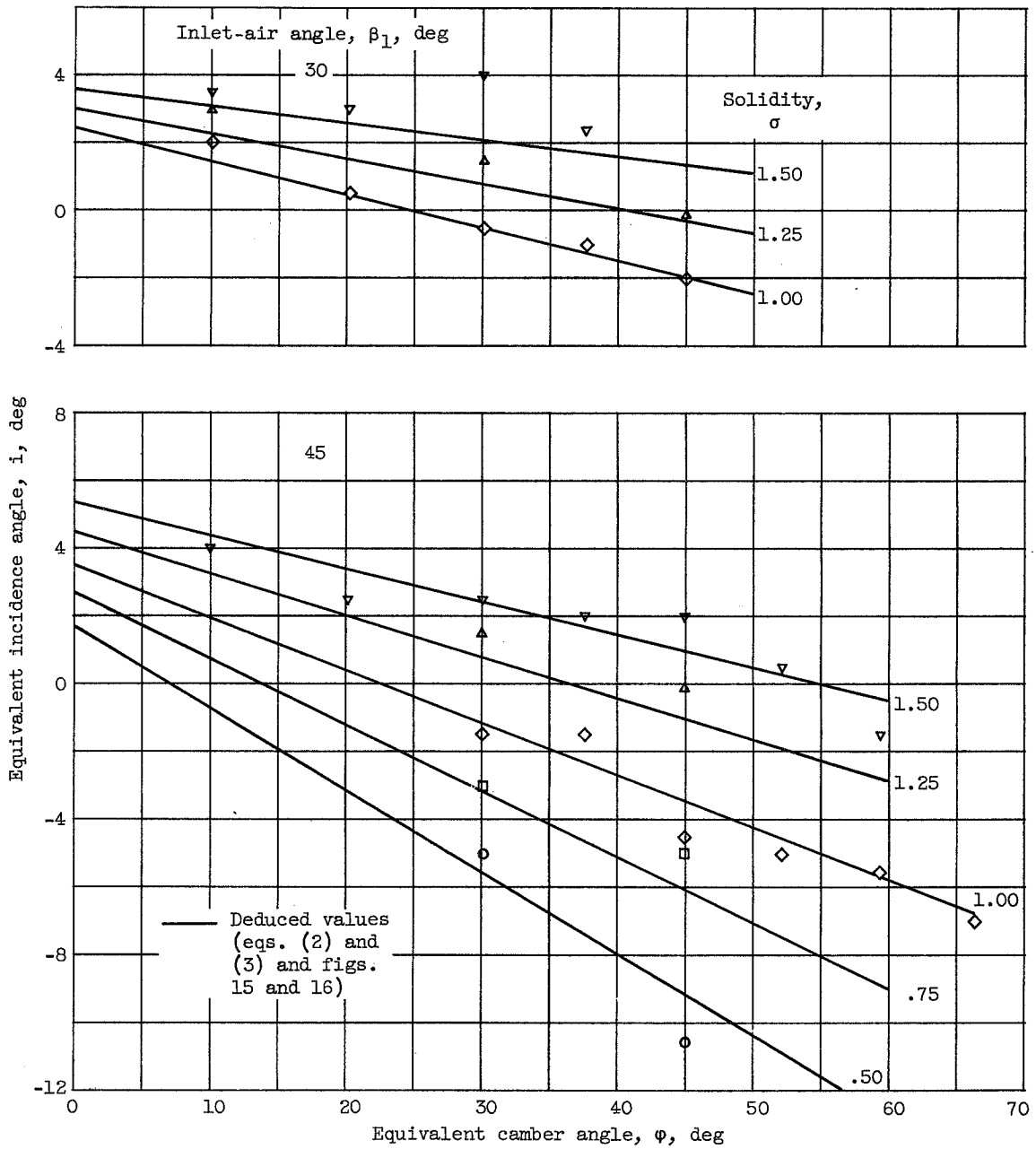

(a) Inlet-air angles of 30° and 45°.

Figure 17. - Comparison of data values and deduced rule values of reference minimum-loss incidence angle for 65-(A_{10})10 blades as equivalent circular arc (ref. 13).

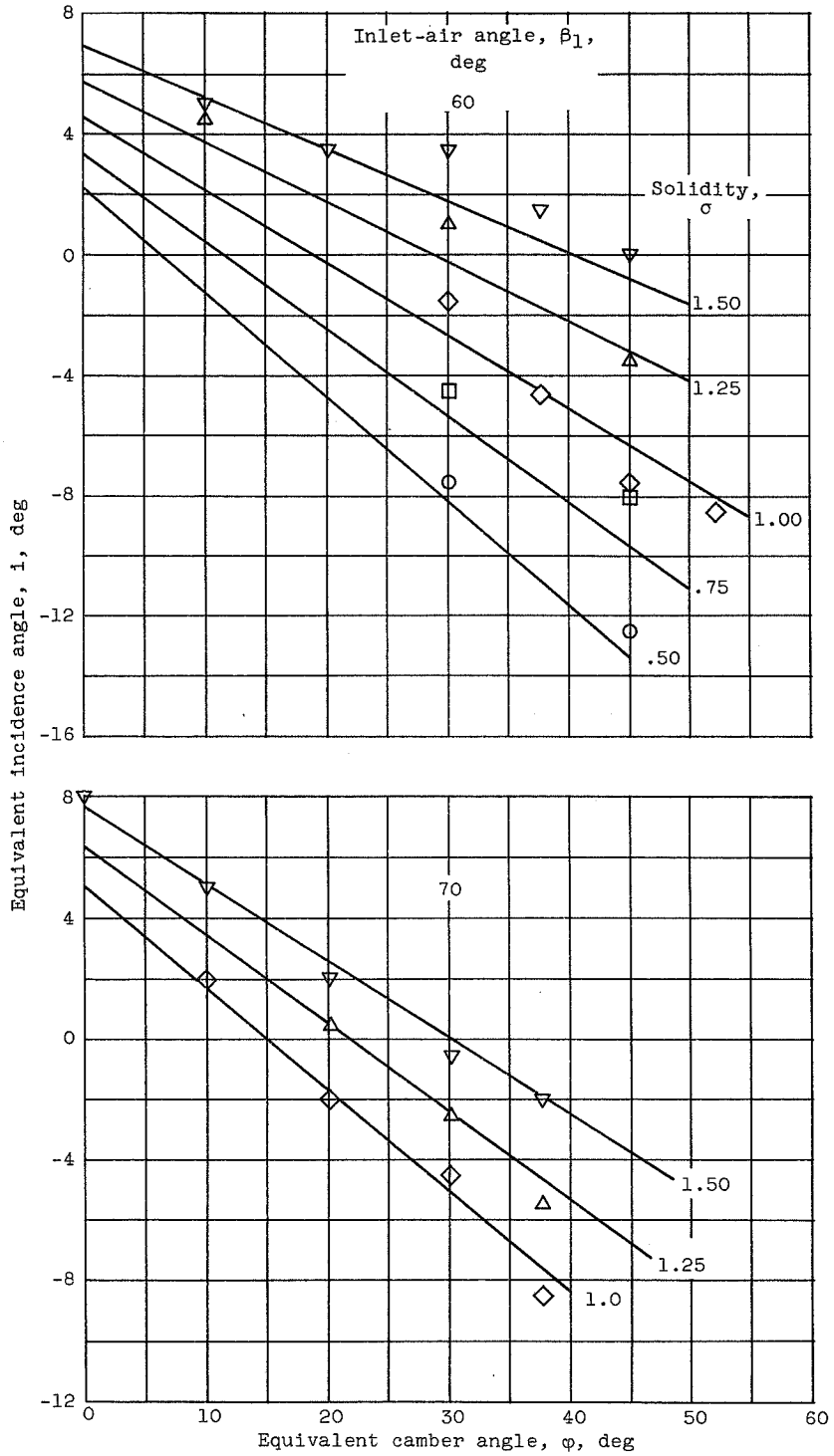

(b) Inlet-air angles of 60° and 70°.

Figure 17. - Concluded. Comparison of data values and deduced rule values of reference minimum-loss incidence angle for 65-(A_{10})10 blades as equivalent circular arc (ref. 13).

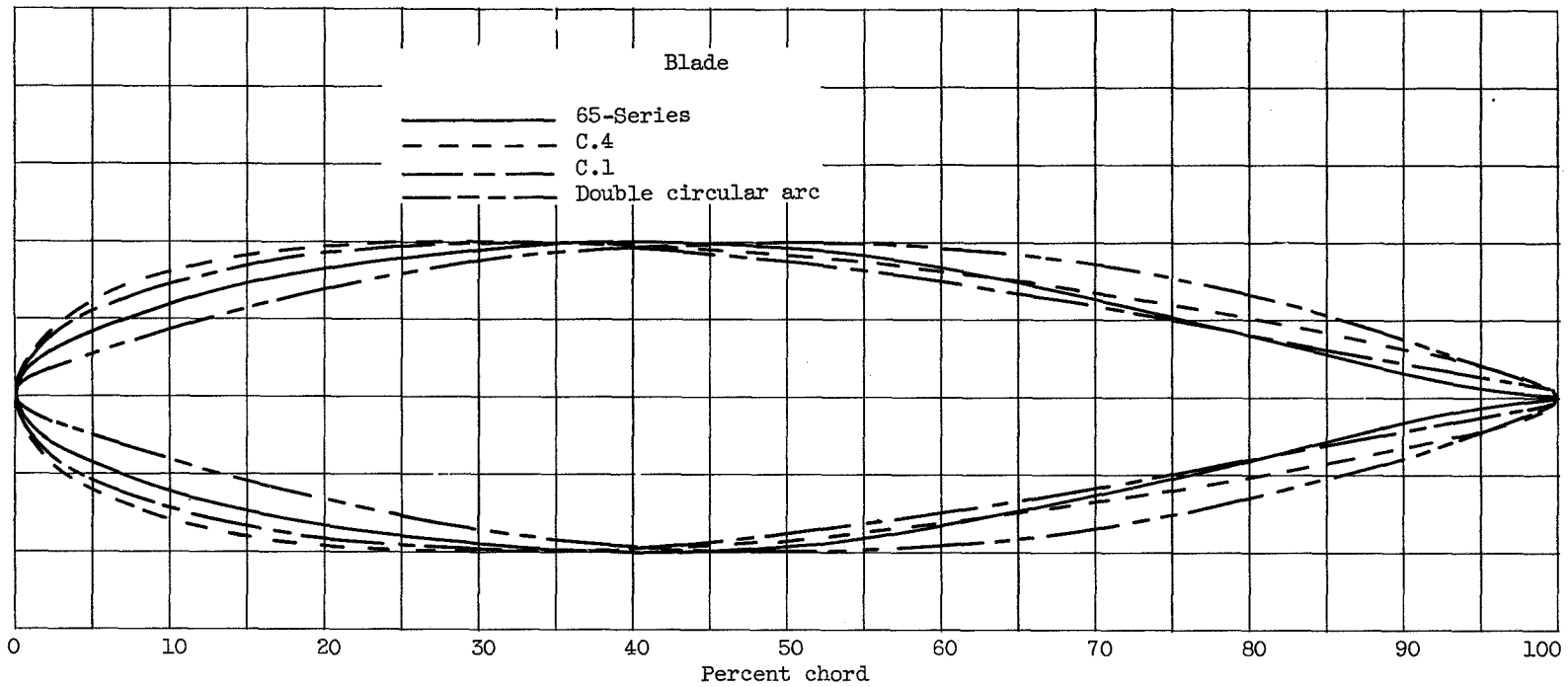

Figure 18. - Comparison of basic thickness distributions for conventional compressor blade sections.

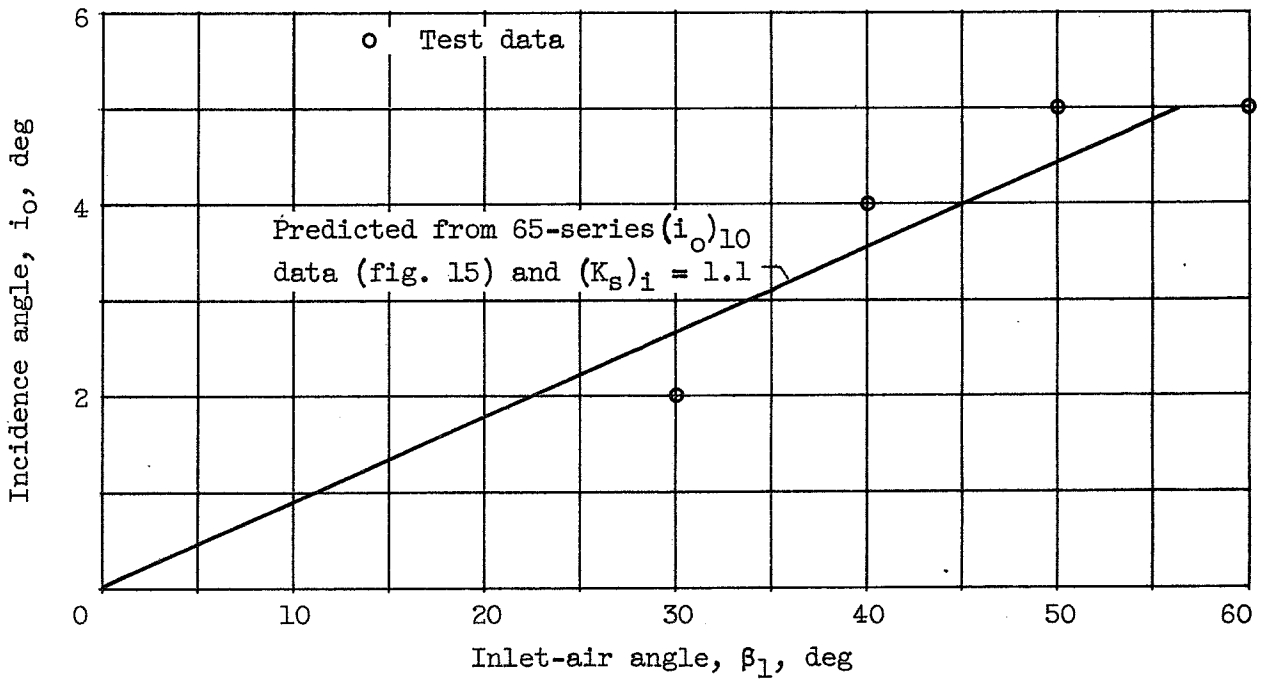

Figure 19. - Zero-camber minimum-loss incidence angle for 10-percent-thick C.4 profile. Solidity, 1.0 (ref. 32).

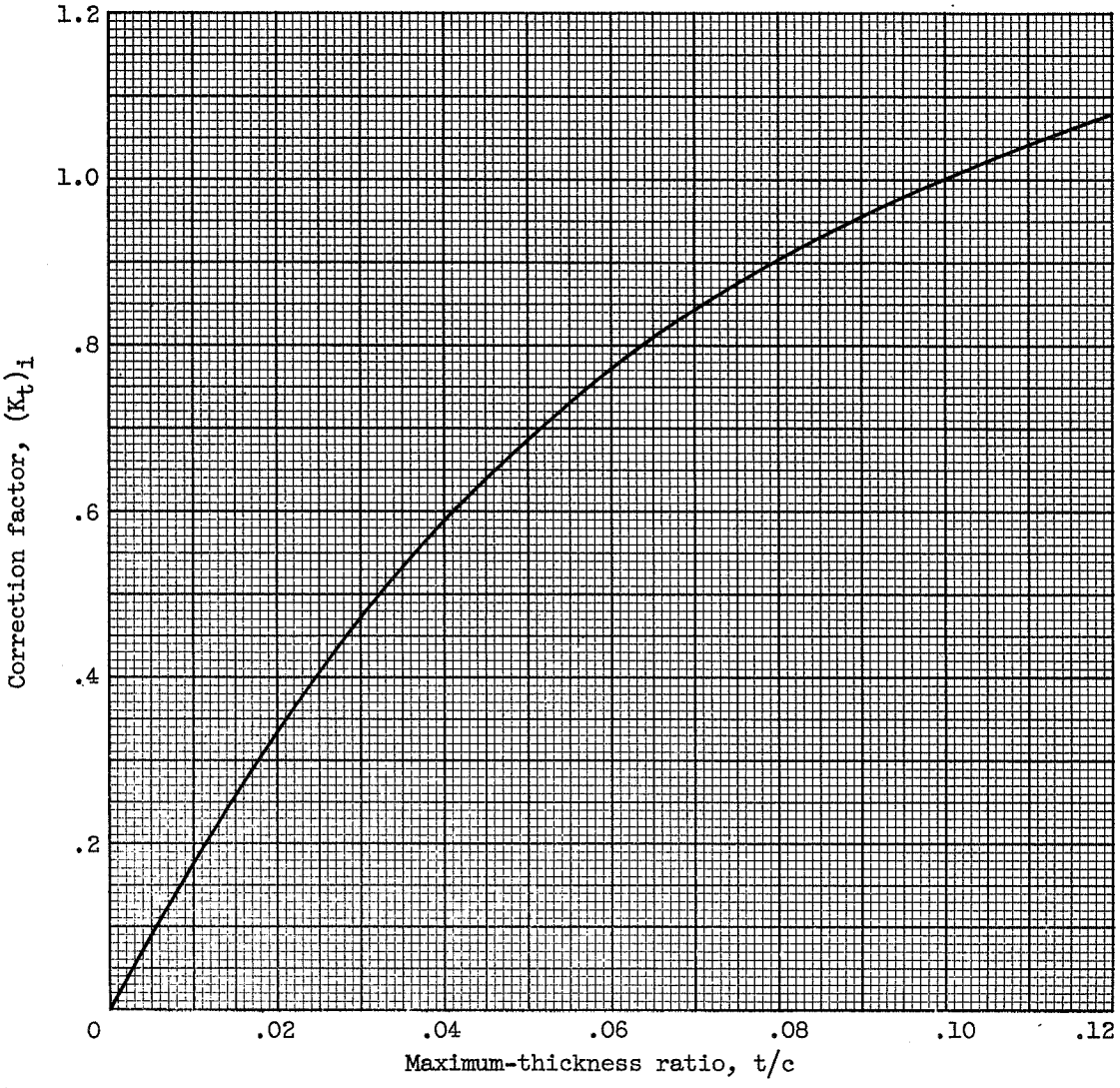

Figure 20. - Deduced blade maximum-thickness correction for zero-camber reference minimum-loss incidence angle (eq. (3)).

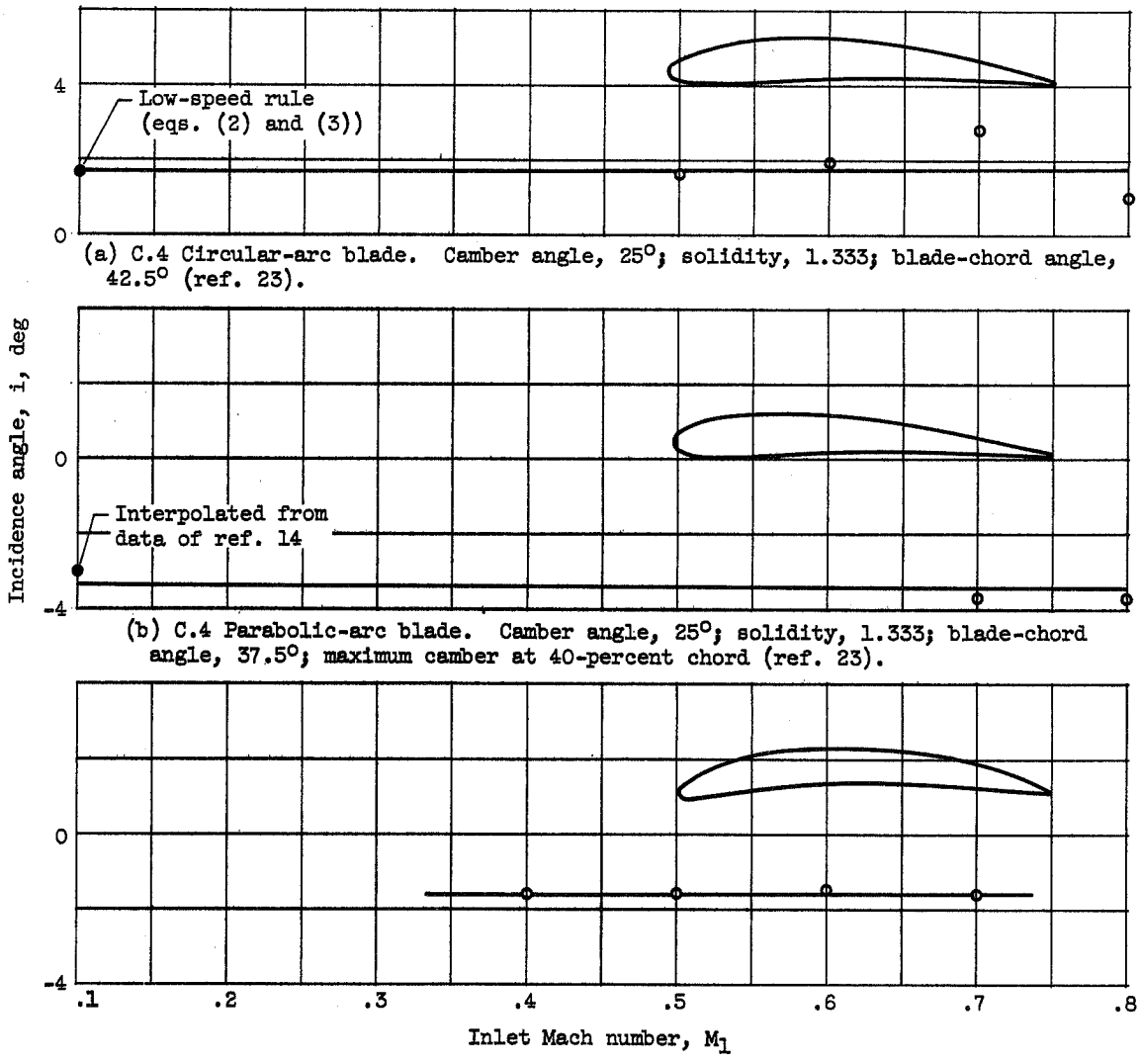

(a) C.4 Circular-arc blade. Camber angle, 25°; solidity, 1.333; blade-chord angle, 42.5° (ref. 23).

(b) C.4 Parabolic-arc blade. Camber angle, 25°; solidity, 1.333; blade-chord angle, 37.5°; maximum camber at 40-percent chord (ref. 23).

(c) C.7 Parabolic-arc blade. Camber angle, 40°; solidity, 1.0; blade-chord angle, 24.6°; maximum camber at 45-percent chord (ref. 55).

Figure 21. - Variation of reference minimum-loss incidence angle with inlet Mach number for thick-nose sections. Maximum-thickness ratio, 0.10.

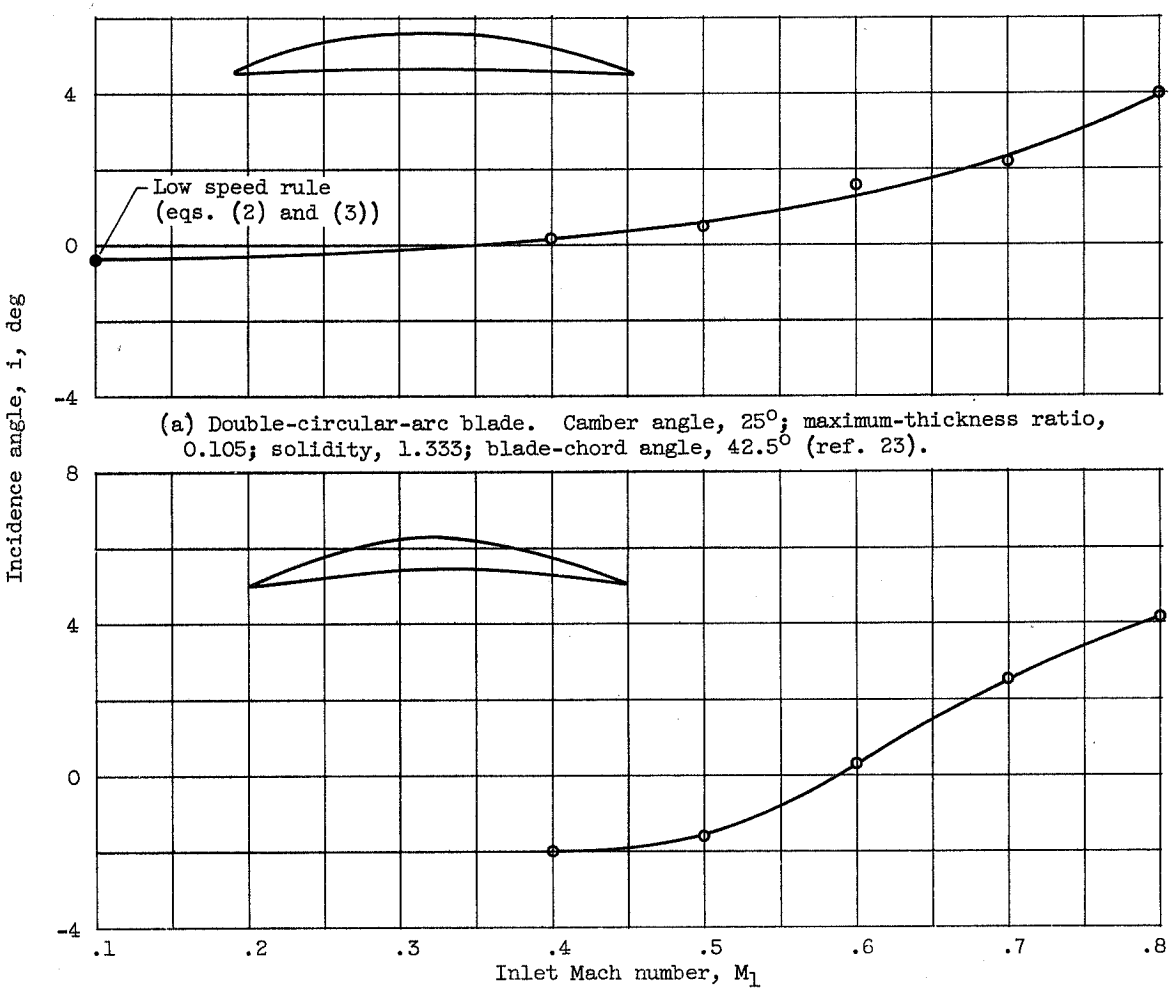

(a) Double-circular-arc blade. Camber angle, 25°; maximum-thickness ratio, 0.105; solidity, 1.333; blade-chord angle, 42.5° (ref. 23).

(b) Blade section of reference 42. Camber angle, 27.5°; maximum-thickness ratio, 0.08; solidity, 1.15; blade-chord angle, 30°; maximum thickness and camber at 50-percent chord.

Figure 22. - Variation of reference minimum-loss incidence angle with inlet Mach number for sharp-nose sections.

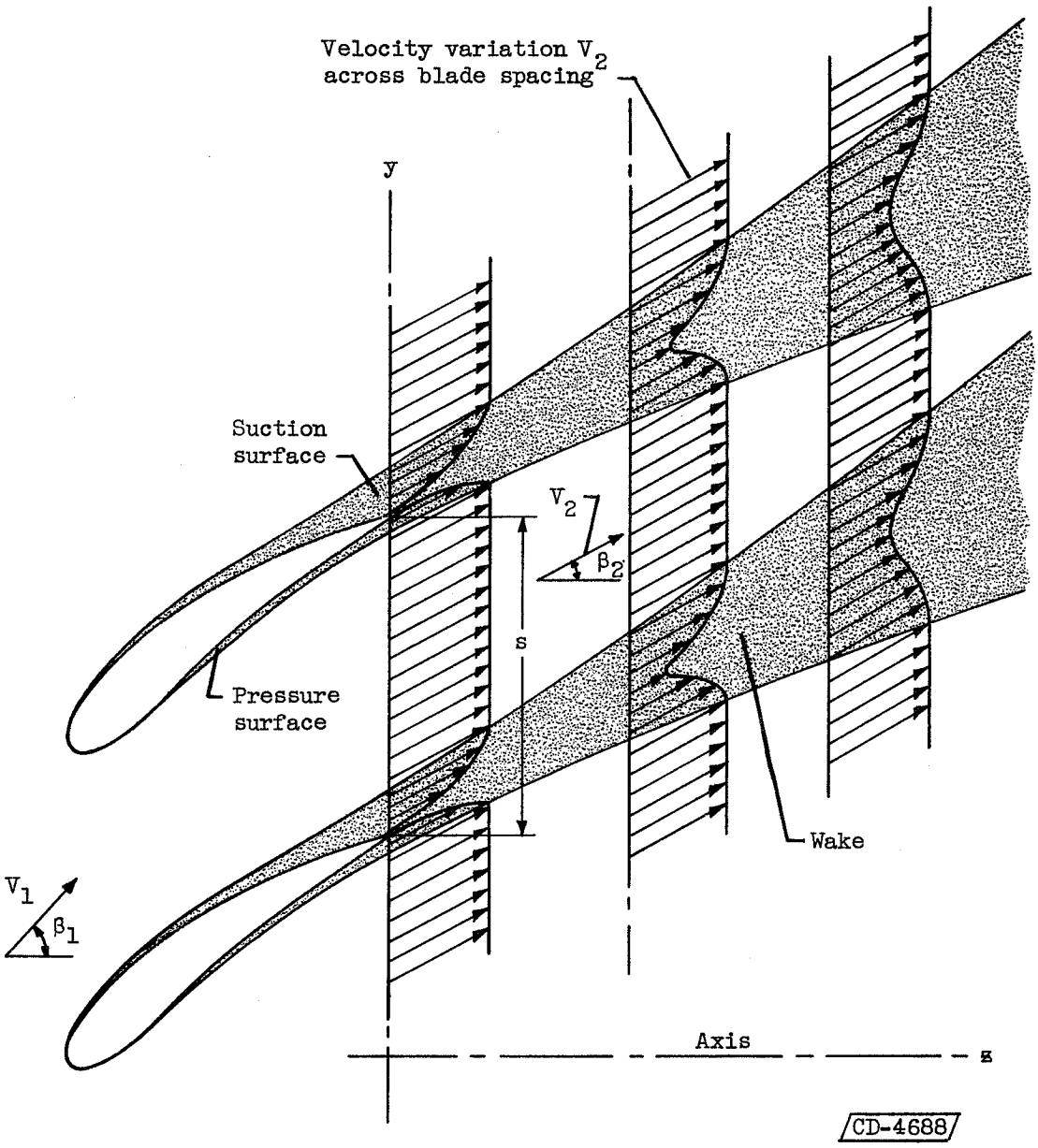

Figure 23. - Schematic representation of development of surface boundary layers and wake in flow about cascade blade sections.

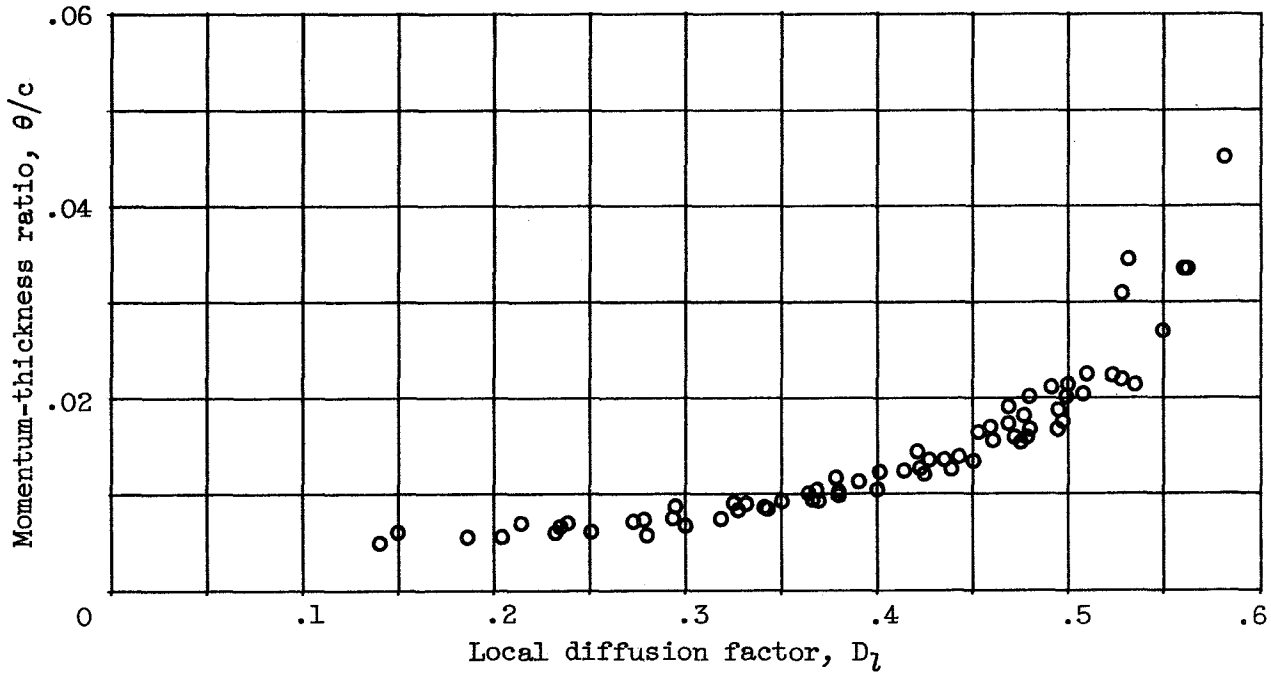

Figure 24. - Variation of computed wake momentum-thickness ratio with local diffusion factor at reference incidence angle for low-speed cascade data of NACA 65-(A_{10})10 blades (ref. 13).

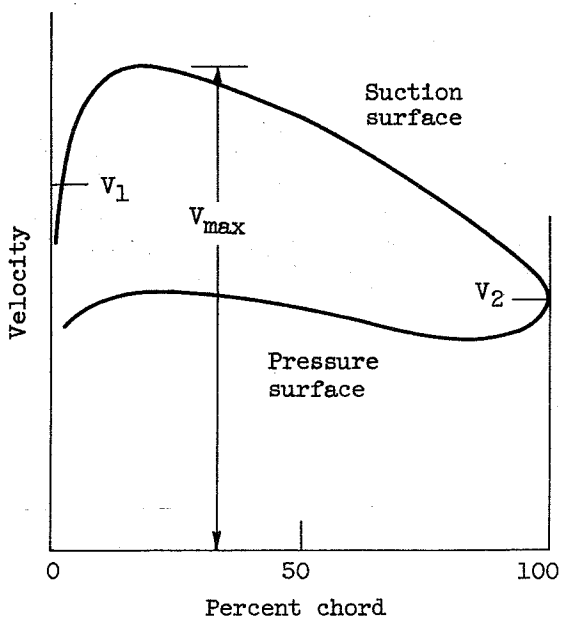

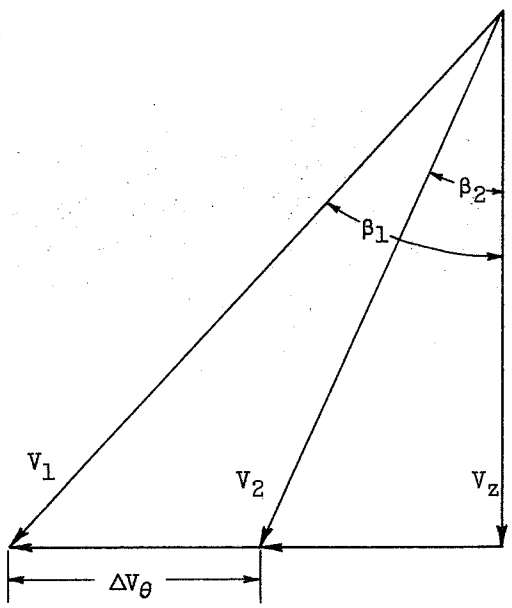

$$D \approx \frac{V_{max} - V_2}{V_{av}} \approx \frac{V_{max} - V_2}{V_1}; \quad V_{max} \approx V_1 + f\left(\frac{\Delta V_\theta}{\sigma}\right)$$

$$\text{Thus, } D = \left(1 - \frac{V_2}{V_1}\right) + \frac{\Delta V_\theta}{2\sigma V_1}$$

$$\text{For two-dimensional flow, with } V_{z,1} = V_{z,2}, \quad D = \left(1 - \frac{\cos \beta_1}{\cos \beta_2}\right) + \frac{\cos \beta_1}{2\sigma} (\tan \beta_1 - \tan \beta_2) \quad \text{(eq. (7))}$$

Figure 25. - Basis of development of diffusion factor for cascade flow from reference 25.

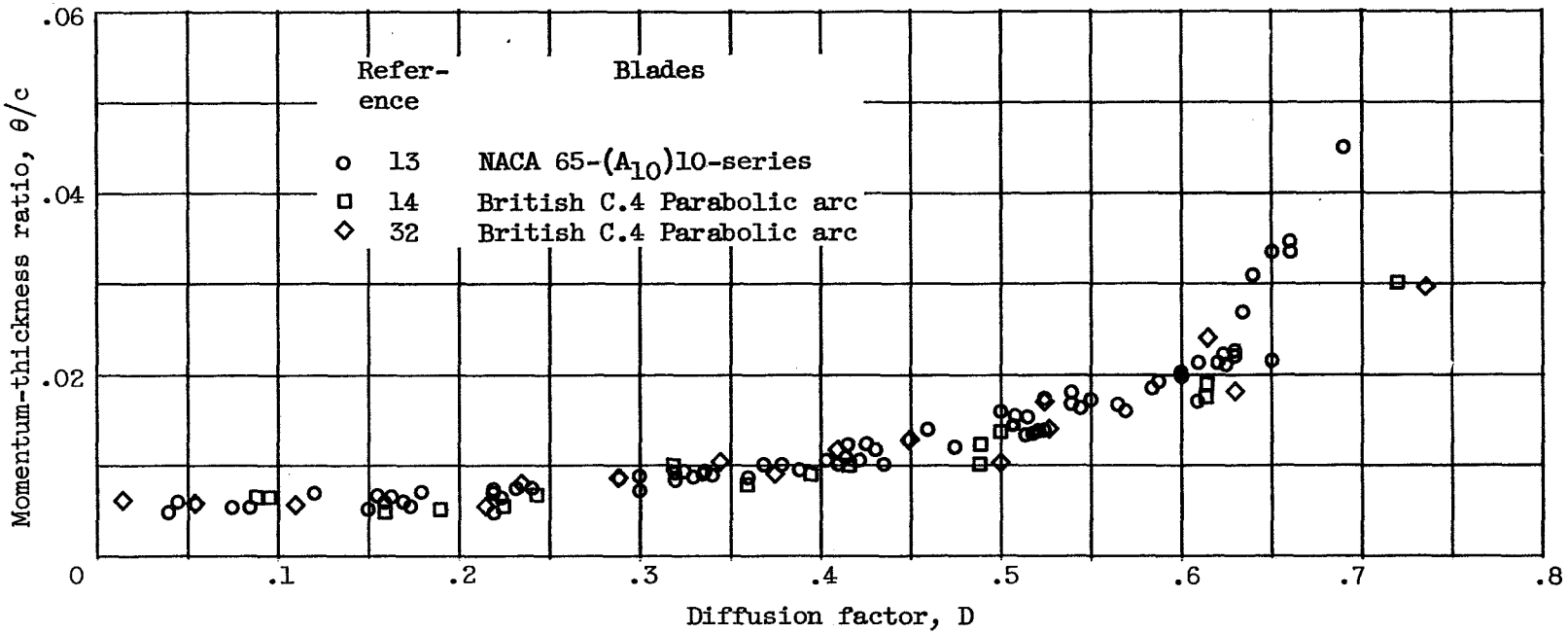

Figure 26. - Variation of computed wake momentum-thickness ratio with over-all diffusion factor at reference incidence angle for low-speed systematic cascade data of references 13, 14, and 32. Blade maximum-thickness ratio, 0.10; Reynolds number, $\sim 2.5\times10^5$.

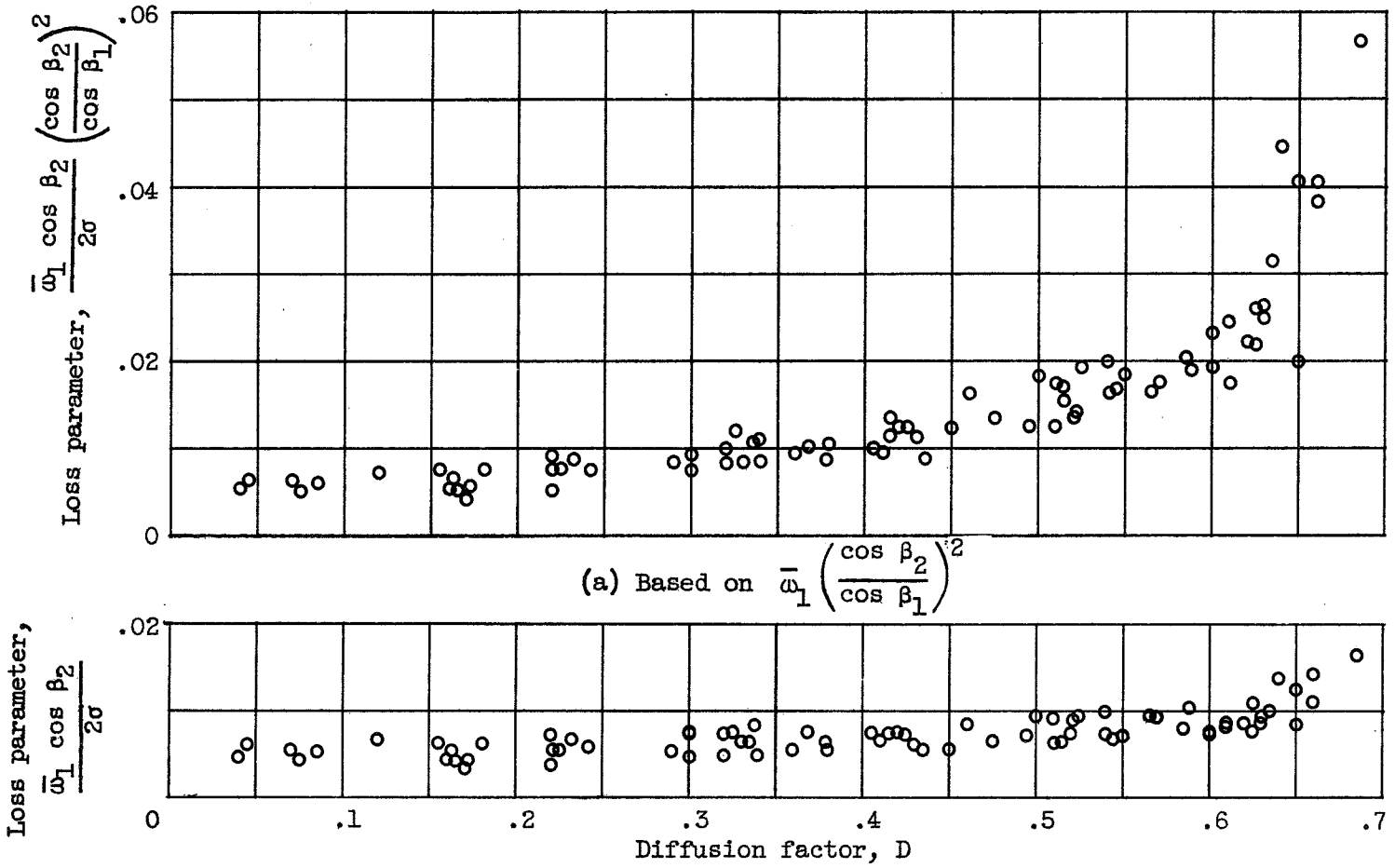

Figure 27. - Variation of loss parameter with diffusion factor at reference minimum-loss incidence angle computed from low-speed-cascade data of NACA 65-(A_{10})10 cascade blades (ref. 13).

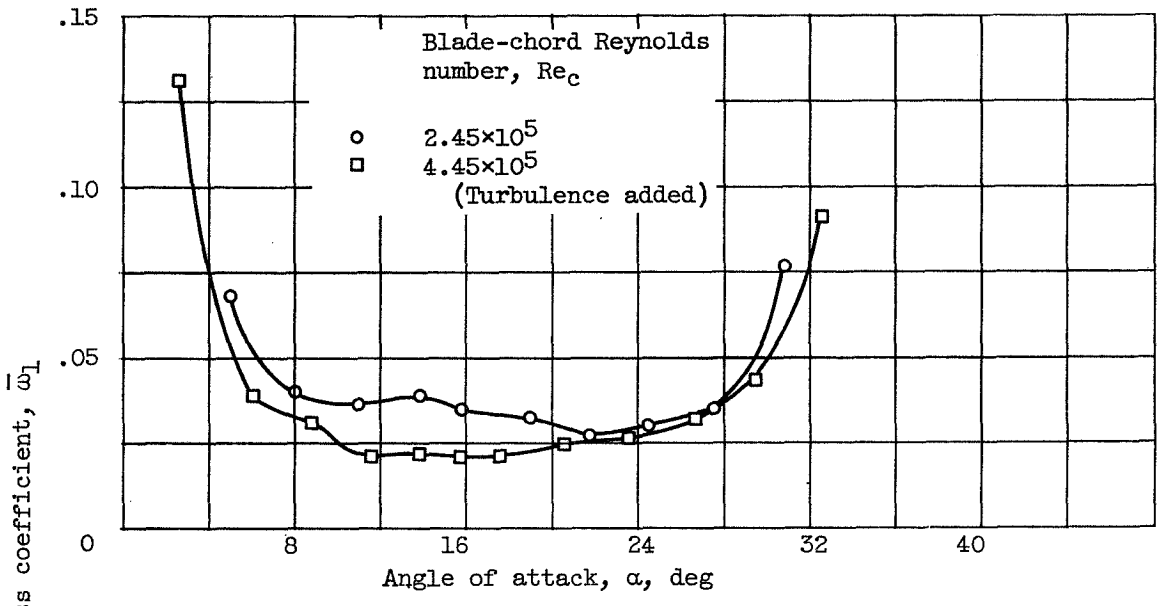

(a) 65-Series blade 65-(12)10. Solidity, 1.5; inlet-air angle, 45° (ref. 13).

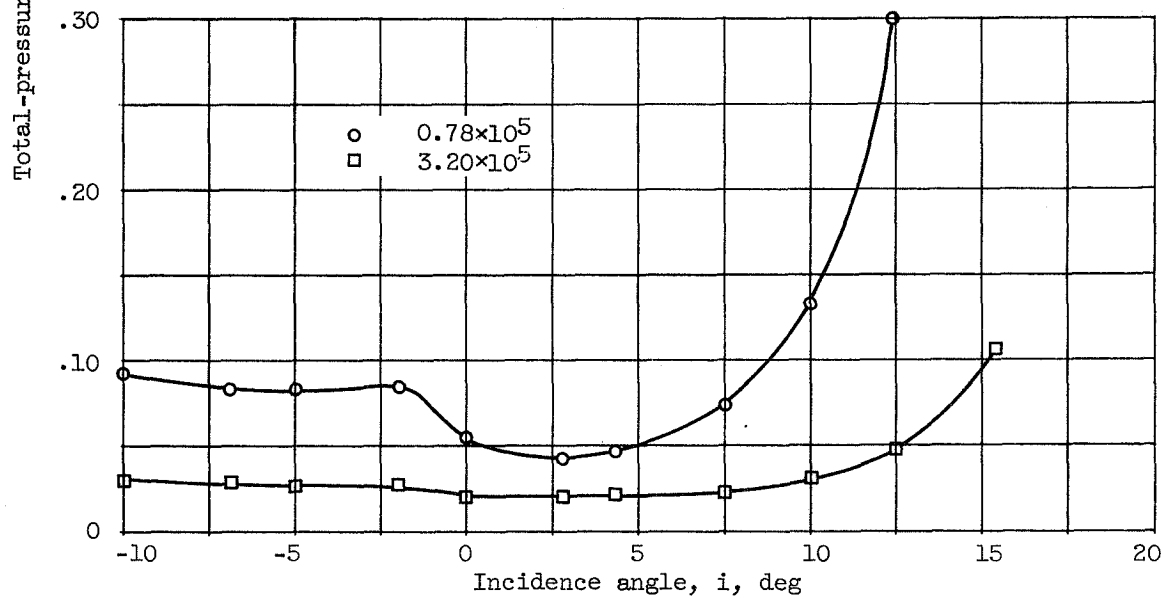

(b) Circular-arc blade 10C4/25C50. Solidity, 1.333; blade-chord angle, 42.5° (ref. 23).

Figure 28. - Effect of Reynolds number on variation of loss with incidence angle.

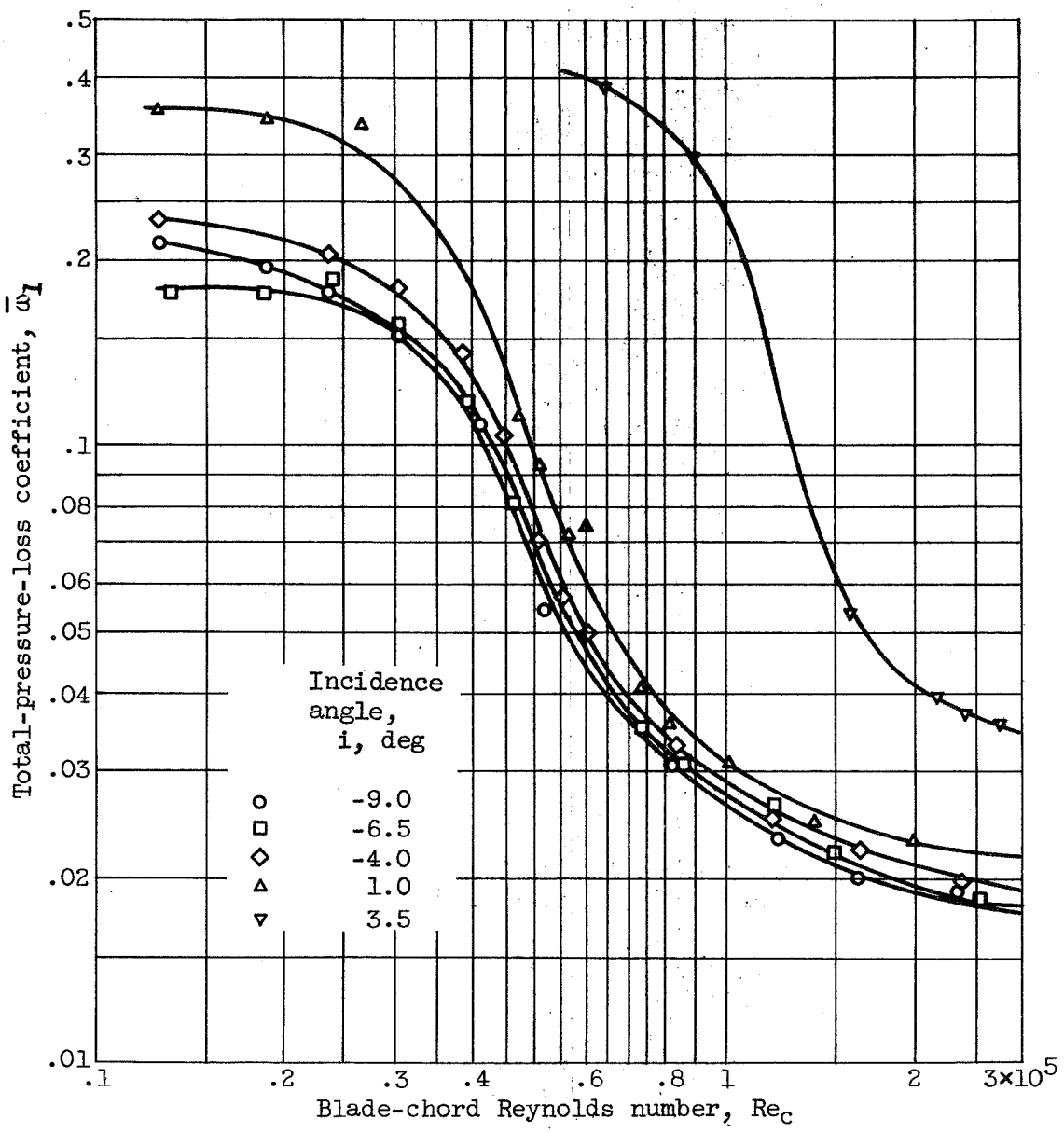

Figure 29. - Variation of total-pressure-loss coefficient with blade-chord Reynolds number for parabolic-arc blade 10C4/40 P40. Inlet-air angle, 28° to 40°; solidity, 1.333 (ref. 41).

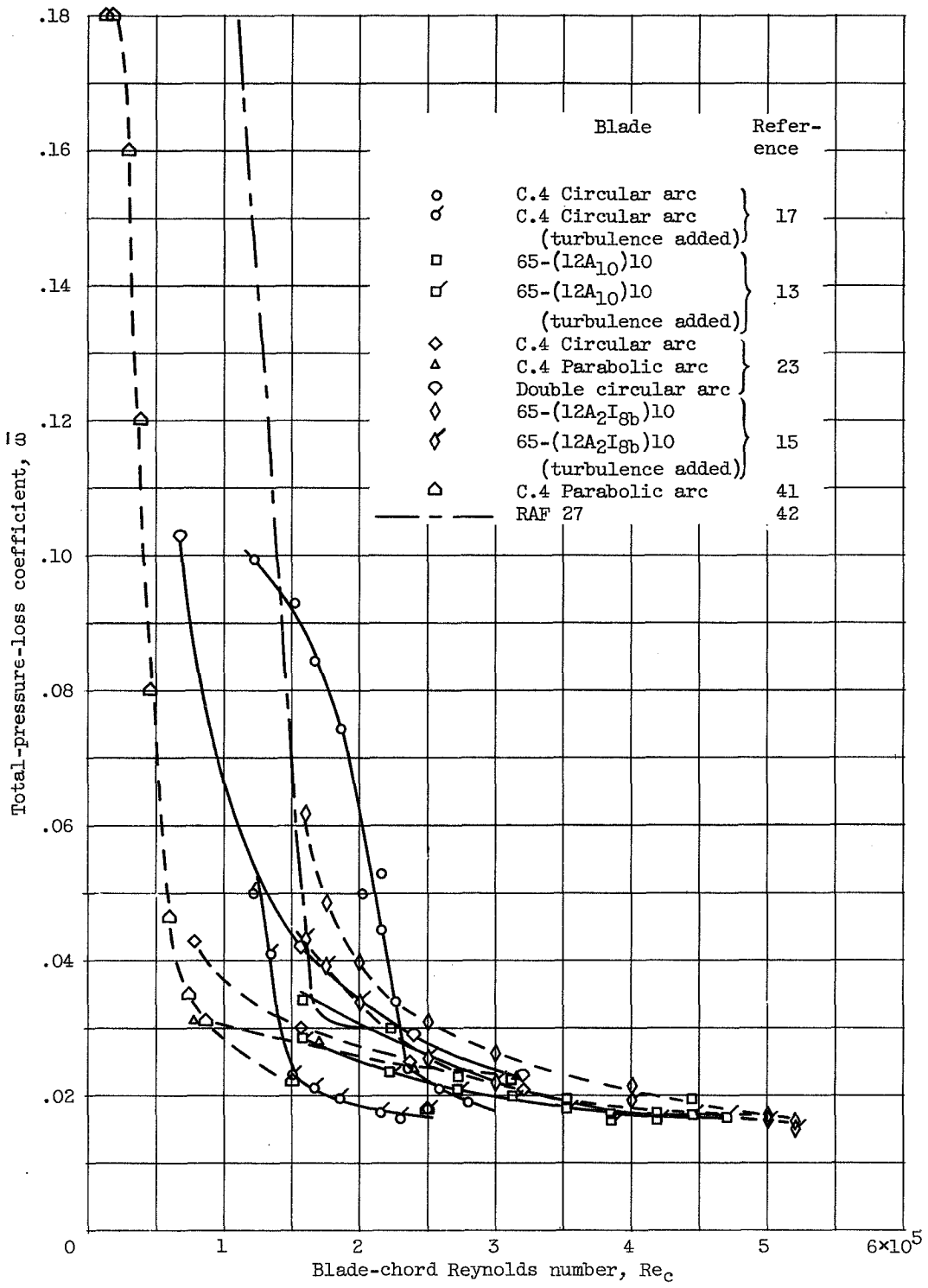

Figure 30. - Composite plot of loss coefficient against blade-chord Reynolds number in region of minimum loss for two-dimensional-compressor cascade blade sections at low speed.

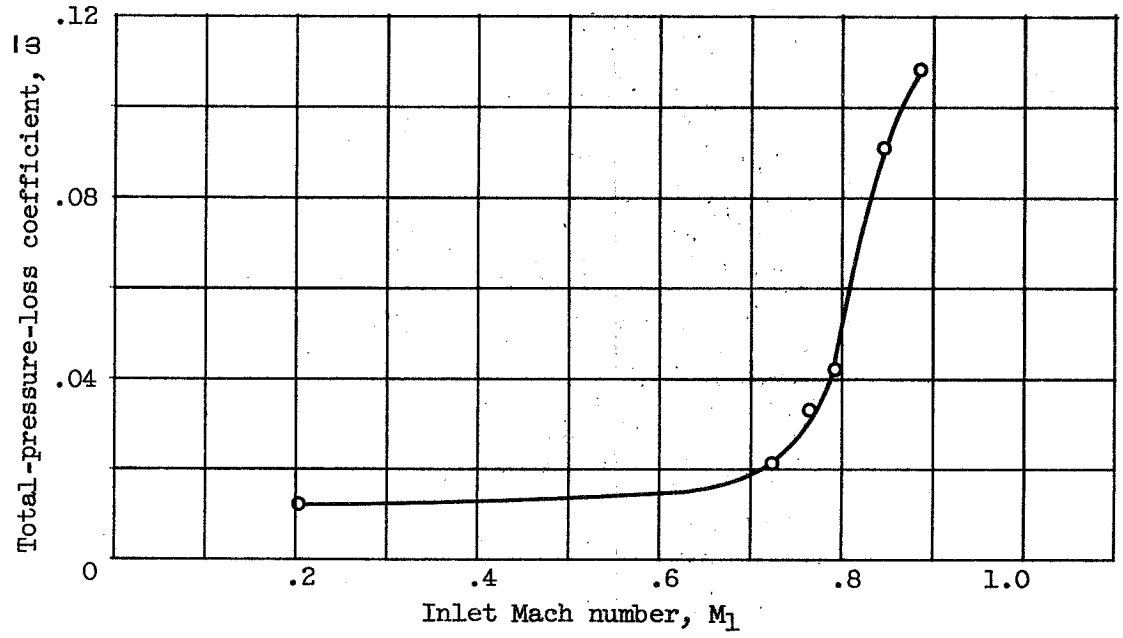

(a) Total-pressure-loss coefficient.

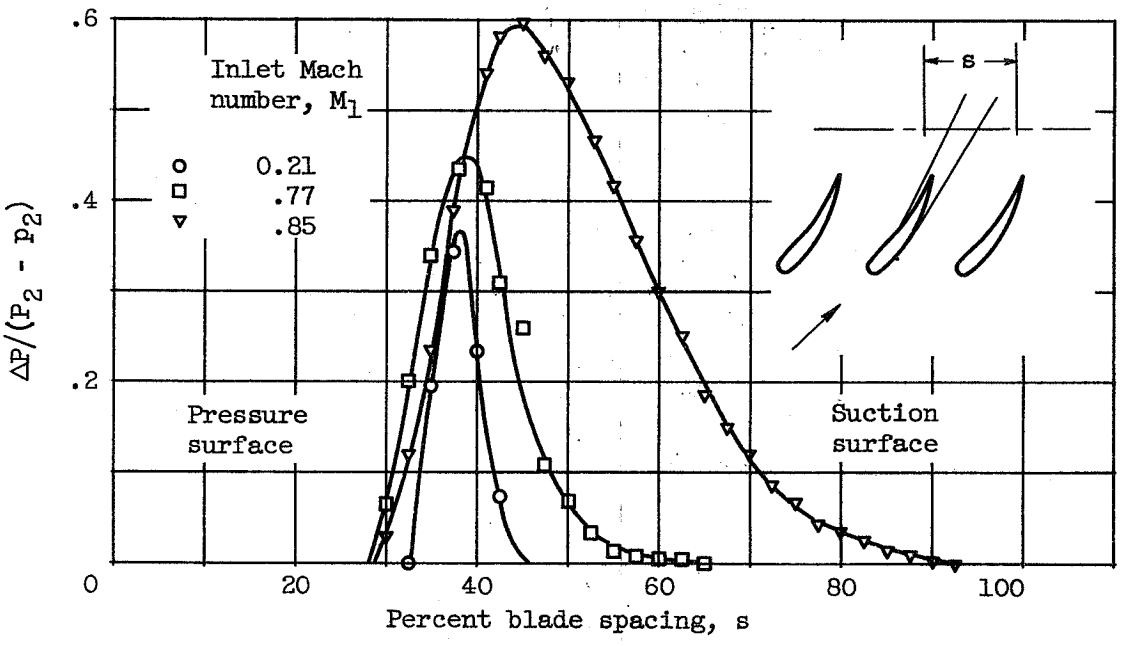

(b) Blade wake.

Figure 31. - Variation of cascade blade loss with inlet Mach number for NACA 65-($12A_{10}$)10 blade in region of minimum loss (ref. 23).

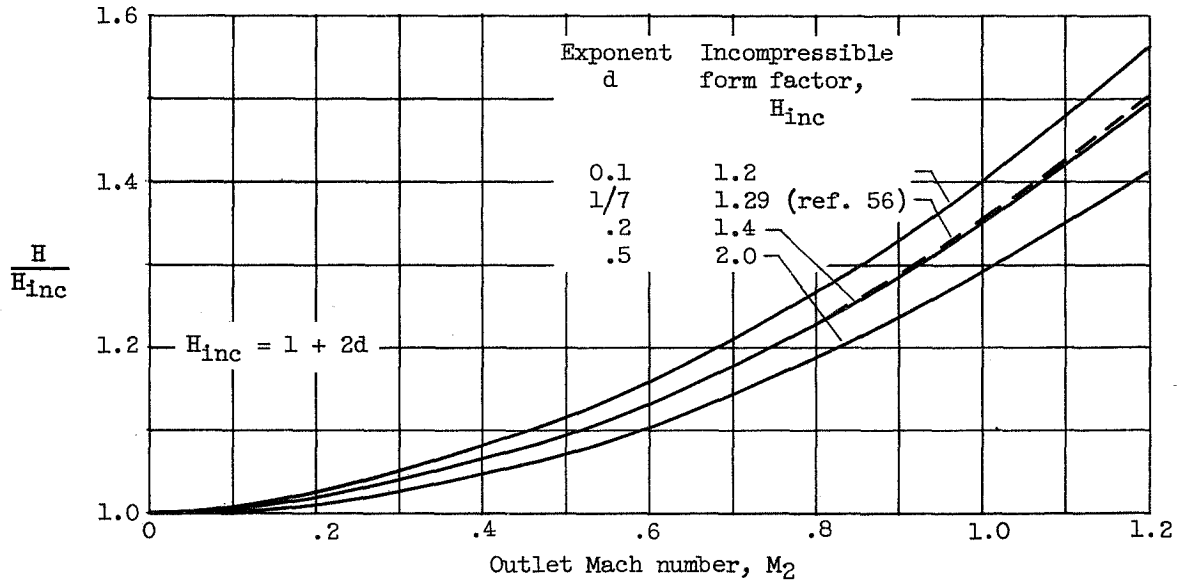

Figure 32. - Ratio of compressible to incompressible form factor for constant value of exponent in power velocity distribution.

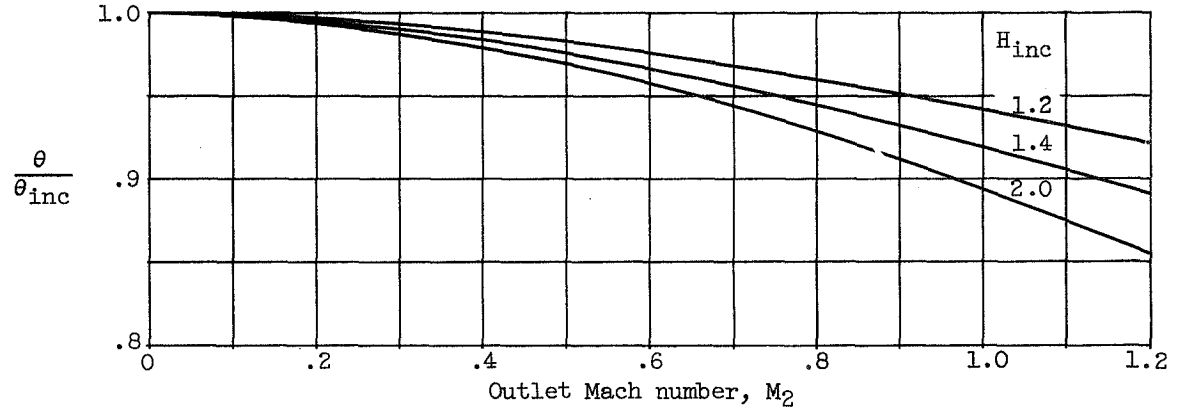

Figure 33. - Ratio of compressible to incompressible momentum thickness for constant full thickness and exponent for power velocity distribution.

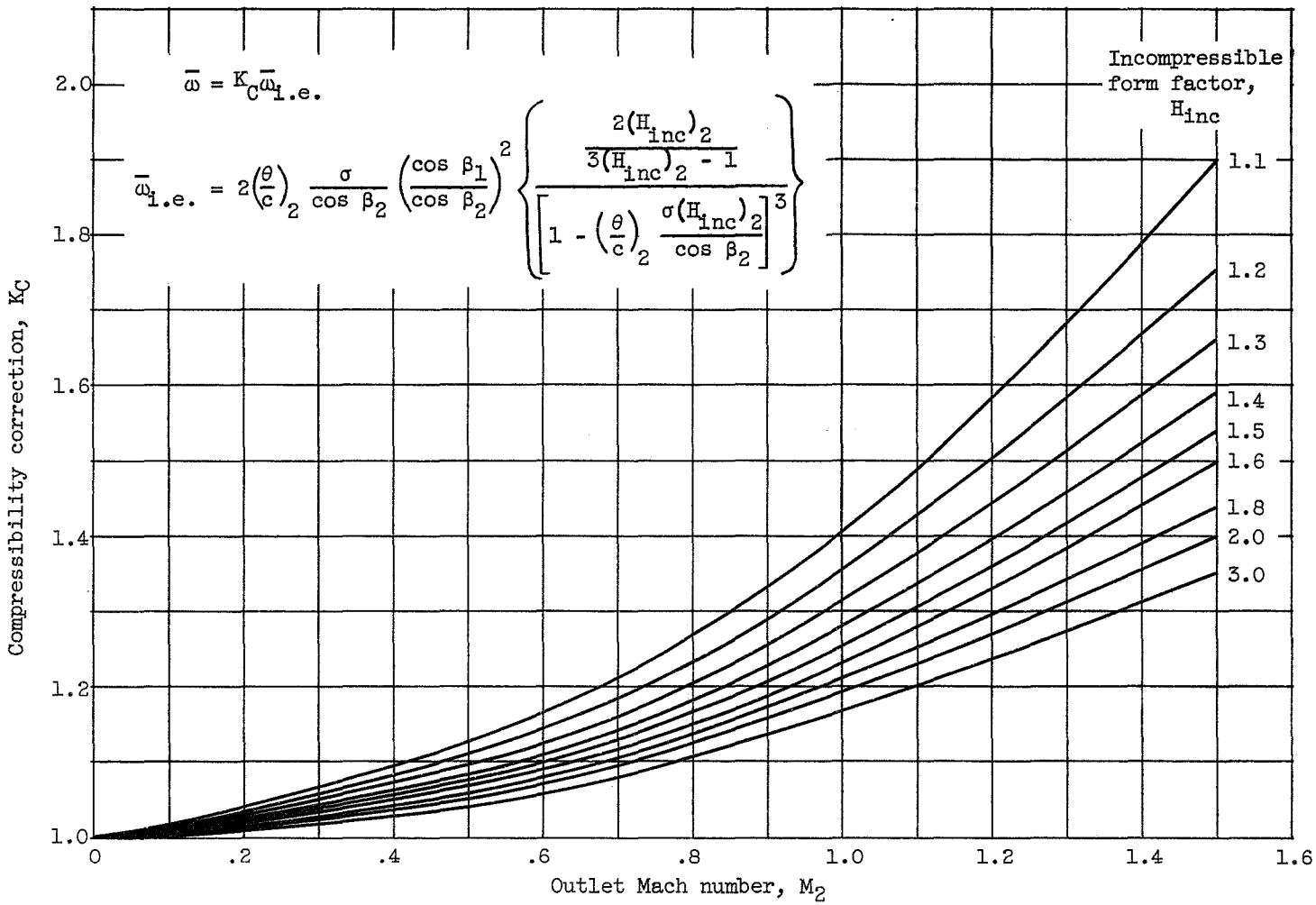

Figure 34. - Correction factor K_c for calculation of total-pressure-loss coefficient for compressible flow on basis of incompressible equation (5) as determined from model wake form with power velocity profile.

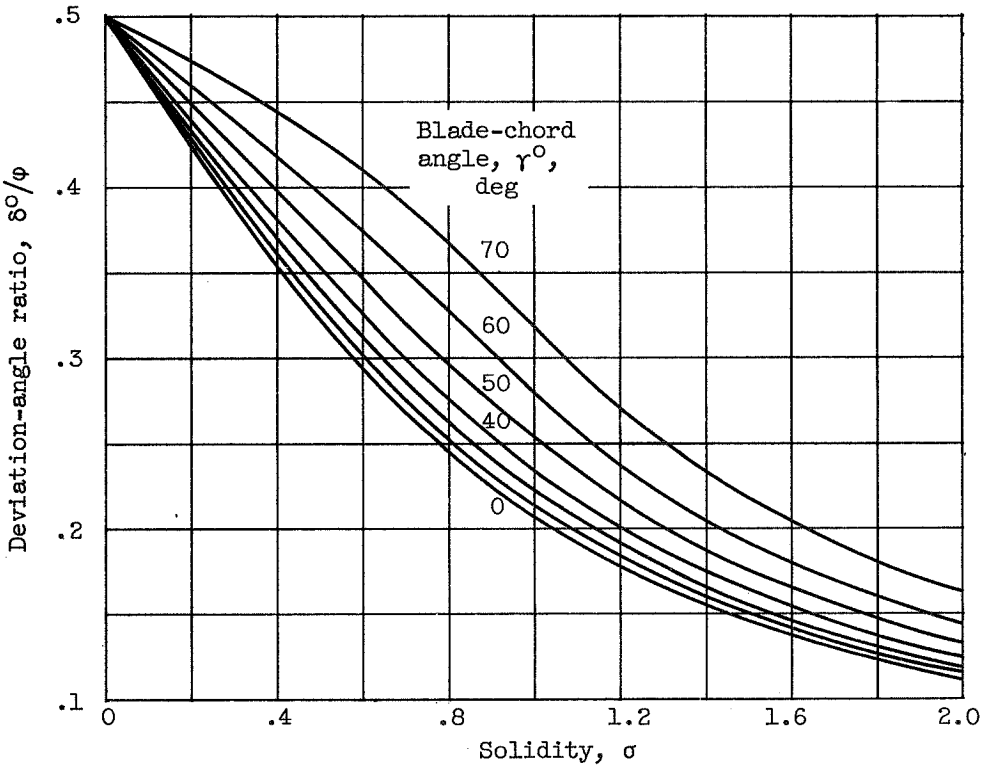

Figure 35. - Theoretical variation of deviation-angle ratio for infinitely thin circular-arc sections at "impact-free-entry" incidence angle according to potential theory of reference 28.

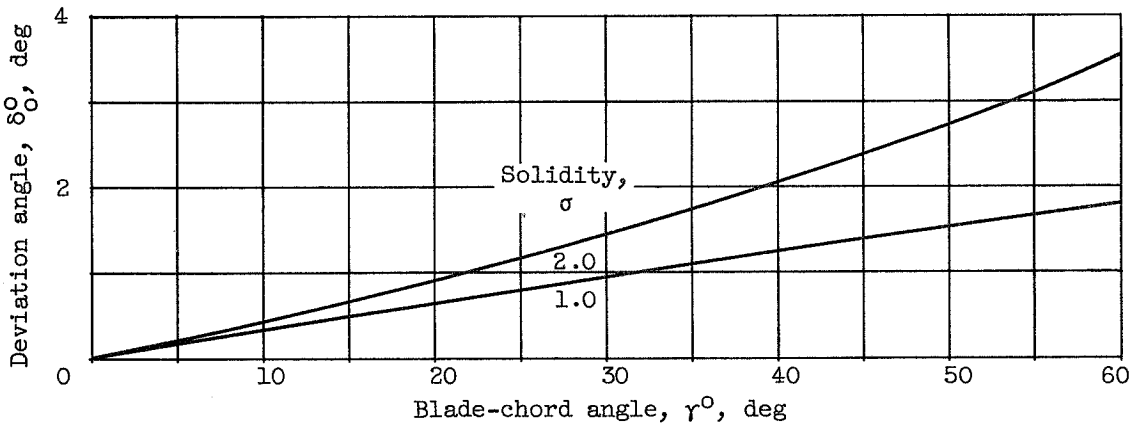

Figure 36. - Theoretical variation of deviation angle for conventional uncambered 10-percent-thick blade section at zero incidence angle as presented in reference 18.

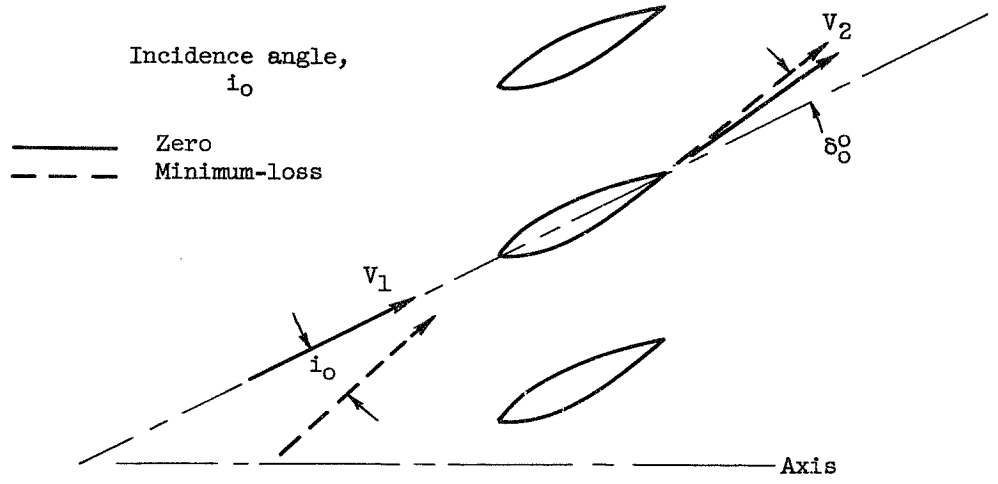

Figure 37. - Outlet flow direction for cascade of staggered uncambered blades.

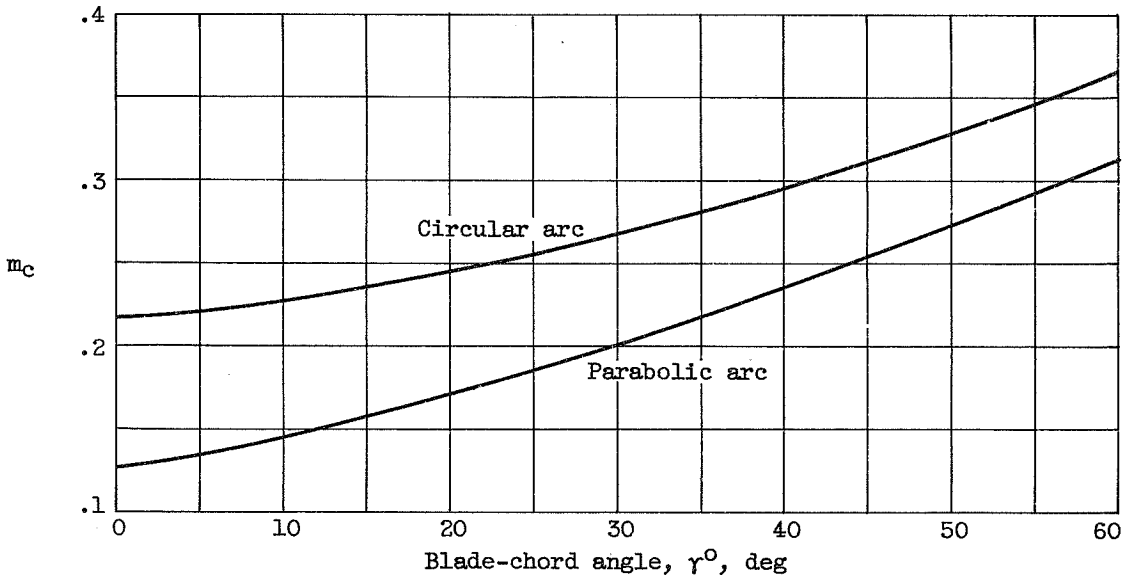

Figure 38. - Variation of factor m_c in Carter's deviation-angle rule (ref. 48).

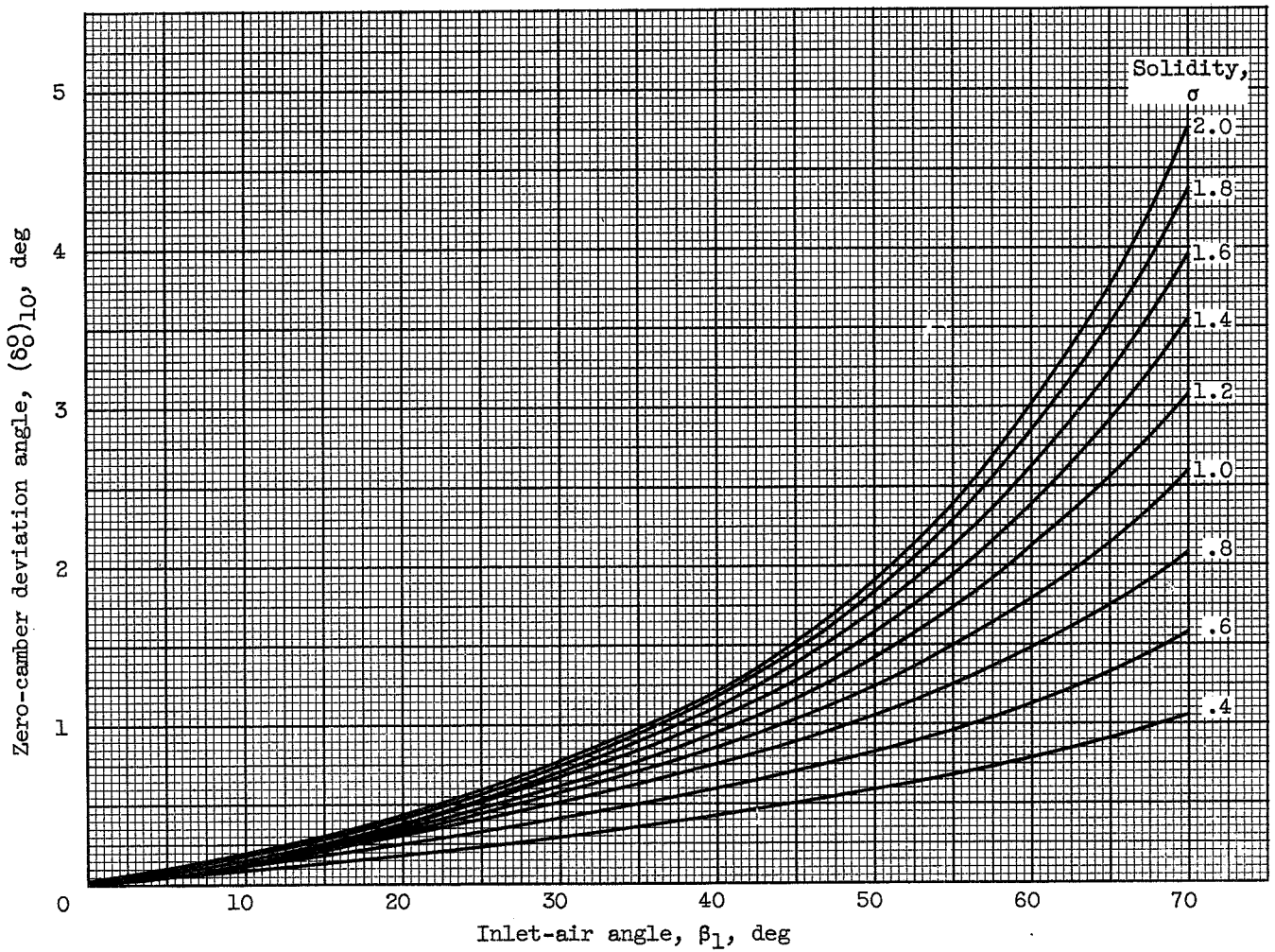

Figure 39. - Zero-camber deviation angle at reference minimum-loss incidence angle deduced from low-speed-cascade data for 10-percent-thick NACA 65-(A_{10})-series blades (ref. 13).

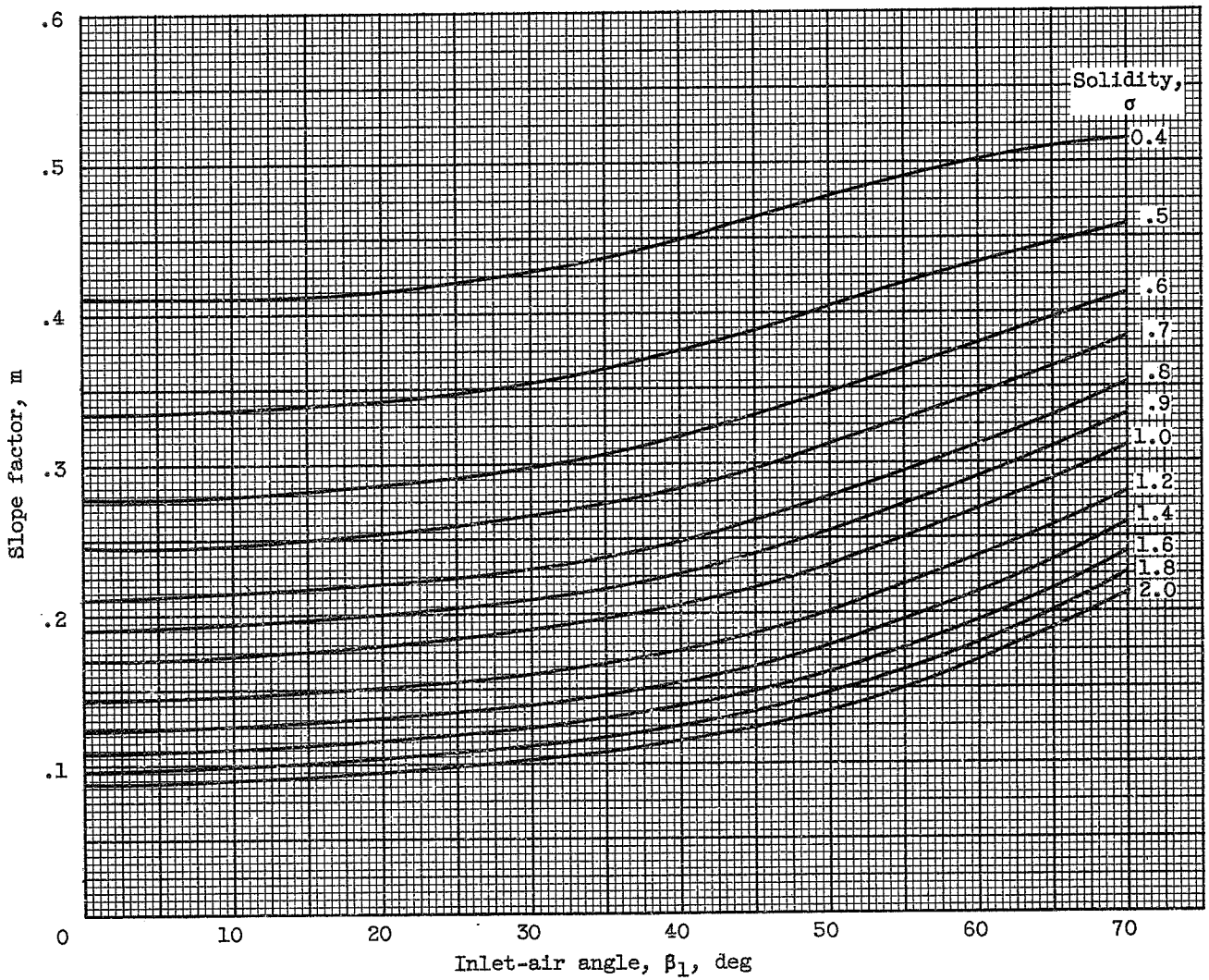

Figure 40. - Deduced variation of slope factor m in deviation-angle rule for NACA 65-(A_{10})-series blades as equivalent circular arc.

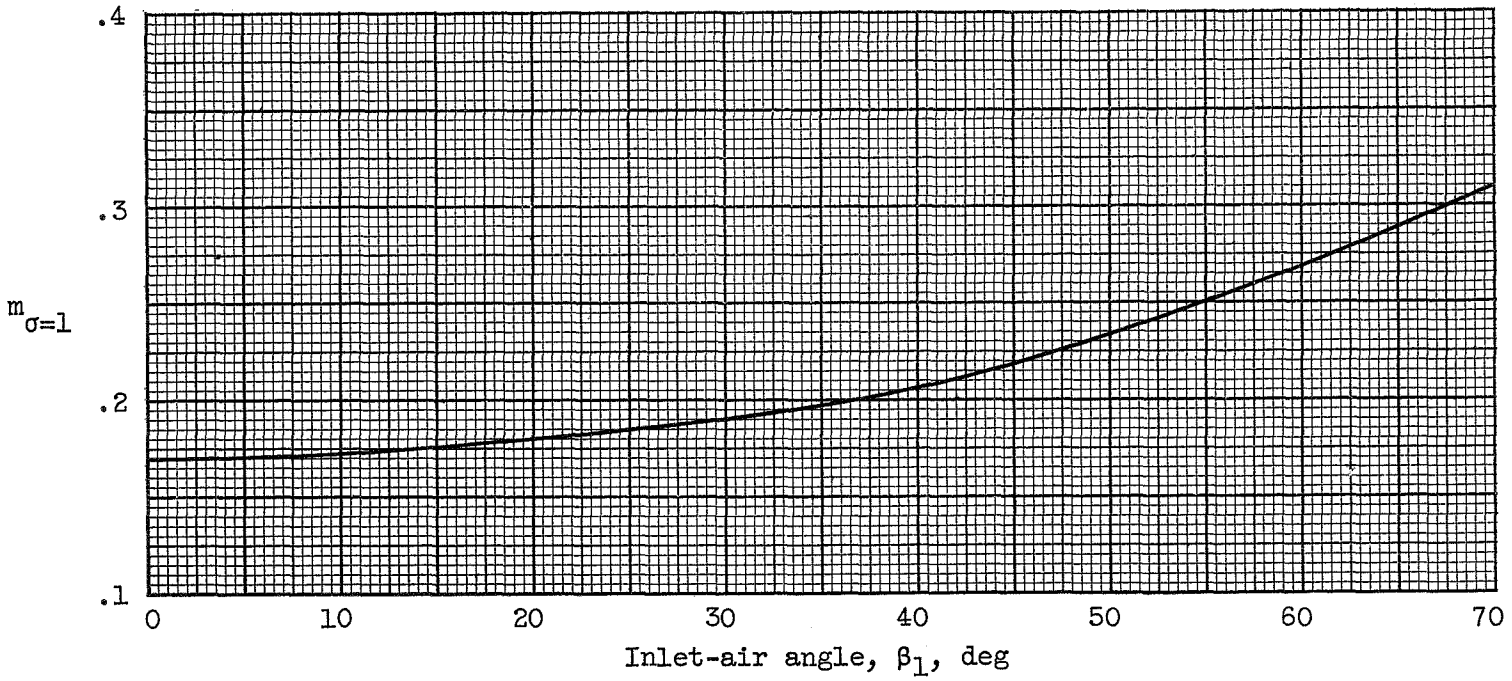

Figure 41. - Value of $m_{\sigma=1}$ in deviation-angle rule for 65-(A_{10})-series blades as equivalent circular arc (deduced from data of ref. 13).

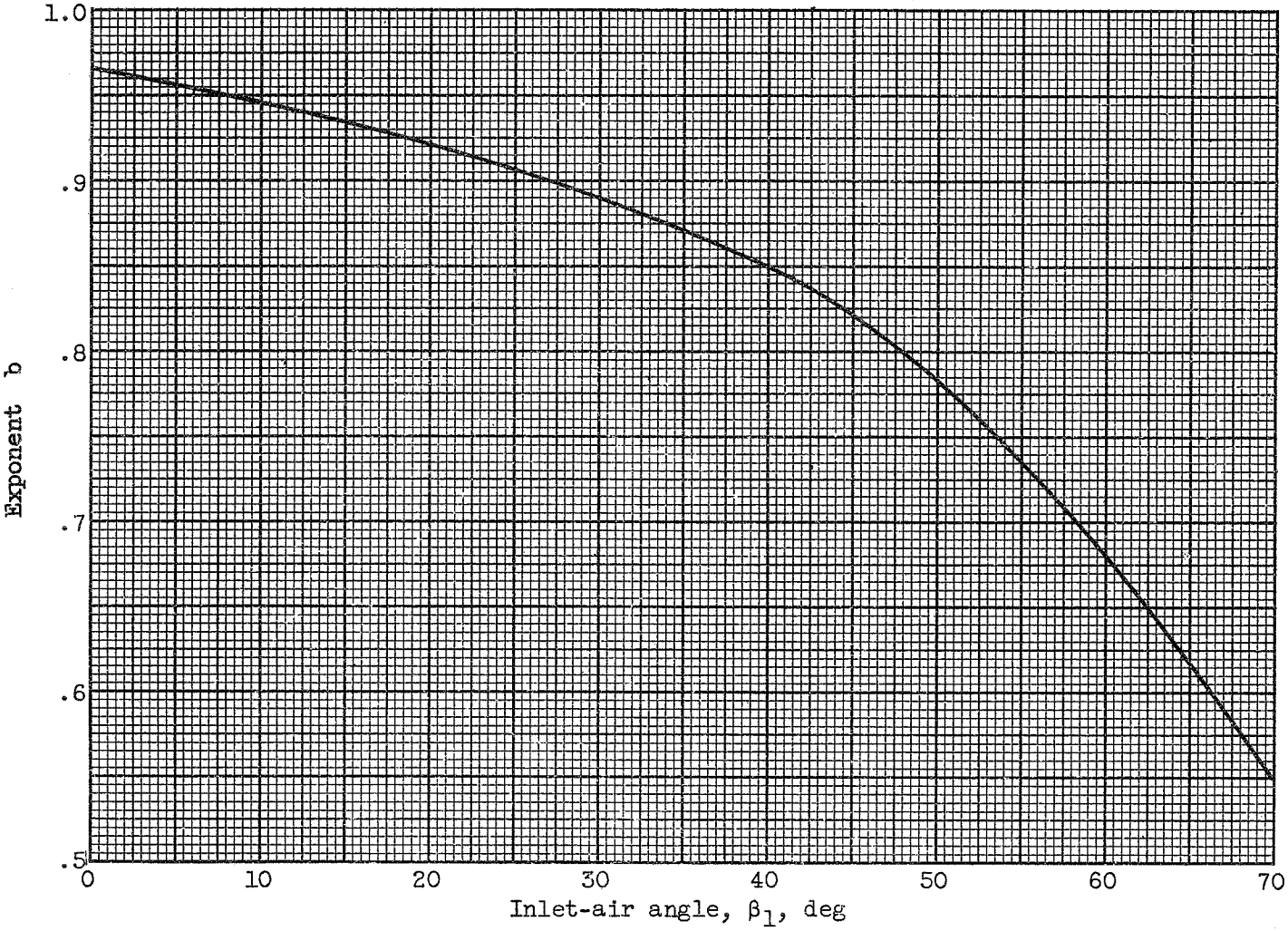

Figure 42. - Value of solidity exponent b in deviation-angle rule (eq. (11)) (deduced from data for 65-(A_{10})-series blades in ref. 13).

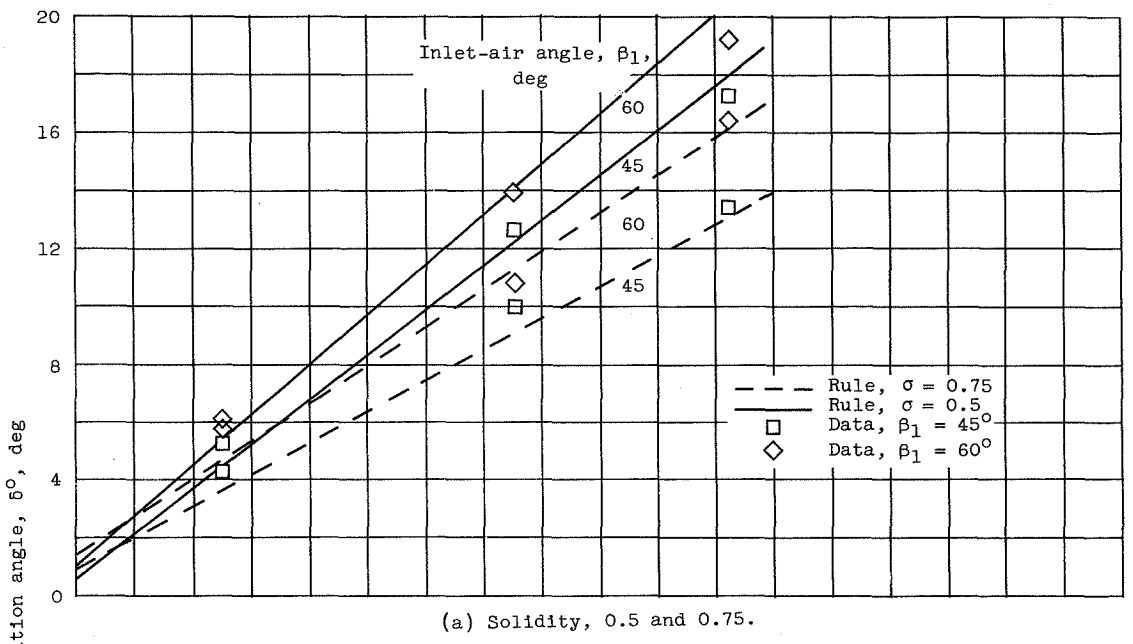

(a) Solidity, 0.5 and 0.75.

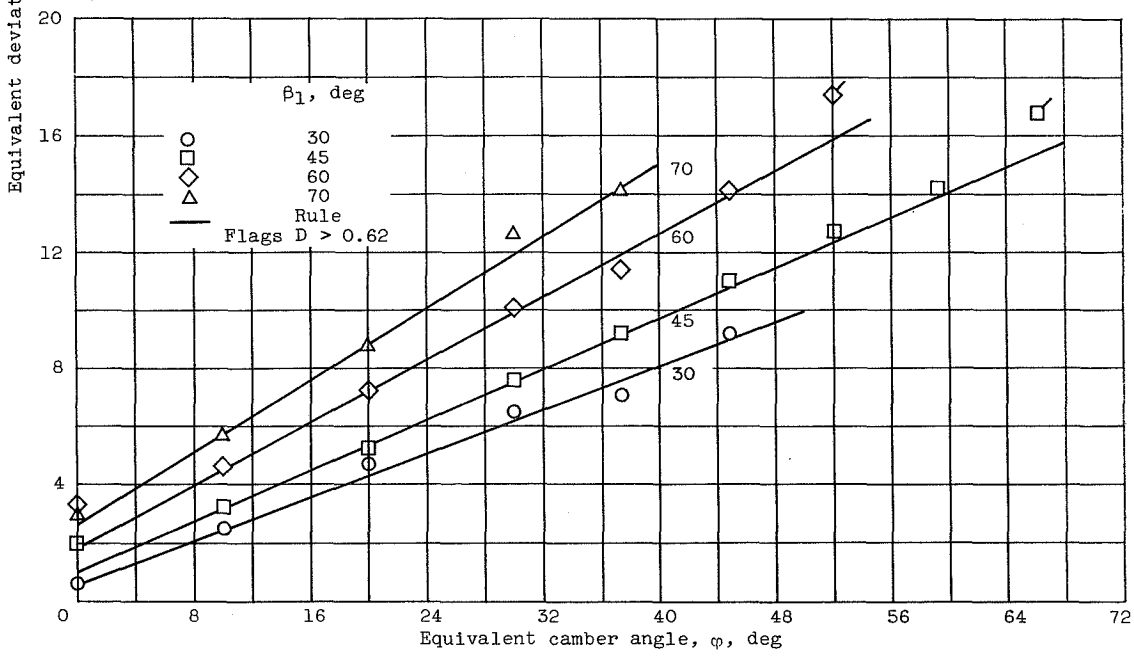

(b) Solidity, 1.0.

Figure 43. - Comparison between data values and deduced rule values of reference minimum-loss deviation angle for NACA 65-(A_{10})10-series blades as equivalent circular arcs (data from ref. 13).

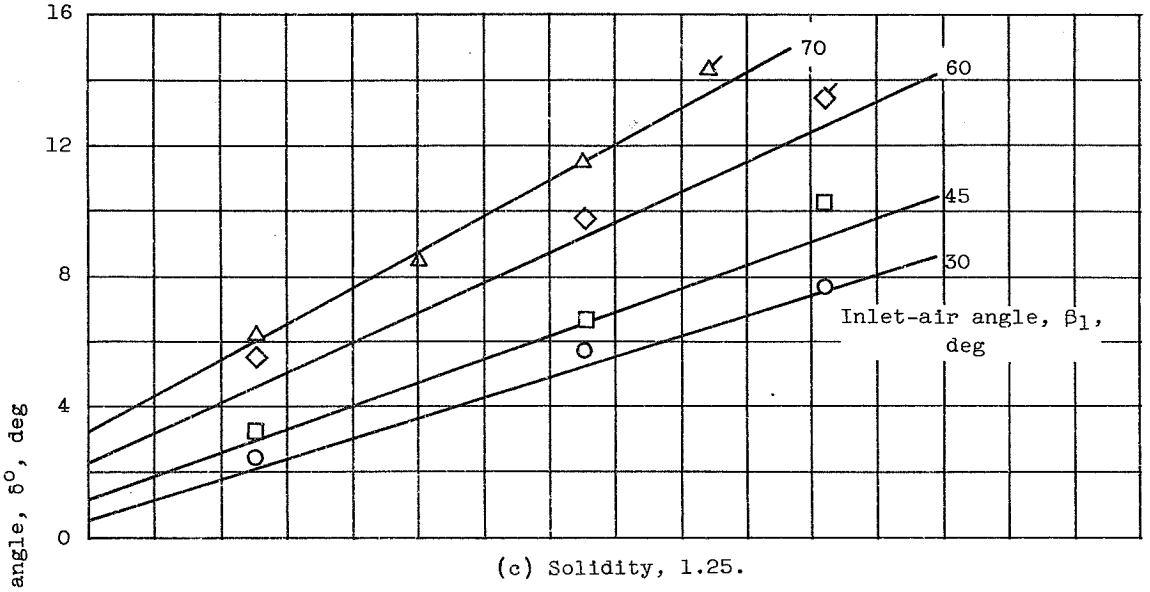

(c) Solidity, 1.25.

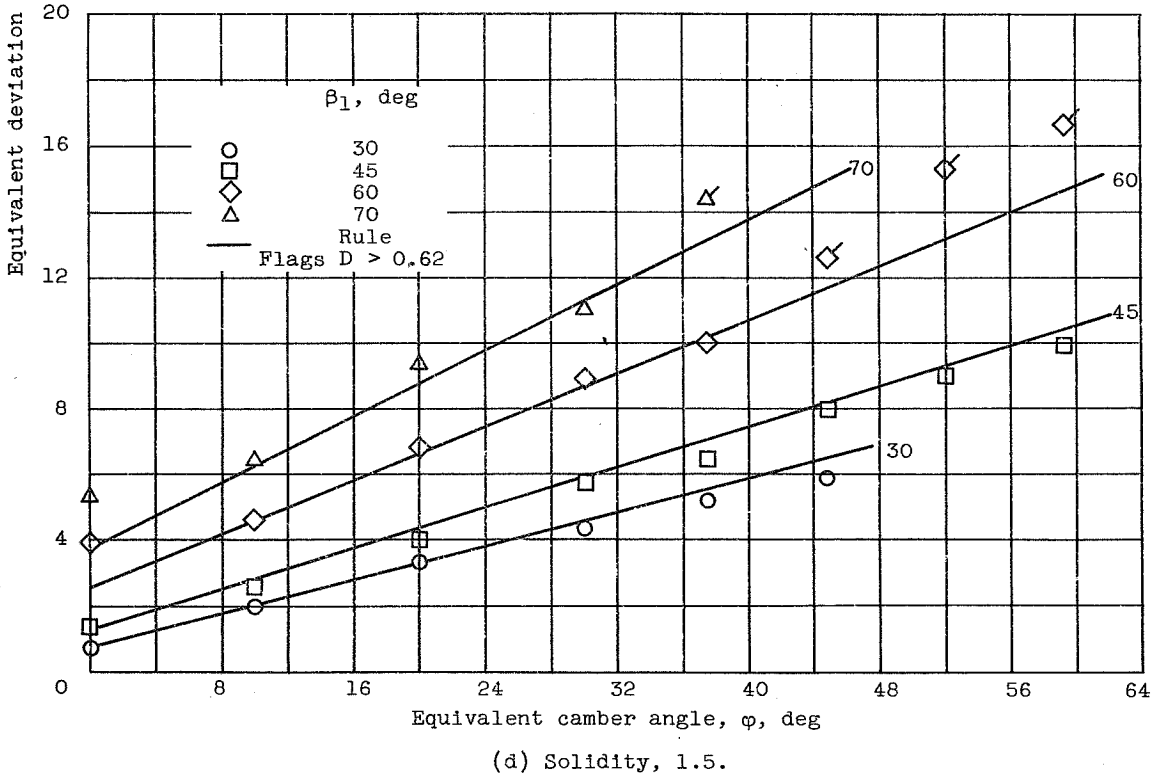

(d) Solidity, 1.5.

Figure 43. - Concluded. Comparison between data values and deduced rule values of reference minimum-loss deviation angle for NACA 65-(A_{10})10-series blades as equivalent circular arcs (data from ref. 13).

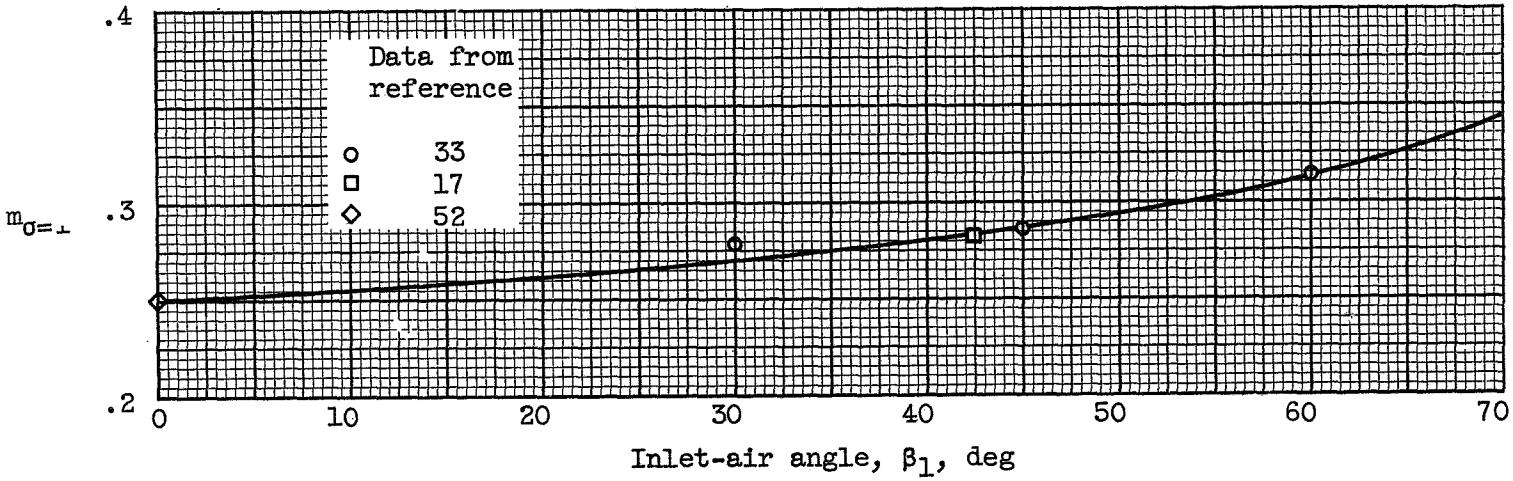

Figure 44. - Deduced values of $m_{\sigma=1}$ for circular-arc mean line.

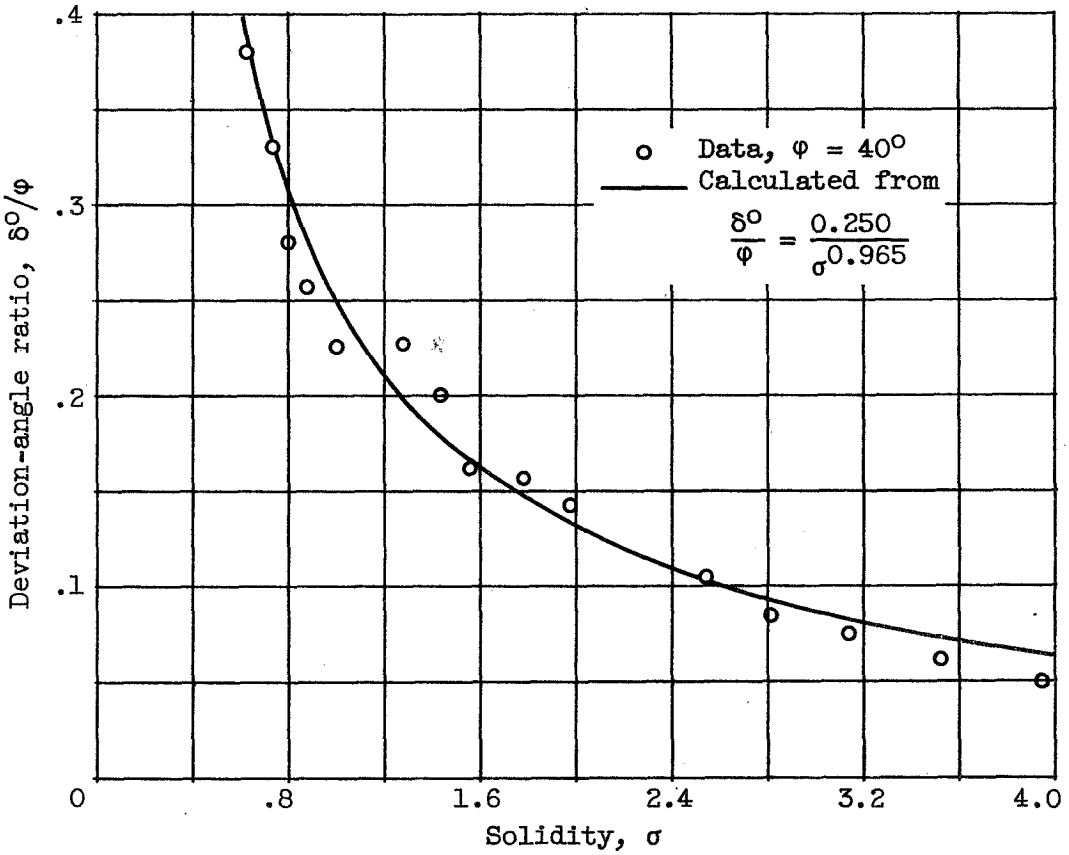

Figure 45. - Comparison of experimental deviation-angle ratio and rule values us ng solidity exponent given by figure 42. Data for cir ular-arc inlet guide vanes in annular cascade (ref. 53).

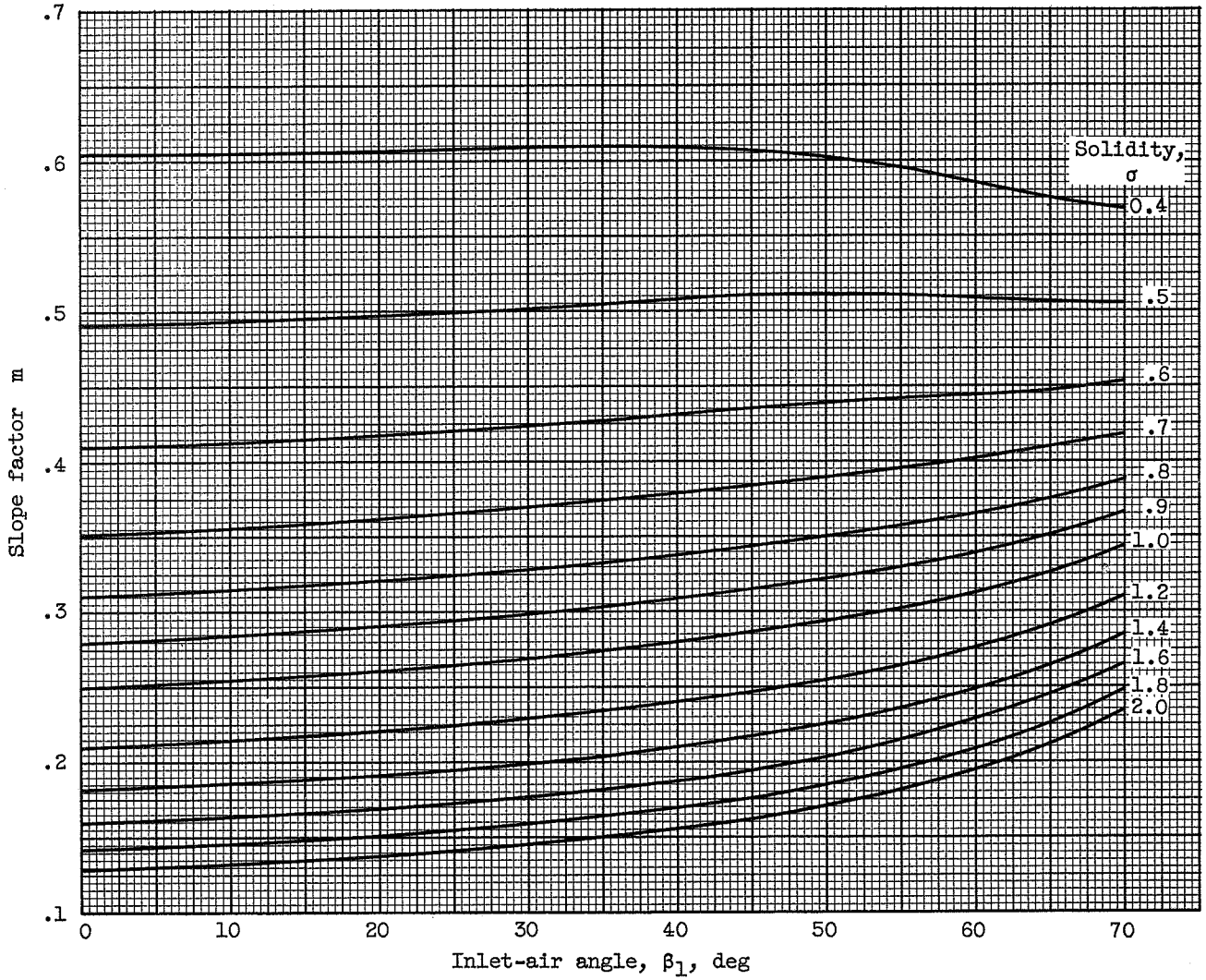

Figure 46. - Deduced variation of slope factor m in deviation-angle rule (eq. (10)) for circular-arc-mean-line blades.

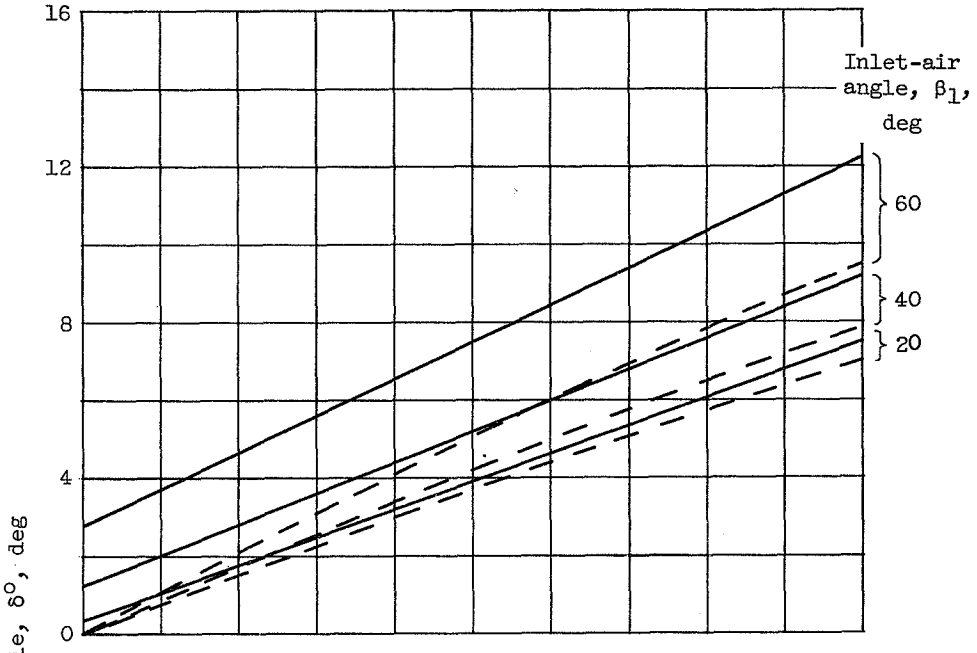

(a) Solidity, 1.5.

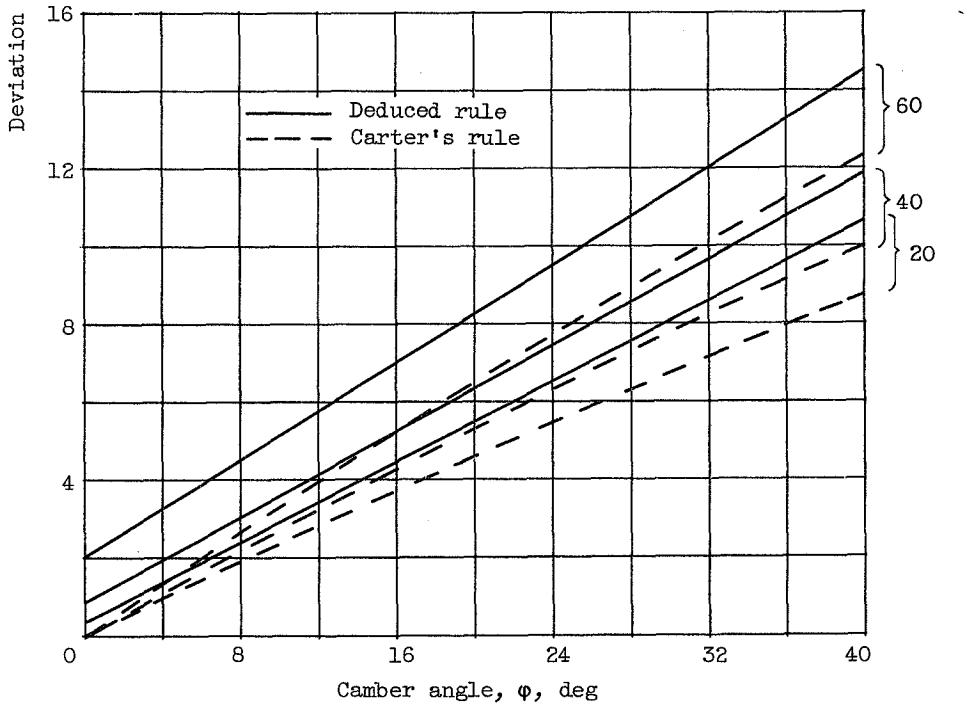

(b) Solidity, 1.0.

Figure 47. - Comparison of calculated reference deviation angles according to Carter's rule and deduced modified rule for 10-percent-thick, thick-nose circular-arc blades.

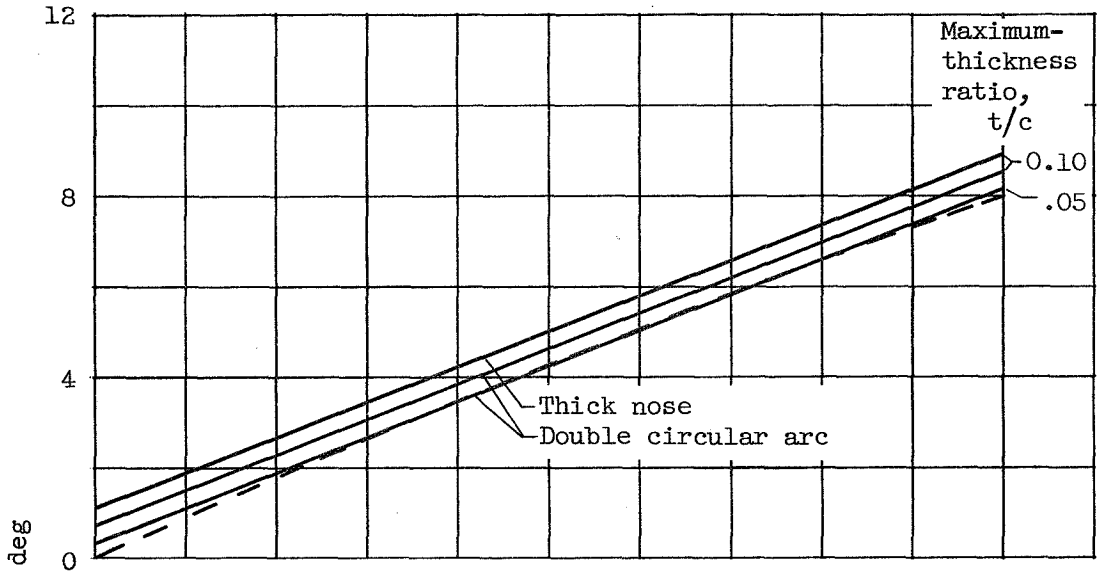

(a) Solidity, 1.5; inlet-air angle, 40°.

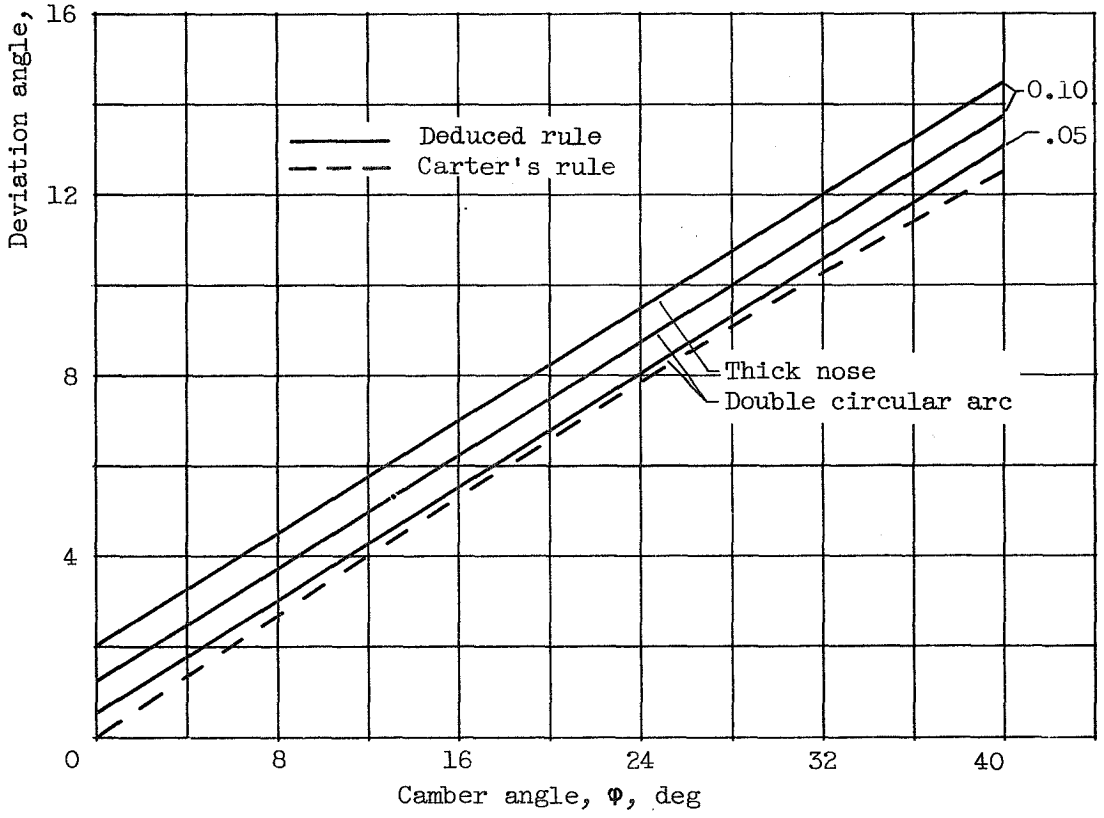

(b) Solidity, 1.0; inlet-air angle, 60°.

Figure 48. - Comparison of calculated reference deviation angles according to Carter's rule and deduced modified rule for circular-arc blades of different thickness.

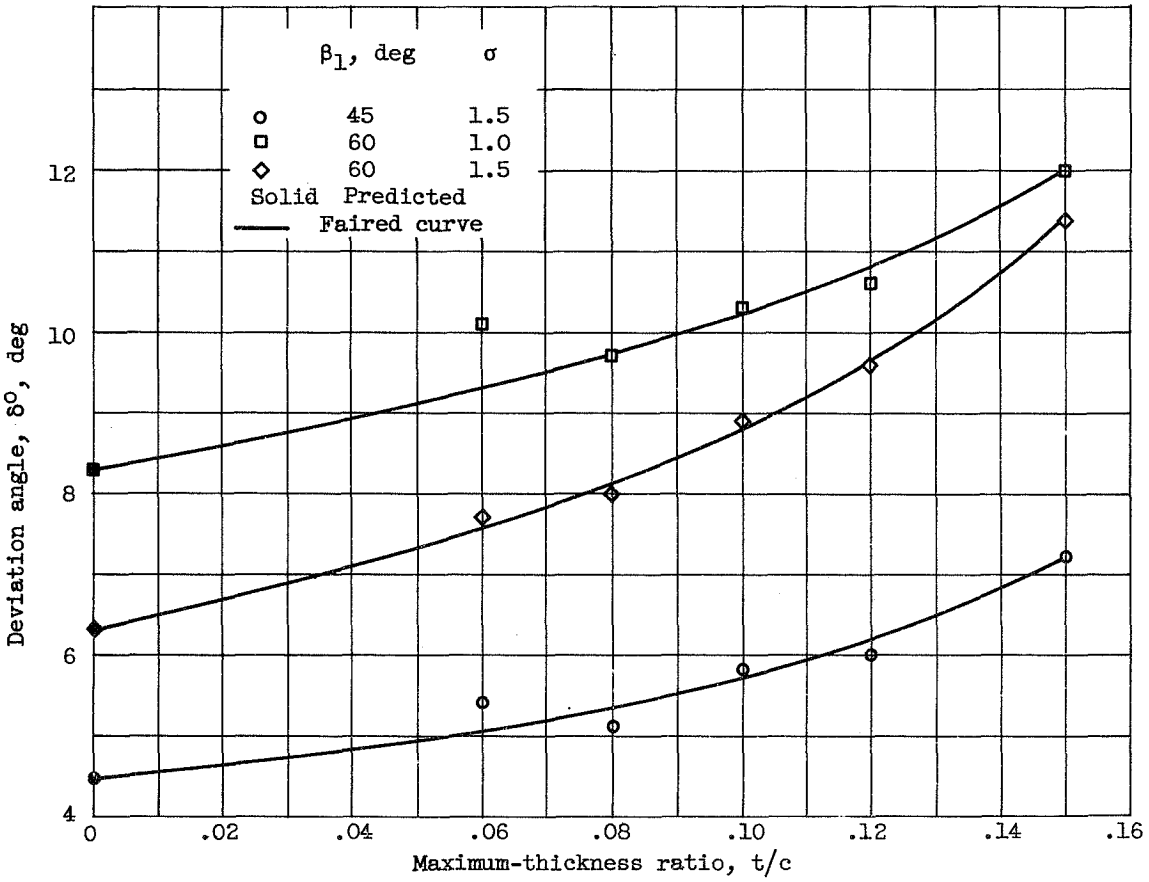

Figure 49. - Variation of deviation angle with blade maximum-thickness ratio for NACA 65-($12A_{10}$) blade in region of minimum loss (data from ref. 36).

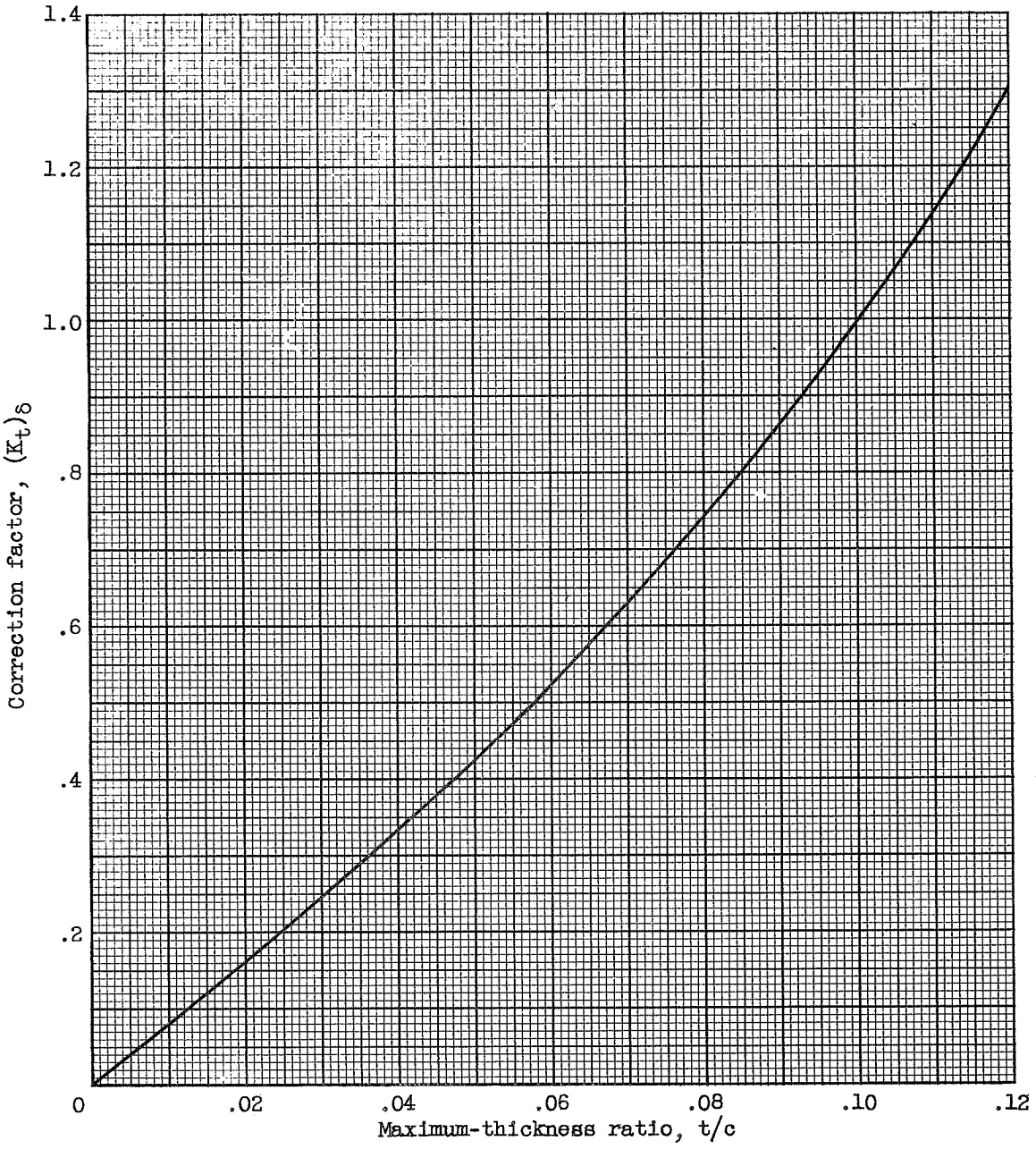

Figure 50. - Deduced maximum-thickness correction for zero-camber reference minimum-loss deviation engle (eq. (13)).

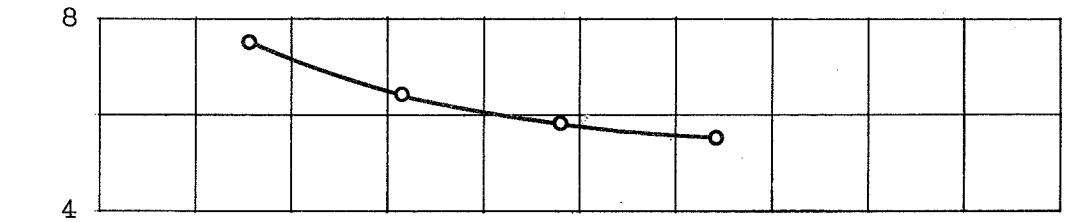

(a) 10C4/25C50 blade. Solidity, 1.33; blade-chord angle, 42.5° (ref. 23).

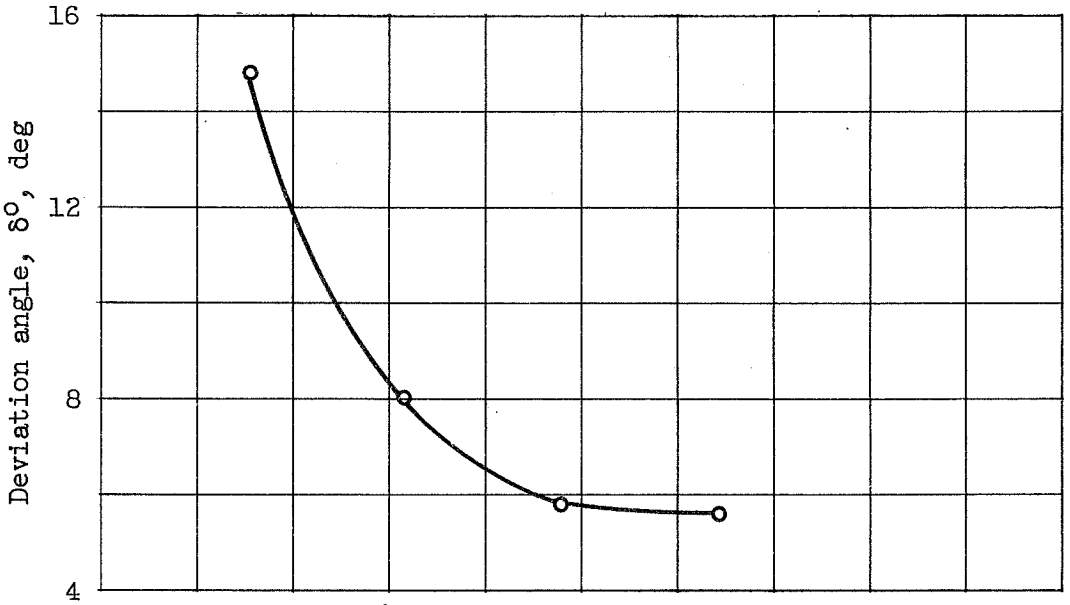

(b) 10.5 2A/25C50 blade. Solidity, 1.33; blade-chord angle, 42.5° (ref. 23).

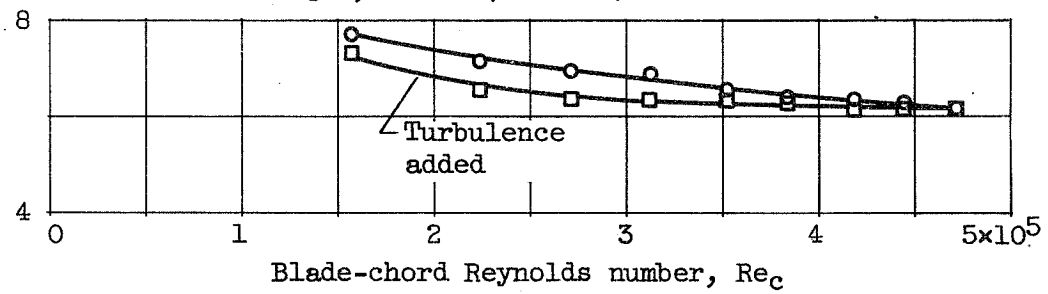

(c) NACA 65-(12)10 blade. Solidity, 1.5; inlet-air angle, 45° (ref. 13).

Figure 51. - Illustrative variations of reference deviation angle with Reynolds number.

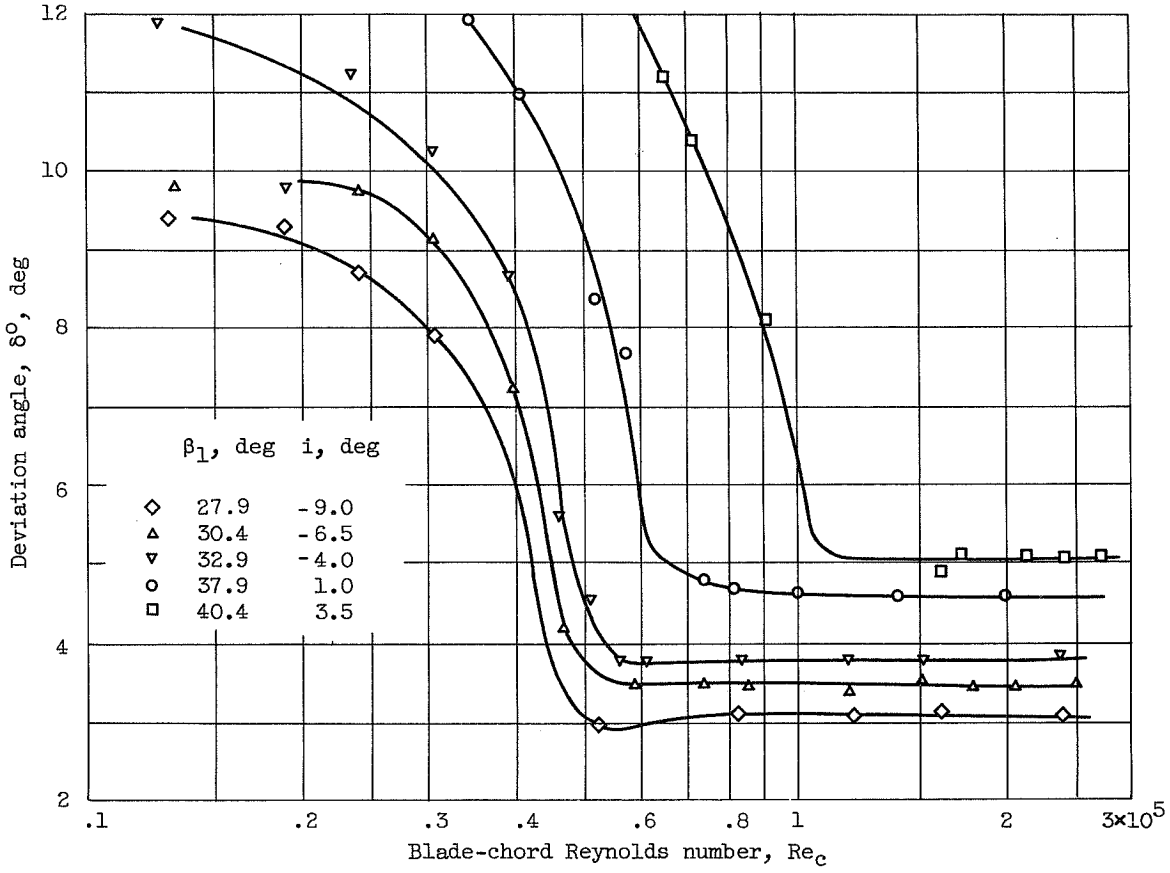

Figure 52. - Variation of deviation angle with Reynolds number for 10C4/40 P40 blade. Solidity, 1.33 (ref. 41).

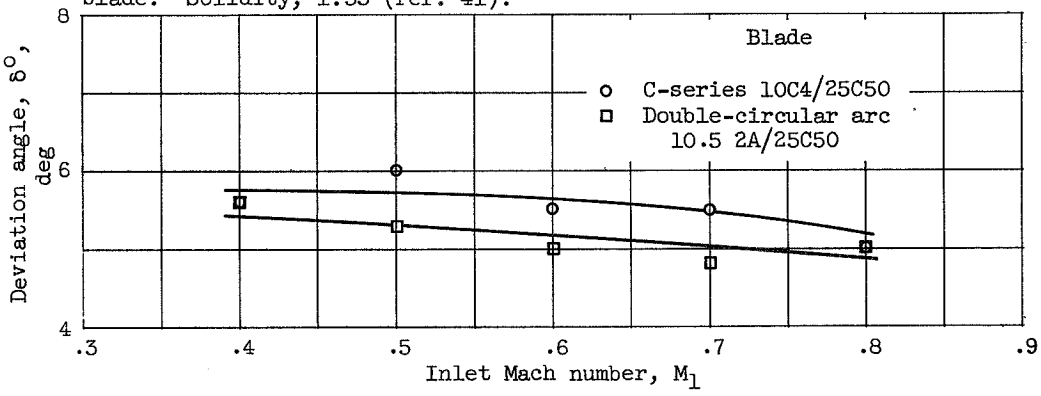

Figure 53. - Variation of reference deviation angle with inlet Mach number for circular-arc blades. Solidity, 1.333; blade-chord angle, 42.5° (ref. 23).

[redacted]

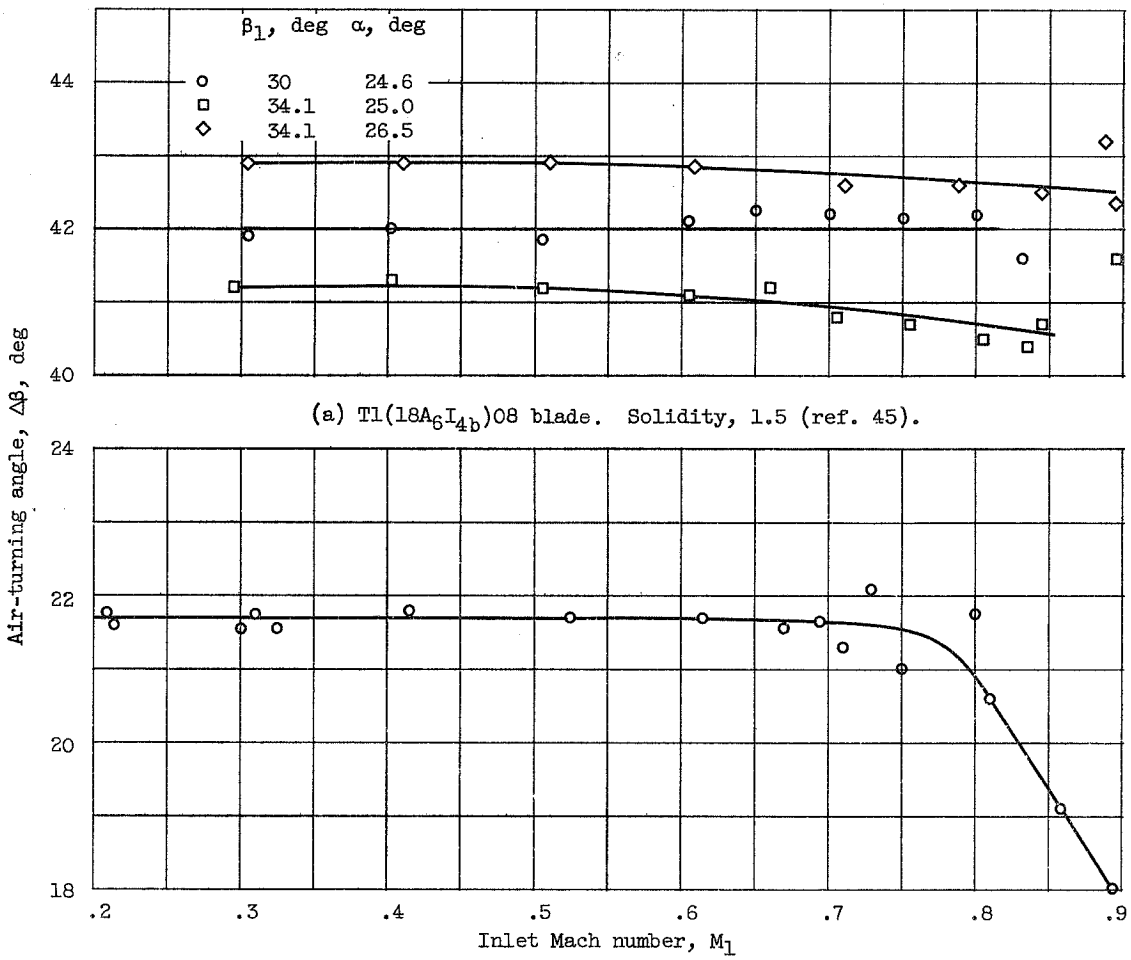

(a) T1($18A_6I_{4b}$)08 blade. Solidity, 1.5 (ref. 45).

(b) 65-($12A_{10}$)10 blade. Solidity, 1.0; inlet-air angle, 45°; angle of attack, 16.5° (ref. 22).

Figure 54. - Variation of air-turning angle with inlet Mach number in region of minimum loss.

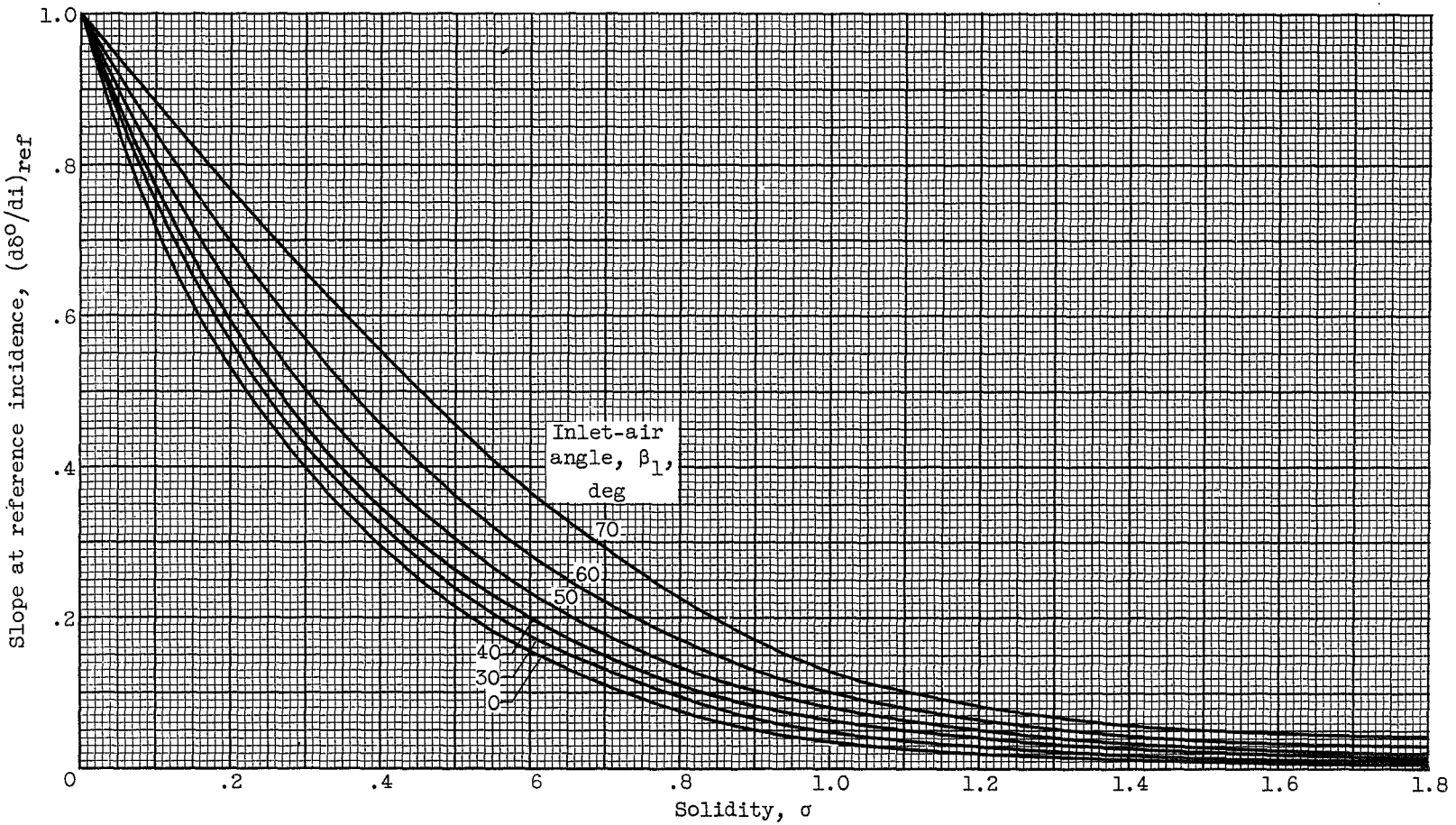

Figure 55. - Deviation-angle slope $d\delta^o/di$ at reference incidence angle deduced from low-speed data for NACA 65-(A_{10})10 blades (ref. 13).

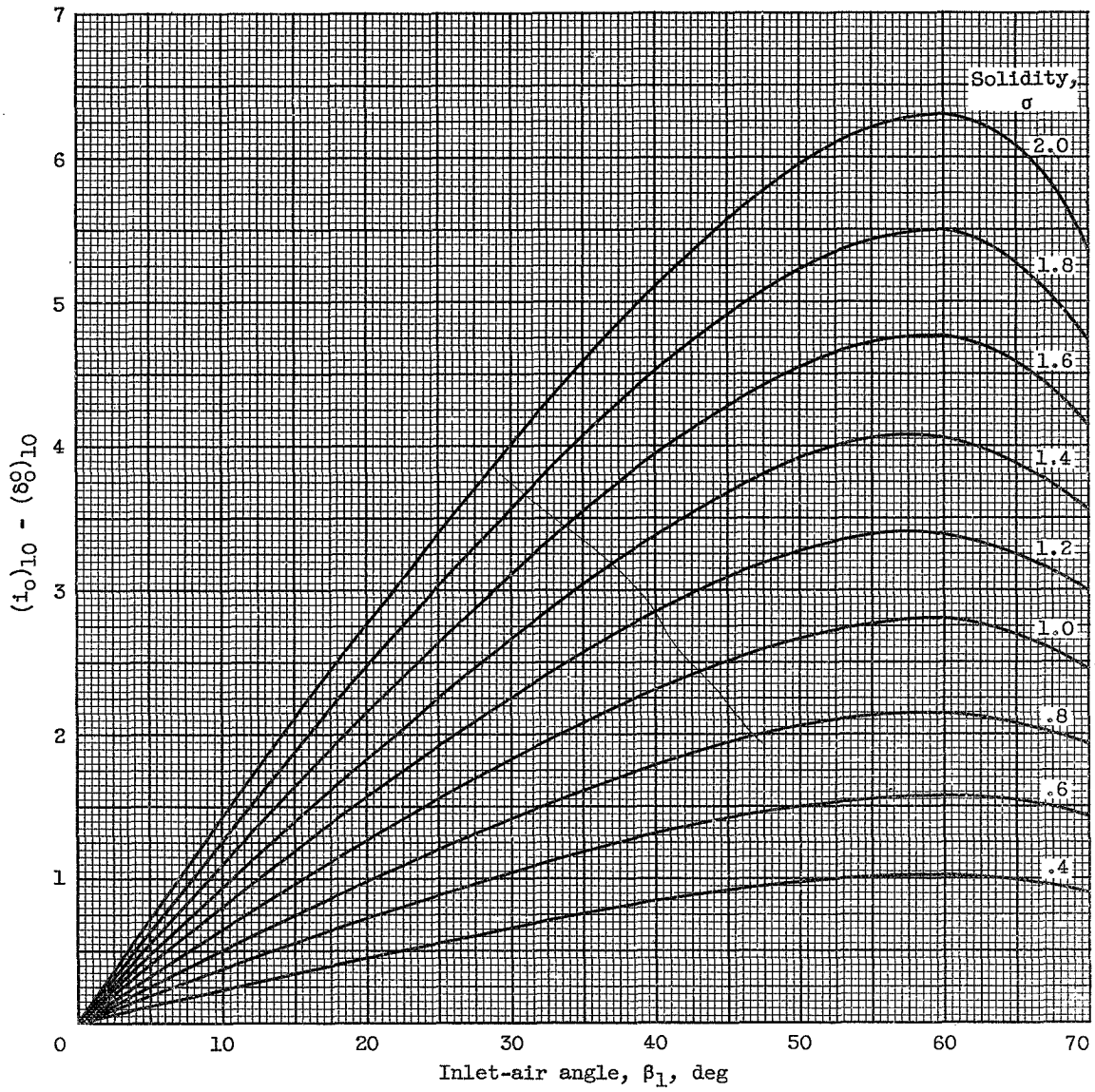

Figure 56. - Variation of $(i_o)_{10} - (\delta_o^o)_{10}$ with inlet-air angle and solidity (eq. (18)).

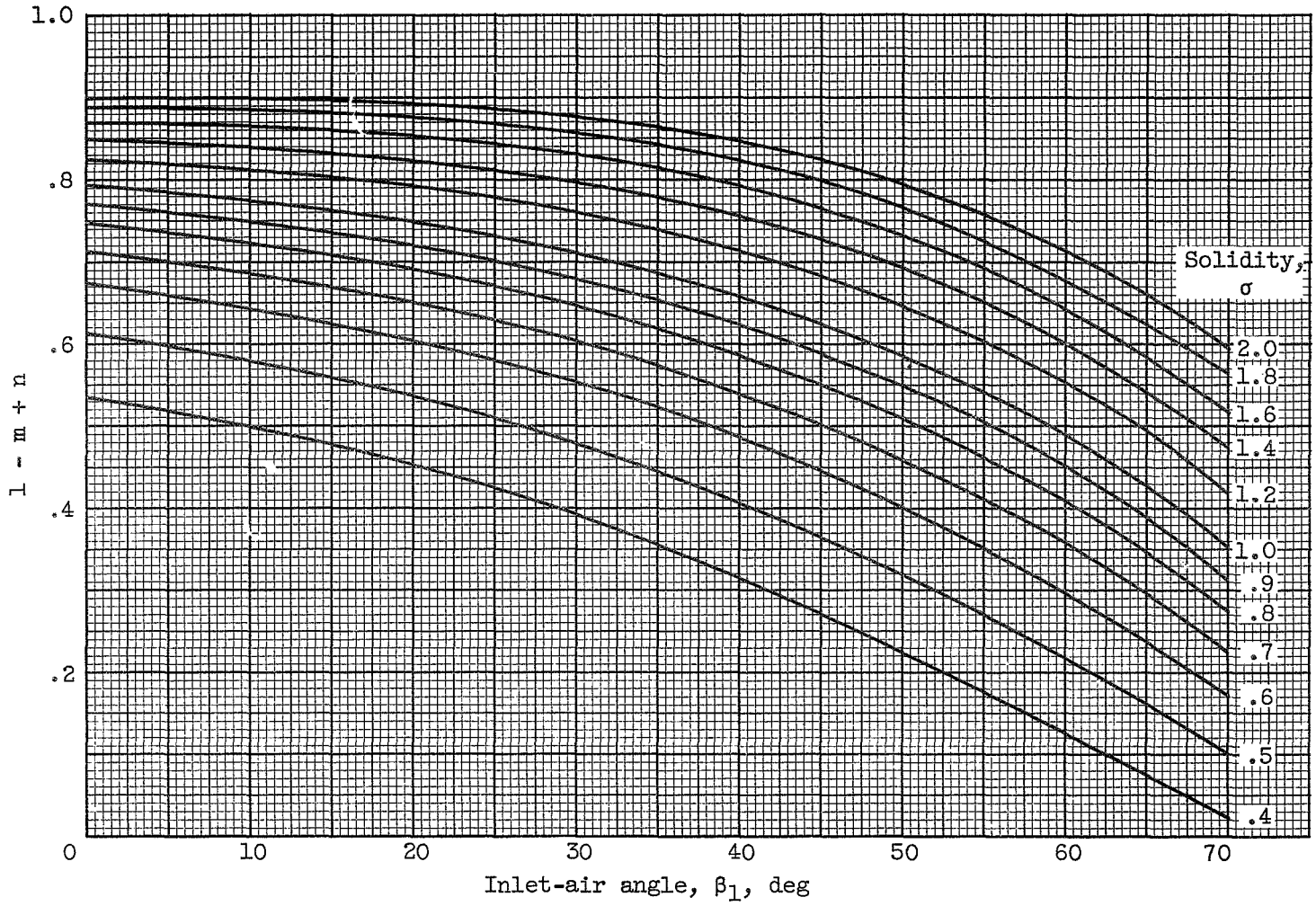

(a) NACA 65-(A_{10})-series blades as equivalent circular arc (eq. 18)).

Figure 57. - Variation of 1 - m + n.

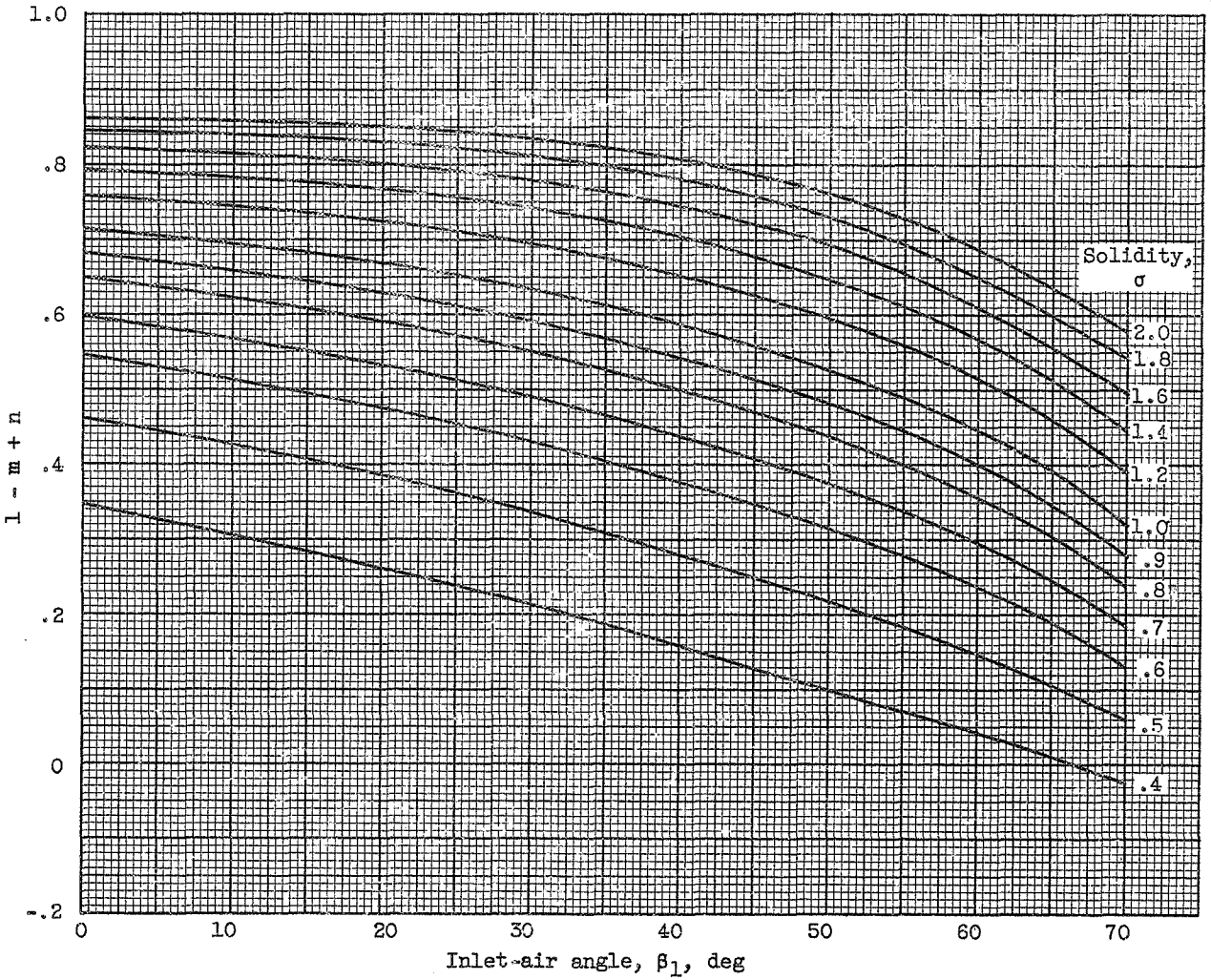

(b) Circular-arc-mean-line blades (eq. (18)).

Figure 57. - Concluded. Variation of 1 - m + n.

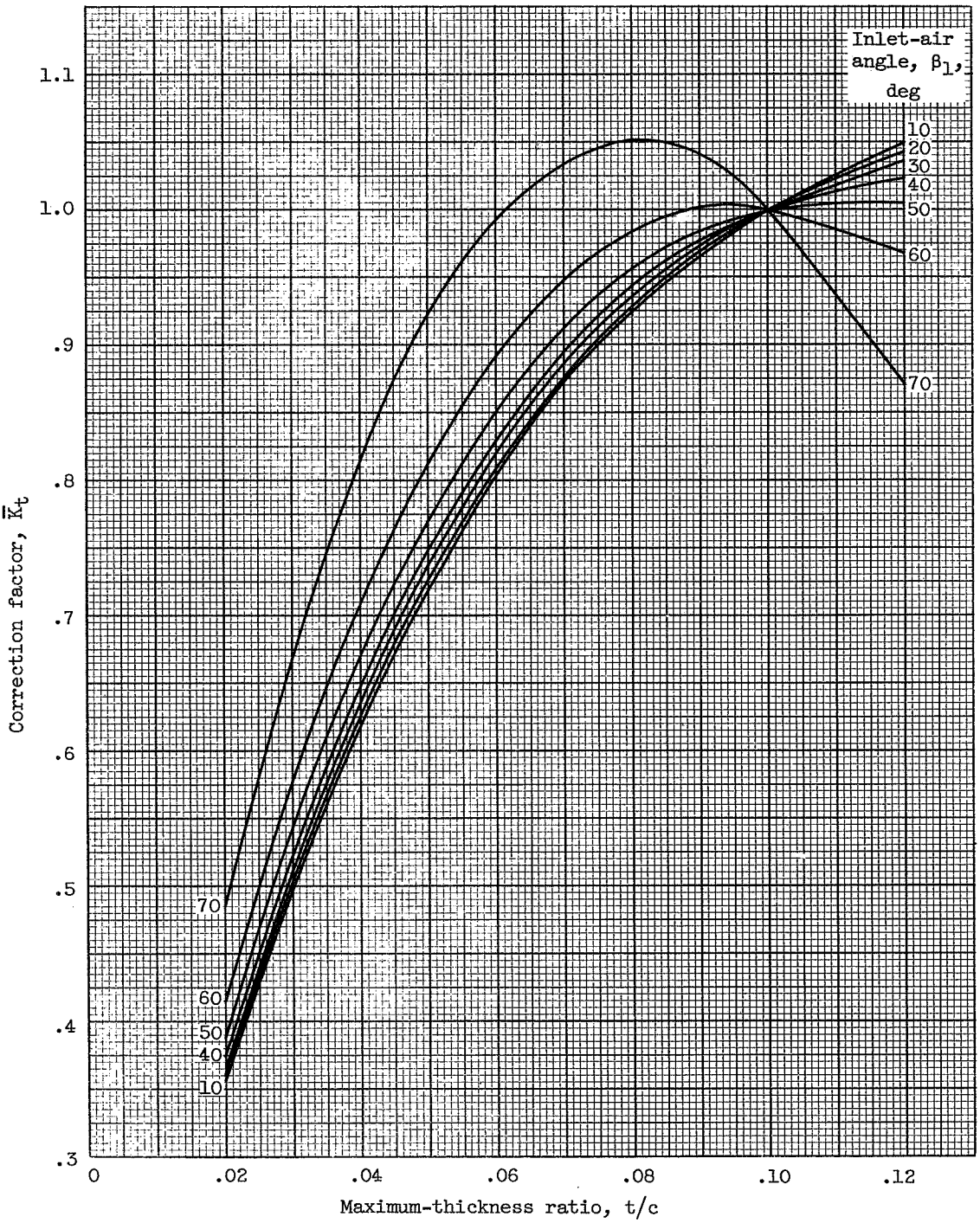

Figure 58. - Variation of thickness-correction factor $\bar{K}_t$ for camber calculation (eq. (18)).

[redacted]

AERODYNAMIC DESIGN OF AXIAL-FLOW COMPRESSORS

VI - EXPERIMENTAL FLOW IN TWO-DIMENSIONAL CASCADES

Seymour Lieblein
Aeronautical Research Scientist
Compressors and Turbines

Approved:

Irving A. Johnsen
Aeronautical Research Scientist
Compressors and Turbines

Robert O. Bullock
Aeronautical Research Scientist
Compressors and Turbines

Oscar W. Schey
Chief, Compressor and Turbine
Research Division

jma - 11/7/55

[redacted]

Cascades, Theory 1.4.5.1

Cascades, Experiment 1.4.5.2

Compressor Flow Theory and Experiment 3.6.1

Compressors - Axial Flow 3.6.1.1

Lieblein, Seymour

AERODYNAMIC DESIGN OF AXIAL-FLOW COMPRESSORS
VI - EXPERIMENTAL FLOW IN TWO-DIMENSIONAL CASCADES

Abstract

Available experimental two-dimensional cascade data for conventional compressor blade sections are correlated at a reference incidence angle in the region of minimum loss. Variations of reference incidence angle, total-pressure loss, and deviation angle with cascade geometry, inlet Mach number, and Reynolds number are investigated. From the analysis and the correlations of the available data, rules and relations are evolved for the prediction of blade-profile performance. These relations are developed in simplified forms readily applicable to compressor design procedures.